HAW HAMBURG

Project

NO_x Emissions of the 50 Most Used Engines for Passenger Aircraft

Author: Ahmed Hasanovic, Muhammed Ali Sarikaya

Supervisor: Prof. Dr.-Ing. Dieter Scholz, MSME
Submitted: 2025-06-13

Faculty of Engineering and Computer Science
Department of Automotive and Aeronautical Engineering

DOI:
https://doi.org/10.15488/xxxxx
URN:
https://nbn-resolving.org/urn:nbn:de:gbv:18302-aero2025-06-13.01
Associated URLs:
https://nbn-resolving.org/html/urn:nbn:de:gbv:18302-aero2025-06-13.01

Any further request may be directed to:
Prof. Dr.-Ing. Dieter Scholz, MSME
E-Mail see: http://www.ProfScholz.de

This work is part of:
Digital Library – Projects & Theses – Prof. Dr. Scholz
http://library.ProfScholz.de

Published by
Aircraft Design and Systems Group (AERO) Department
of Automotive and Aeronautical Engineering Hamburg
University of Applied Science

This report is deposited and archived:

- Deutsche Nationalbibliothek (https://www.dnb.de)
- Repository of Leibniz University Hannover (https://www.repo.uni-hannover.de)
- Internet Archive (https://archive.org),
  Item: https://archive.org/details/TextHasanovicSarikaya.pdf

This report has associated data published in Harvard Dataverse: https://doi.org/10.7910/DVN/4KYGVU

Abstract

Purpose – This study investigates NO_x emissions from the 50 most used commercial jet aircraft engines. The primary aim is to derive regression models to estimate NO_x emissions based on engine parameters.

Methodology – The analysis begins by determining the 50 most used engine families in passenger aviation, based on the World Airliner Census 2020 and aircraft delivery data from the major commercial aircraft manufacturers. NO_x emissions were obtained using the ICAO Engine Emissions Databank (EEDB). Emissions were analyzed for different flight phases from the ICAO Landing and Take-Off (LTO) Cycle (taxi, take-off, climb, and approach) and for cruise. For the cruise phase NO_x emissions were calculated a) with the Boeing Fuel Flow Method 2 (BFFM2) based on LTO NO_x and cruise fuel flow and b) with a method developed by the German Aerospace Center (DLR). Non-linear regression analysis was applied to estimate NO_x emissions based on one or two selected engine parameters. Separate models were developed for the full dataset and for 13 specific combustor technology subgroups.

Findings – NO_x emissions from aircraft contribute to local air pollution near airports and to global warming at cruise altitude. Legal limits for NO_x emissions are defined for the total LTO emissions per thrust as a function of Overall Pressure Ratio (OPR), with stricter standards introduced since 2004. The 50 selected engine families represent around 95 % of the global commercial jet fleet. NO_x emissions from the BFFM2 and the DLR method agree well ($R^2 = 0.99$). The most predictive engine parameters are OPR, thrust and fuel flow, while Bypass Ratio (BPR) has limited influence. Engine design is a trade-off. Low fuel burn requires higher OPR, which increases NO_x emissions. Some combustors can reduce NO_x but may lead to more soot emissions, causing denser contrails with more global warming potential. Combustor-specific regression significantly improves prediction accuracy. A model incorporating all combustor types yields a coefficient of determination of only $R^2 = 0.398$ and a Mean Absolute Percentage Error (MAPE) of only 62.5 %. In contrast, combustor-specific models are much better. E.g. a model for the Twin Annular Premixing Swirler (TAPS) II achieves $R^2 = 0.788$ and a MAPE of 12.7 %. This underlines the necessity of considering combustor technology in NO_x estimation.

Research Limitations – In this study, regression analysis was limited to a maximum number of two input parameters. However, more parameters seem not to lead to a substantially higher accuracy.

Practical Implications – The study provides equations for three NO_x emission cases: total emissions during the LTO cycle, emission index at take-off, and emission index during cruise. For each of these three cases and for each of the 13 investigated combustor technologies, one equation is proposed based on one engine parameter and a second equation based on the best combination of two engine parameters. This leads overall to 78 equations.

Social Implications – Easy to use equations make NO_x emission from passenger jet aircraft more accessible to a wider community of people to discuss the implications of aviation as a means of transport.

Originality – No other study seems to be available that offers such a simple way to predict NOx emissions form jet engines for aircraft design or aircraft operation while accounting for different combustor technologies.

DEPARTMENT OF AUTOMOTIVE AND AERONAUTICAL ENGINEERING

NOx Emissions of the 50 Most Used Engines for Passenger Aircraft

Task for a Project (Master studies)

Background

Nitrogen oxide is produced when nitrogen (N) and oxygen (O) are heated. NOx stands for any combination of N and O as explained here in detail. Inhalation of the pure NO and NO2 is rapidly fatal. Nitrogen oxides form by natural and technical combustion processes. Chemically bound nitrogen from fuels (such as kerosene) also reacts with oxygen during combustion to NOx. Elevated levels of nitrogen dioxide can cause damage to the human respiratory tract and can lead to asthma. NOx forms acid rain, smog (haze) and contributes to particulate matter and ozone. At higher altitudes NOx is a potent greenhouse gas. As such, NOx from aircraft lead to local air pollution near airports. NOx emitted at altitude in cruise flight contributes to global warming.

Task

The task of this project is to determine, list and compare the NOx emissions of the 50 most used engines in commercial passenger aircraft. The subtasks are:

- Provide short(!) background information to the task: What are NOx? How do aircraft produce NOx? How do NOx cause damage? How can NOx be reduced? What are the trade-offs in NOx reduction? What are legal NOx limits for aviation?
- Determine the 50 most used engines for passenger aircraft.
- Determine the NOx emissions from the selected aircraft engines: Landing and Take Off Cycle; Cruise.
- Produce statistics: How do NOx emissions compare to legal limits? How do NOx emission depend on other aircraft parameters? Estimate the relationships between parameters with regression analysis.
- Discuss your findings and draw conclusions.

The report has to be written in English based on German or international standards on report writing.

Table of Contents

List of Figures

List of Tables

List of Symbols

Symbols

δ_{amb}	Non-dimensional ambient OPR
δ_{total}	Non-dimensional stagnation OPR
θ_{amb}	Non-dimensional ambient temperature ratio
θ_{total}	Non-dimensional stagnation temperature ratio
τ	Temperature ratio used in vapor pressure model
ϕ	Relative humidity
ω	Specific humidity
π_{OPR}	Engine OPR
T_{TO}	Take-off thrust
$EI_{\text{NO}_\text{x},\text{TO}}$	Emission index of NO_x at take-off [g/kg fuel]
$NO_{x,\text{LTO}}$	NO_x emissions over the LTO cycle [g]
$NO_{x,\text{Cr}}$	Emission index of NO_x at cruise [g/kg fuel]
$m_{\text{f,LTO}}$	Total fuel mass burned during the LTO cycle [kg]
$\dot{m}_{\text{f,CO}}$	Fuel mass flow rate during climb-out [kg/s]
$\dot{m}_{\text{f,IDLE}}$	Fuel mass flow rate during idle [kg/s]
$\dot{m}_{\text{f,Cr}}$	Fuel mass flow rate during cruise [kg/s]

Indices

amb	Ambient (static)
f	Fuel
ff	Fuel (reference conditions)
ref	Reference conditions
total	Total (stagnation conditions)

List of Abbreviations

BC	Black Carbon
BFFM2	Boeing Fuel Flow Method 2
CAEP	Committee on Aviation Environmental Protection
CH_4	Methane
CO	Carbon Monoxide
CO_2	Carbon Dioxide
DLR	German Aerospace Center (Deutsches Zentrum für Luft- und Raumfahrt)
Dp/Foo	NO_x Emission Rate (g NO_x per kN thrust; ICAO metric)
EEDB	Engine Emissions Databank
EI	Emission Index (g of emission per kg of fuel)
$EINO_x$	Emission Index of NO_x
FOI	Swedish Defence Research Agency
HC	Hydrocarbons
ICAO	International Civil Aviation Organization
ISA	International Standard Atmosphere
ISG	Impacts and Science Group
LTO	Landing and Take-Off (cycle)
NO	Nitric Oxide
NO_2	Nitrogen Dioxide
NO_x	Nitrogen Oxides
O_3	Ozone
OC	Organic Carbon
OH	Hydroxyl Radical
OPR	Overall Pressure Ratio
$PM_{2.5}$	Particulate Matter < 2.5 µm
R&D	Research and Development
RQL	Rich-Quench-Lean (combustion principle)
SFC	Specific Fuel Consumption
SLE	Staged Low Emission
TALON	Technology for Advanced Low NO_x
DAC	Double Annular Combustor
HPC	High Pressure Compressor
HPT	High Pressure Turbine
LPT	Low Pressure Turbine
SAC	Single Annular Combustor
TAPS	Twin Annular Premixing Swirler
TI	Tech Insertion (advanced engine variant)

List of Definitions

CAEP

"The Committee on Aviation Environmental Protection (CAEP) is a technical committee of the ICAO Council established in 1983 (ICAO 2025)."

EEDB

"The ICAO Aircraft Engine Emissions Databank contains information on exhaust emissions of production aircraft engines, measured according to the procedures in ICAO Annex 16, Volume II (EASA 2025)."

Emission Index

"The mass of pollutant (CO, HC, NOx, nvPM mass or nvPM number), in grams, divided by the mass of fuel used in kilograms (EASA 2023)."

Fuel Flow Correlation Method

"A semi-empirical method for estimating NO_x emissions based on engine fuel flow data, used especially when detailed thermodynamic data are unavailable (Deidewig 1996)."

LTO Cycle (Landing and Take-Off Cycle)

"LTO cycle is defined by ICAO. It covers four modes of engine operation, namely idle, approach, climb out and take-off, each of which is associated with a specific engine thrust setting and a time in mode (EUROCONTROL 2025)."

1 Introduction

1.1 Motivation

Commercial aviation plays a critical role in global transportation, but it also contributes significantly to environmental degradation. While the focus has long been on carbon dioxide (CO_2) emissions, increasing attention is being directed toward nitrogen oxides (NO_x) due to their impact as both local air pollutants and indirect greenhouse gases. NO_x emissions from aircraft engines affect atmospheric chemistry by promoting ozone (O_3) formation in the troposphere and stratosphere, which affects climate change (Grewe 2002a, Pitari 2002).

Aviation-related NO_x emissions are of specific concern during the landing and take-off (LTO) cycle, when pollutants are released close to the ground and directly affect surrounding populations. According to recent studies at major international airports, including those in Los Angeles and Copenhagen, aircraft operations are a primary source of NO_x and particulate matter emissions, often exceeding those from road traffic in the local area (Shirmohammadi 2017, Winther 2015). These emissions contribute to higher $PM_{2.5}$ and O_3 levels, with well-documented health impacts including an increased risk of respiratory and cardiac diseases (Benosa 2018).

Furthermore, the emissions reported in certification databases, such as those from ICAO, often underestimate real-world emissions during idle and taxi phases. Empirical research at London Heathrow and Athens International Airport shows significant deviations between modelled and measured NO_x values, particularly due to variable engine operating conditions and ageing engines (Koudis 2017b, Synylo 2017). Considering the projected growth in air traffic and the increasingly stringent international emission standards, it is crucial to refine emission databases using high-resolution, engine-specific data. The accurate assessment of NO_x emissions, particularly in the LTO phase, is essential for supporting effective environmental regulations, local air quality management, and technological innovation in engine design.

This study aims to provide a comprehensive analysis of NO_x emissions from civil aviation, focusing on variations across aircraft types and operating conditions. Using updated empirical data and modelling approaches, the study will evaluate the real-world emission performance of widely used engines and identify potential measures for reducing emissions.

1.2 Title Terminology

NO_x

The term NO_x refers to the combined presence of nitric oxide (NO), "produced in the combustion of hydrocarbon fuels by oxidation of atmospheric nitrogen" and nitrogen dioxide (NO_2), "a toxic brown gas which contributes to the irritant properties of smog" (AGARD, 1980).

Emissions

The term *emissions* refers to “a substance discharged into the air, as by an internal combustion engine. Exhaust emissions contain pollutants” (Crocker 2005).

Most

The term *most* refers to “the largest in number or amount” (Oxford University Press 2023).

Used

The term *used* refers to something that “has already been put to the purpose it was intended for” (Cambridge University Press 2023).

Engines

The term *engine* refers to “any machine that converts energy in one form into another form suitable for the required use, e.g., heat to torque in a reciprocating engine” (AGARD 1980).

Passenger

A passenger can be defined as “a person who is travelling in a vehicle, or on a train or plane, but is not driving it, flying it, or working on it”. (Cambridge University Press 2025).

Aircraft

The term *aircraft* refers to “a machine that is able to travel through the air. Aeroplanes, gliders, balloons, airships, helicopters, etc., are all aircraft”(Crocker 2005).

1.3 Objectives

The primary objective of this study is to provide a comprehensive assessment of nitrogen oxides (NO_x) emissions associated with the most widely used passenger aircraft engines in commercial aviation. The specific goals of this work are as follows:

1. To provide background information on NO_x emissions, including their thermal formation mechanisms in aircraft gas turbines, the environmental and public health consequences,

technical mitigation strategies and related trade-offs, along with the existing international regulatory framework, particularly the emission standards set by ICAO.

2. To identify the 50 most used engines in passenger aircraft, based on current fleet data, in order to ensure that the analysis reflects the real-world impact of engine emissions on a global scale.

3. To quantify NO_x emissions during different phases of flight, specifically during the LTO cycle using certified ICAO data and during cruise flight using calculation methods validated in published scientific literature.

4. To conduct statistical analyses comparing measured and calculated NO_x values to existing regulatory limits, and to investigate correlations between NO_x emissions and aircraft-specific parameters such as engine thrust and overall Pressure Ratio (OPR).

5. To apply regression models to identify and quantify key variables influencing NO_x emissions.

6. To discuss the results in terms of their impact on future engine design, environmental regulations and areas of research that could help to reduce the environmental impact of aviation.

1.4 Previous Research

Over recent decades, extensive research has examined aircraft engine emissions of nitrogen oxides (NO_x) and their effects on atmospheric chemistry, human health, and climate. The *AERONOX project* in the 1990s was pivotal in showing that NO_x emissions at cruising altitudes significantly influence the upper troposphere and lower stratosphere by promoting ozone (O_3) formation, a short-lived climate forcer (Schumann 1997). Wasiuk (2016) quantified increases in NO_x and O_3 between 2005 and 2011, linking them to air quality and radiative forcing. Vedantham (1998) projected that rising air traffic will intensify these effects unless mitigated by technological or operational measures.

Several studies have assessed the local and regional air quality impacts of NO_x emissions at airports. Schürmann (2007) measured emission indices at Zurich Airport, revealing significant variability between engines and deviations from ICAO certification data. Similarly, Unal (2005) found that aircraft NO_x at Atlanta Airport contributed to local O_3 and $PM_{2.5}$ levels, particularly under stagnant conditions. Ekici (2022) evaluated Turkey's largest airline and found NO_x to be among the most economically harmful pollutants due to its role in forming secondary pollutants and affecting respiratory health. Stettler (2011) and Xu (2020) further showed that health impacts can extend far beyond airport boundaries, affecting urban populations tens of kilometers downwind.

Research has also focused on strategies to reduce NO_x emissions. Koudis (2017a) showed that

reduced thrust procedures at London Heathrow can lower take-off NO_x emissions by approximately 10.7 % ... 47.7 %, depending on engine type and aircraft mass. Technological developments include low-NO_x combustors, staged combustion, and lean-burn systems, though these often involve trade-offs such as increased weight, complexity, or reduced efficiency (Miller 2022). Higher overall pressure ratios (OPR), typical of more efficient engines, lead to increased combustion temperatures and thus higher thermal NO_x formation rates (Grewe 2002b). Consequently, efficient engines may comply with CO_2 targets while exceeding NO_x limits, or vice versa. Miller (2022) proposed a social cost framework to better account for these conflicting effects in future ICAO regulations.

For emission quantification, the aviation sector primarily relies on the ICAO Engine Emissions Databank (EEDB), which provides certified NO_x, CO, and HC values under standardized LTO conditions. However, studies such as Herndon (2004) and Klapmeyer (2012) have shown that certified values can deviate from actual emissions, especially during idling and take-off. To overcome this, empirical models based on fuel flow and engine parameters have been developed. Notable examples include the *Boeing Fuel Flow Method 2 (BFFM2)* and the *DLR fuel flow correlation method*, which use limited reference data (e.g. ICAO modes) to estimate emissions during cruise.

Previous student theses and projects at the University of Applied Sciences Hamburg have contributed to the development of methods for assessing the environmental impact of air travel. Velasco (2020), Hurtecant (2021), and Mattausch (2024) developed ecolabels and evaluation tools for aircraft, flights, and multimodal travel. The list of the 50 most used passenger aircraft, compiled by Kühn (2023), serves as the basis for identifying the corresponding engines. In addition, the engine fuel flow values during cruise were obtained from the work of Mattausch (2024), where they were calculated using the BFFM2 model.

Despite recent progress, there is still a lack of detailed emissions data that covers entire aircraft fleets and includes both LTO and cruise-phase emissions across different engine types. Most existing studies focus on single airports or regional fleets, which limits how well their results apply to a wider range of engines and flight phases. By focusing on the 50 most used passenger aircraft engines and analysing their NO_x emissions during both LTO and cruise, this study builds on the existing research while expanding it to cover engine-specific trends, emission correlations, and regulatory implications on a global scale. The approach combines existing knowledge from ICAO data, fuel flow models, and statistical analysis, thus providing a solid framework for evaluating NO_x emissions in modern civil aviation.

1.5 Structure of the Work

This study is structured into eight main sections, each building upon the previous one to provide a complete understanding of NO_x emissions from the most used engines in commercial passenger aviation.

The main body of this work contains the following sections:

Section 2 introduces the definition of NO_x emissions in aviation, providing a detailed explanation of their formation in aircraft engines, the environmental and health implications of NO_x, strategies for reducing such emissions, the associated trade-offs and an overview of the current legal emission limits.

Section 3 presents the methods for calculating NO_x emissions. It describes three existing methods: the p_3/T_3 method, which uses the pressure and temperature at the combustor inlet, and two fuel flow correlation methods developed by the German Aerospace Center (DLR) and Boeing.

Section 4 describes the process of identifying the 50 most used engines in passenger aviation. This selection is based on delivery data obtained from aircraft manufacturers.

Section 5 focuses on quantifying NO_x emissions for the selected engines. The analysis is divided into emissions emitted during the LTO cycle, which are calculated using ICAO-certified data, and emissions produced during cruise, which are calculated using the methods described in Section 3.

Section 6 contains a statistical analysis of the NO_x emission data. It explores relationships between emissions and aircraft parameters, such as thrust rating and OPR. Regression analyses are applied to identify and quantify significant correlations.

Appendix A includes selected plots based on available engine data. Limited or unrepresentative cases were excluded. The full dataset allows further analysis.

2 Fundamentals

2.1 Definition and Characteristics of NO_x

Nitrogen oxides, often referred to as NO_x, are a group of chemically reactive gases composed of nitrogen and oxygen. The two most common forms are nitric oxide (NO) and nitrogen dioxide (NO_2). These are formed mainly through high-temperature combustion processes, such as those occurring in jet engine turbines. The chemical behavior of NO_x is complex: while NO itself is relatively stable at low concentrations, it oxidises rapidly in the atmosphere to form NO_2, which is far more toxic and plays a key role in atmospheric processes. NO_x formation in aircraft engines is dominated by what is known as thermal NO_x formation. This process occurs when atmospheric nitrogen and oxygen combine at high temperatures, typically above 1800 K. The rate of NO_x formation increases exponentially with temperature, making it a key issue in gas turbine engines that operate under high thermal loads to maximize efficiency (Birch 2000, Miller 2022).

The social and environmental impacts of NO_x emissions become particularly clear when considering the distribution of fuel production costs, climate impacts and air quality damages across engine designs. As shown in Figure 2.1, the relative contribution of air quality damage increases at higher OPR, becoming the dominant component of social cost as engine OPR increases. This highlights the trade-offs faced in the design of modern high-efficiency engines.

A unique feature of NO_x formation in aviation is its varying behaviour during different phases of flight. During high-thrust conditions, such as take-off and climb, NO forms the majority of NO_x, often accounting for more than 90 % of total emissions. At lower thrust settings, such as taxiing or idling, NO_2 becomes more dominant, sometimes making up as much as 98 % of NOx emissions (Stettler 2011). From an environmental and health perspective, NO_x plays a dual role. Near the ground, it contributes to the formation of ozone (O_3) and particulate matter ($PM_{2.5}$), both of which are harmful to human health. At cruising altitudes, NO_x affects atmospheric chemistry by changing the ratio of greenhouse gases, which contributes to ozone formation (a warming effect) and methane reduction (a cooling effect). This influences radiative forcing and climate change (Miller 2022, Yu 2021). Despite accounting for only an estimated 1.5 % ... 2 % of total global NO_x emissions, emissions from aviation are of particular concern due to their altitude-specific effects and the increasing amount of air traffic. These emissions are released directly into sensitive layers of the atmosphere, where they have a much greater impact than ground-level emissions (Tsilingiridis 2008).

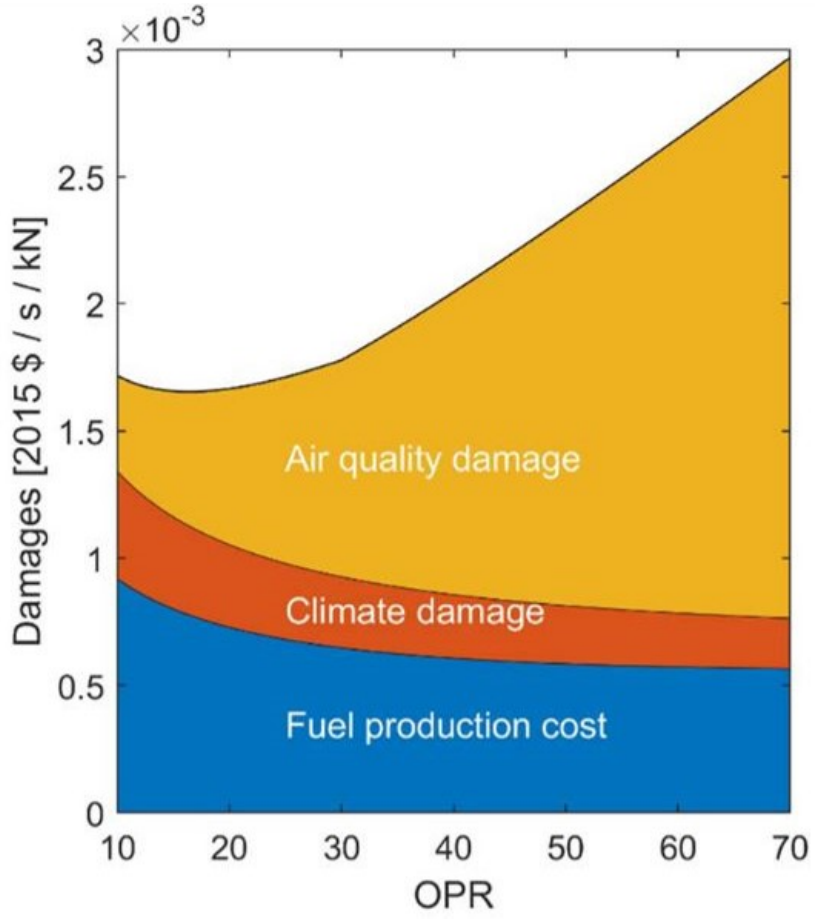

Figure 2.1: Social cost analysis broken into marginal production cost of fuel, climate damage, and air quality damage using the mean of the Monte Carlo runs (Miller 2022).

Figure 2.2 illustrates the distribution of emissions over the different phases of the LTO cycle for several pollutants, further differentiated by chemical composition into organic carbon (OC), black carbon (BC), and sulfate. In particular, NO_x and $PM_{2.5}$ are emitted primarily during high-thrust phases such as take-off and climb, while CO and HC are emitted primarily during low-thrust phases such as taxiing and idling. CO_2 emissions closely follow the thrust profile due to their proportionality to fuel flow. These results highlight the complex trade-offs in emission reduction strategies at airports. For example, while single-engine taxiing can help reduce CO, HC, and CO_2 emissions, it has little effect on NO_x or $PM_{2.5}$. In addition, atmospheric conditions such as mixing height introduce additional variability in emission estimates, especially for CO_2, SO_x, NO_x, and $PM_{2.5}$, while CO and HC remain largely unaffected.

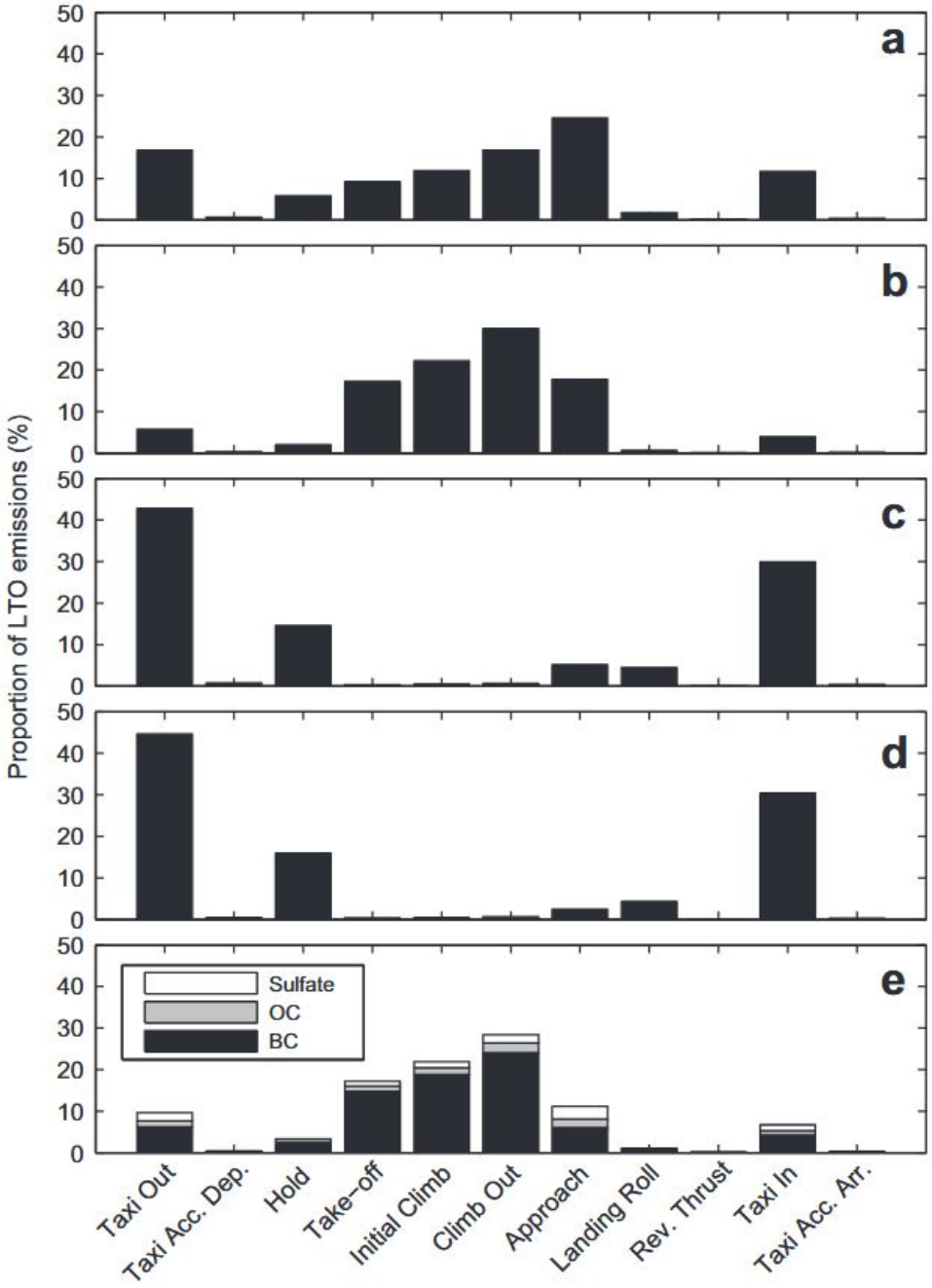

Figure 2.2: Relative proportion of emissions attributable to each phase of the LTO for (a) CO_2, (b) NO_x, (c) CO, (d) HC, and (e) $PM_{2.5}$, differentiated by chemical composition: organic carbon (OC), black carbon (BC), and sulfate (Stettler 2011).

The importance of NO_x in aviation is further underscored by its role as a regulatory focus. Unlike other pollutants such as CO_2 or SO_2, NO_x emissions are closely related to engine design and combustion parameters. Therefore, understanding the characteristics of NO_x is essential for developing both technological and operational strategies to reduce emissions.

2.2 Formation of NO_x in Aircraft Engines

The formation of nitrogen oxides (NO_x) in aircraft engines is primarily controlled by thermodynamic and chemical conditions within the combustion chamber. Modern aircraft engines are designed to operate at very high pressures and temperatures to maximize thermal efficiency and minimize fuel consumption. However, these same conditions contribute to the formation of NO_x, making it one of the most challenging aviation emissions to mitigate (Birch 2000, Miller 2022).

There are three primary mechanisms through which NO_x is formed in combustion processes: thermal NO_x, prompt NO_x, and fuel-bound NO_x. Of these, thermal NO_x is the most relevant in gas turbine engines used in aviation.

- **Thermal NO_x** is generated through the high-temperature oxidation of atmospheric nitrogen in the combustion air. This process becomes important at flame temperatures above 1800 K, which are common in the high-pressure turbines of modern jet engines. The reaction rate is exponentially related to temperature, meaning even slight increases in combustion temperature can result in substantial increases in NO_x production (Miller 2022).

- **Prompt NO_x** is formed when hydrocarbon radicals react with nitrogen at the flame front. While it usually contributes little to total NO_x emissions from aircraft, its impact can be significant in certain conditions, especially in fuel-rich combustion areas (Herndon 2004).

- **Fuel-bound NO_x** is produced when nitrogen, which is chemically bound in the fuel, reacts with oxygen during combustion. In aviation kerosene (Jet A-1), the nitrogen concentration is relatively low, making this process less impactful than thermal NO_x (Stettler 2011).

Figure 2.3 illustrates the relative contributions of these three mechanisms as a function of combustion temperature. It is evident that thermal NO_x becomes the dominant source at temperatures above about 1850 K due to its exponential dependence on temperature, while prompt and fuel-bound NO_x remain comparatively minor over the entire range.

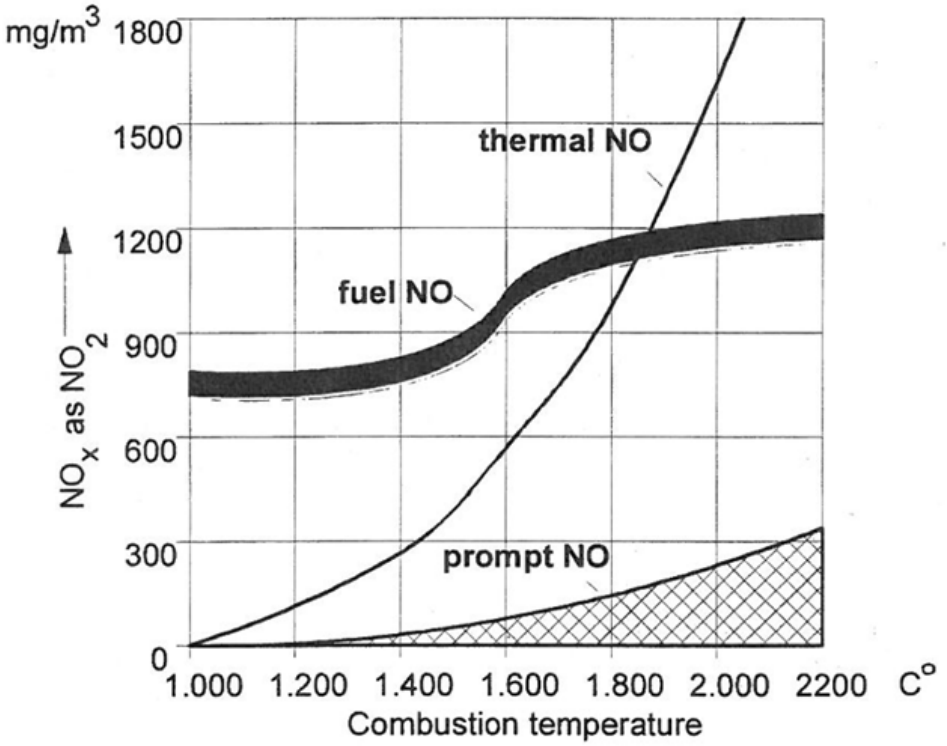

Figure 2.3: Influence of combustion temperature on the formation of thermal, prompt, and fuel-bound NO_x.(Technical Secretariat of the TFTEI 2023)

NO_x formation in aircraft engines is not consistent throughout the different phases of a flight. For emissions certification, ICAO divides the engine operating cycle into four modes: idle, approach, climb-out and take-off. Each mode is associated with different engine power settings, residence times, and atmospheric conditions, all of which influence NO_x production. The highest NO_x emissions occur during the take-off and climb-out phases due to the high thrust settings and elevated combustion temperatures. In comparison, the idle and approach phases generate relatively low NO_x emissions but higher emissions of other pollutants such as CO and unburned hydrocarbons (Klapmeyer 2012, Chilongola 2019). During cruise, although it is not part of the LTO cycle, NO_x continues to be produced in high quantities and has a notable impact on atmospheric chemistry due to the altitude at which emissions occur (Schumann 1997).

Furthermore, engine design has an impact on NO_x formation. The OPR of a jet engine is directly correlated with NO_x production. Engines with higher OPRs achieve greater thermodynamic efficiency, but also tend to produce more NO_x. This has led to a design trade-off between reducing CO_2 emissions by improving efficiency and increasing NO_x emissions, which is a core challenge in sustainable aviation engineering (Miller 2022). Figure 2.4 illustrates this trade-off by showing how specific fuel consumption (SFC) decreases with increasing OPR, while the NO_x emissions index increases. As engine efficiency improves, NO_x formation rises sharply unless mitigated by advanced combustor technologies. The dotted lines indicate the potential reductions in NO_x emissions that could be achieved through such improvements, highlighting the importance of combustion innovation in meeting efficiency and emissions goals.

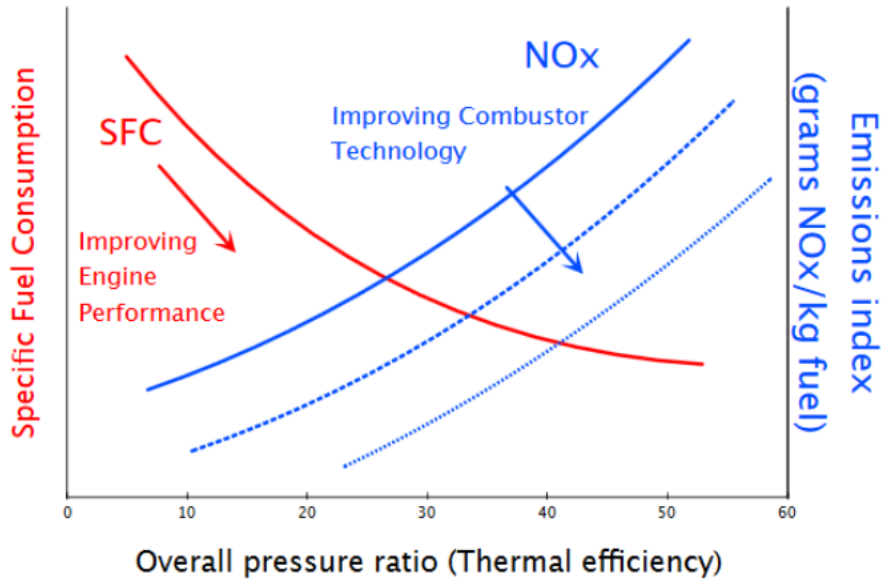

Figure 2.4: Relationship between OPR, specific fuel consumption (SFC), and NO_x emissions index (Mazur 2017).

To manage NO_x emissions, engine manufacturers have introduced technologies such as staged combustion chambers, lean-burn designs and improved fuel-air mixing techniques. These innovations aim to control flame temperature and reduce the residence time of gases in high-temperature zones, therefore reducing NO_x formation without any loss of performance (Birch 2000).

2.3 Environmental and Health Impacts of NO_x

NO_x emitted from aircraft engines have significant environmental and health impacts. The altitude and geographic distribution of NO_x emissions greatly increases the impact they have on atmospheric chemistry and public health (Tsilingiridis 2008). At ground level, NO_x emissions contribute to the formation of tropospheric ozone (O_3) and particulate matter ($PM_{2.5}$). Both of these are associated with negative health effects. NO_2, a primary component of NO_x, is known to cause airway inflammation, aggravate asthma, and reduce lung function, especially in vulnerable populations such as children and the elderly (Winther 2015). Residents living near major airports, such as Los Angeles International Airport (LAX) and London Heathrow, are exposed to higher concentrations of these pollutants compared to urban traffic areas (Shirmohammadi 2017, Koudis 2017a). Such exposure is associated with an increased risk of cardiovascular disease, respiratory disease and premature mortality (Hertel 2013). Recent assessments show that cruise emissions, which account for more than 90 % of aviation NO_x, can significantly affect ground-level air quality by contributing to background O_3 and $PM_{2.5}$ levels. In fact, cruise emissions may dominate aviation-induced surface particulate concentrations globally. Increases of 0.14 ... 0.4 % are expected in high-traffic regions, with cruise emissions accounting for a large proportion of aviation-related cases of premature mortality (Miake-Lye 2022).

In the upper troposphere, NO_x emissions have a different effect. They contribute to the formation of ozone, a short-lived greenhouse gas that warms the atmosphere, while simultaneously

breaking down methane (CH_4), a long-lived greenhouse gas, resulting in a net effect that is complex and regionally dependent. Figure 2.5 illustrates these atmospheric interactions. Following additional NO_x emissions, a short-lived increase in ozone is observed (Figure 2.5a), which decays within a few months (Figure 2.5b). This is accompanied by a longer-term decrease in CH_4 concentrations (Figure 2.5c) due to increased OH levels. Since methane is also an ozone precursor, its reduction eventually results in a slight negative ozone anomaly, which cancels out the initial increase. The scientific consensus, supported by the ICAO Impacts and Science Group (ISG), is that NO_x emissions from aviation have resulted in a net warming effect on climate over the period 1940–2018 (Stevenson 2009, Lee 2021, Miake-Lye 2022).

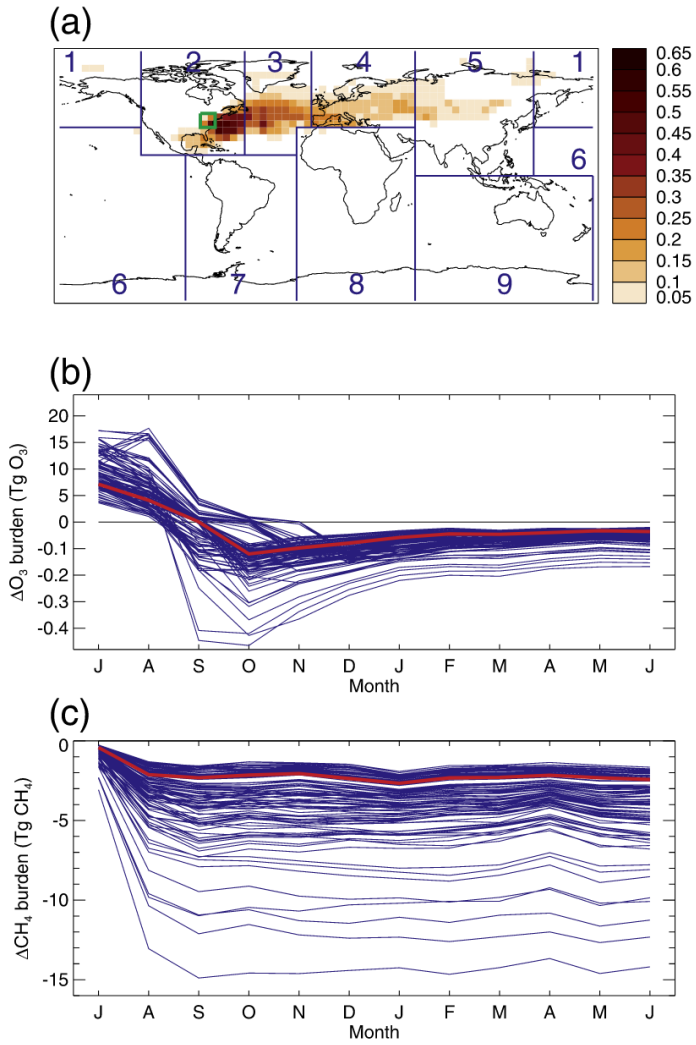

Figure 2.5: (a) Monthly mean change in ozone (ppb) at 250 hPa for July due to extra aircraft NO_x emissions over eastern North America. (b) Change in global tropospheric ozone burden, and (c) change in global methane burden over 12 months. All values are normalized to a 1 Tg(NO_2) pulse (Stevenson 2009).

In addition to the environmental and health consequences, NO_x emissions also have major economic costs. These costs result from health care expenses, reduced labour productivity, crop damage and ecosystem degradation. Recent studies have introduced the concept of the "social cost" of NO_x, which attempts to quantify these impacts in economic terms. For example, Miller (2022) shows that air quality damage due to NO_x can account for more than 60 % of the total social cost of aircraft emissions, often surpassing the direct climate impact of CO_2. These findings highlight the importance of addressing NO_x not only from a technical and regulatory perspective, but also from a broader environmental justice and economic perspective (see Figure 2.1).

Several certified commercial engines already incorporate low-NO_x combustors, with the Rich-Quench-Lean (RQL) design being one of the most common architectures. One example is the General Electric CF6-80E1A4 engine, available in standard and low-emissions configurations. Both versions use an RQL combustor and have the same thermodynamic design characteristics, including OPR, bypass ratio, and rated thrust. However, the low-emissions variant has been optimized to reduce NOx emission values across multiple operating points without altering the propulsion system's overall architecture. Table 2.1 summarizes the key emission characteristics for both configurations. The low-emissions version shows substantial reductions in EI_{NOx}, with 27 % and 22 % lower values at take-off and climb-out, respectively. Interestingly, the approach condition exhibits a slightly higher EI_{NOx}, likely due to altered air-fuel mixing or flame temperature control strategies. Cruise emissions drop by approximately 35 % (from 13.90 to 9.05 g/kg), demonstrating the effectiveness of targeted combustor modifications under realistic flight conditions.

Table 2.1: Comparison of emission characteristics for GE CF6-80E1A4 variants (standard vs. low-emissions) from ICAO Database

Parameter	**Standard**	**Low Emissions**
Combustor Type	RQL	RQL
OPR	34.5	34.5
Rated Thrust (kN)	297.44	297.44
$EI_{NOx,\ T/O}$ (g/kg)	43.15	31.28
$EI_{NOx,\ C/O}$ (g/kg)	30.30	23.54
$EI_{NOx,\ App}$ (g/kg)	10.13	12.66
$EI_{NOx,\ Idle}$ (g/kg)	4.62	4.77
$EI_{NOx,\ Cruise}$ (DLR) (g/kg)	13.90	9.05
NO_x Total Mass (LTO) (g)	18,055	15,027
NO_x Dp/Foo Characteristic (g/kN)	60.69	50.52
Fuel Flow T/O (kg/s)	2.933	2.933
Fuel Flow C/O (kg/s)	2.367	2.367
Fuel Flow App (kg/s)	0.759	0.759
Fuel Flow Idle (kg/s)	0.250	0.250
Fuel Flow Cruise (kg/s)	1.015	1.015
Fuel LTO Cycle (kg)	963	963

2.4 Strategies for NO_x Reduction and Trade-Offs

Reducing NO_x emissions from aircraft engines has become a key objective of environmental and public health policy. A variety of strategies have been developed or proposed to achieve this goal, ranging from technological improvements in engine design to operational changes at airports. However, each reduction strategy comes with trade-offs, particularly regarding fuel efficiency, CO_2 emissions and cost. One of the most significant technological approaches is the development of low-NO_x combustors. These include staged combustion systems, where combustion occurs in separate zones optimized for different power settings, and lean-burn technologies that ensure more complete combustion at lower flame temperatures (Birch 2000). By controlling the peak flame temperature and improving the air-fuel mixing process, these technologies can substantially reduce thermal NO_x formation. The Rich-Quench-Lean (RQL) approach achieves this by initially burning in a rich zone with low oxygen concentrations, followed by a rapid cooling process involving the addition of air, which forms a lean mixture that burns at reduced temperatures. However, such systems often increase complexity, cost and maintenance requirements and may lead to lower combustion efficiency at certain operating points. According to Moran (2007), fast quenching and uniform fuel-air premixing are essential to avoid stoichiometric pockets where NO_x formation is most intense. A newly emerging trade-off has been identified between reducing NO_x and increasing soot emissions. While low-NO_x combustors reduce ozone-related climate impacts, they tend to generate higher levels of soot (non-volatile particulate matter, nvPM), especially under rich or staged combustion conditions (Scholz 2023). This soot facilitates the formation of persistent contrails that significantly contribute to radiative forcing, particularly during night-time or under cold and humid atmospheric conditions (Theo 2022). Thus, reducing NO_x may inadvertently increase overall climate impact due to enhanced contrail effects. For example, a single aircraft type using such engines accounted for only 2.4 % of all flights, yet was responsible for 18 % of flights with strongly warming contrails. Overall, nearly half of these contrails that warm the atmosphere came from aircraft with this type of engine. These findings demonstrate that designing environmentally friendly aircraft engines involves balancing conflicting objectives. The classic trade-off between fuel efficiency and NO_x reduction is now compounded by a second dilemma, as reducing NO_x through advanced combustors can lead to increased soot emissions and thus enhance climate impact through contrail formation. This underlines the need to evaluate propulsion systems not only by their isolated emissions, but also by their integrated climate effect, including CO_2, NO_x, nvPM, and contrails.

Lean-staged combustion is an alternative technology that reduces flame temperature through a lean fuel-air mixture. This can theoretically result in NO_x reductions at high power, especially with complete vaporisation and uniform premixing of the fuel. Challenges include ensuring flame stability at low power through a dedicated pilot zone, managing dynamic pressures and avoiding fuel coking and pre-ignition (Moran 2007). While industrial gas turbines have demonstrated over 90 % NO_x reduction with lean-staged combustors, translating such performance to aviation involves overcoming constraints such as weight, size, acceleration profiles, and airworthiness certification. Several certified aircraft engines already incorporate RQL-based combustors, such as TALON I and II (PW), LEC (GE), and the Phase 5 combustor (RR), showing improved emission control without compromising reliability (Moran 2007).

Figure 2.6 illustrates the NO_x formation characteristics of both RQL and lean-staged combus-

tion systems as a function of fuel-air ratio. It highlights how both approaches shift operation away from the stoichiometric region, where NO_x formation peaks, toward regimes with significantly lower NO_x production, thereby indicating their potential for emission reduction.

Another promising approach is the use of alternative aviation fuels, particularly synthetic fuels and biofuels with low nitrogen content. These fuels can reduce overall NO_x emissions by 5–10 %, depending on their composition and the combustion characteristics of the engine (Benosa 2018). Additionally, they emit much lower levels of particulate matter and sulfur oxides. However, alternative fuels are currently limited by production capacity, high costs and logistical challenges related to global fuel infrastructure. Operational strategies also offer great potential for NO_x reduction. Technologies such as single-engine taxiing, reduced thrust take-off and optimized climb procedures can lead to measurable emissions reductions. For instance, reduced thrust take-off procedures can lower NO_x emissions during the most intense phase of ground-level operation by up to 47 %, depending on aircraft type and engine configuration (Koudis 2017b). Nevertheless, these measures may slightly increase fuel consumption or require changes in pilot procedures and airport scheduling.

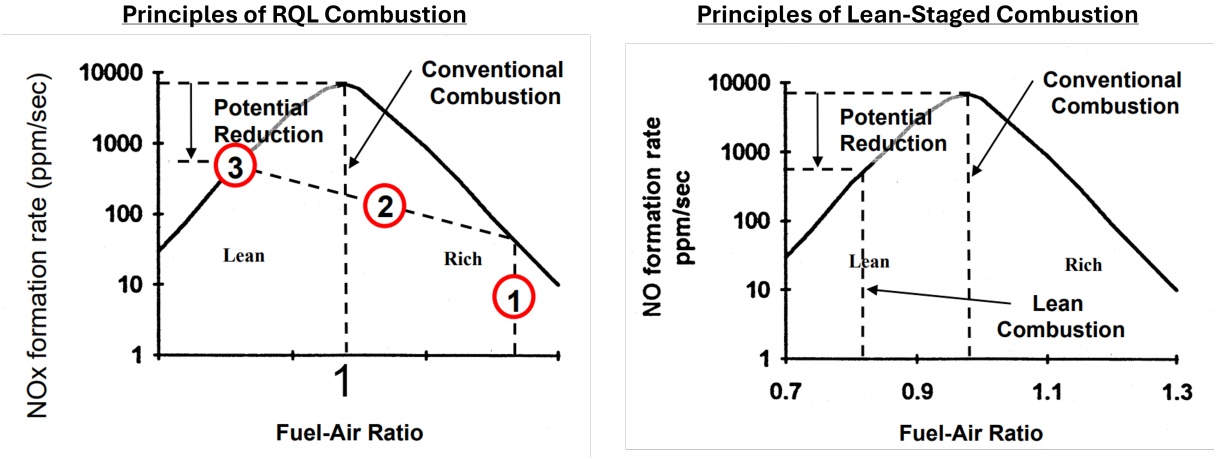

Figure 2.6: Comparison of NO_x formation principles in RQL (Rich-Quench-Lean) and Lean-Staged combustion systems (Moran 2007).

At a regulatory level, ICAO has implemented increasingly stringent NO_x standards over the past decades. These standards define allowable NO_x emissions as a function of the engine's rated thrust and OPR, reflecting the thermodynamic efficiency of the engine (Miller 2022). However, this approach inherently creates a trade-off: higher OPRs improve fuel efficiency and reduce CO_2 emissions, but also increase NO_x formation due to higher combustion temperatures. This is evident in recent certification data, where newer engines with OPRs up to 42.9 still meet CAEP/6 NO_x limits, albeit with limited margin (Moran 2007). As a result, engine manufacturers must balance between compliance with NO_x standards and the pursuit of better fuel economy. This NO_x–CO_2 trade-off illustrates a fundamental challenge in sustainable aviation design. Reducing one type of emission often increases another, unless innovative technologies or systems-level optimizations are introduced. For example, Miller et al. Miller (2022) suggest evaluating engine performance based on a combined social cost of fuel use, air quality impact, and climate damage to ensure more balanced environmental outcomes. Moran (2007) similarly highlights that reducing combustor volume or enriching fuel in early stages helps reduce NO_x, but can lead to increased CO and HC emissions or operational instabilities at altitude.

In summary, there is no one-size-fits-all solution to NO_x reduction in aviation. A combination of cleaner combustion technologies, alternative fuels, improved operational practices and adaptive regulatory frameworks will be needed to meaningfully reduce NO_x emissions while managing the associated trade-offs with fuel efficiency and climate goals. The transition from research and development (R&D) to product certification, as demonstrated by the 25-year development of staged low emission (SLE) combustors, highlights the importance of long-term investment, thorough testing procedures and consistent policy support at national and international levels (Moran 2007).

2.5 Legal NO_x Limits in Aviation

The regulation of nitrogen oxides (NO_x) emissions from commercial aircraft engines is primarily governed by the International Civil Aviation Organization (ICAO) through its Committee on Aviation Environmental Protection (CAEP). ICAO standards define legally binding emission limits for newly certified and newly manufactured turbofan engines, with the goal of reducing the environmental and health impacts of aviation-related air pollution on a global scale (Miller 2022).

ICAO regulates NO_x emissions based on performance during the LTO cycle, which includes the taxi/idle, take-off, climb-out and approach modes. The NO_x limits are defined as a function of two critical engine design parameters: the rated take-off thrust and the OPR of the engine. This approach reflects the fact that engines with higher thermodynamic efficiency (i.e., higher OPR) tend to produce more NO_x due to elevated combustion temperatures (Birch 2000).

Over time, ICAO has introduced increasingly stringent NO_x emission limits through a series of CAEP standards: CAEP/2, CAEP/4, CAEP/6, and CAEP/8. Each new standard modifies the slope and intercept of the regulatory function that defines the maximum allowable NO_x emissions per unit of thrust. Starting with CAEP/4, a bifurcated regulation was introduced that applies different equations to engines with an OPR above or below 30, in order to better address variations in engine architecture. These standards are visualized as limit lines in performance graphs and provide a benchmark for assessing engine compliance (ICAO 2014).

In addition to the mandatory certification thresholds, ICAO has defined “technology goals” that are intended to encourage long-term innovation in combustor and engine design. These goals, introduced in 2010, aim to support the development of ultra-low NO_x technologies that go beyond what is required by law. The two main targets are:

- A 45 % reduction in NO_x emissions from CAEP/6 levels by 2016, and
- A 60 % reduction from CAEP/6 levels by 2026.

Although these goals are not legally binding, they serve as strategic indicators for the industry and research community, guiding the design of future engine generations and supporting ICAO’s broader climate and air quality strategies.

It is important to differentiate between legal standards and technological goals when evaluating the environmental performance of aircraft engines. While many engines on the market today meet the certification limits set out in CAEP/8, only a few approach the aspirational targets set for 2026. This distinction is key to assessing regulatory compliance and the potential for reducing emissions further.

Moreover, the current regulatory framework inherently involves trade-offs. Since NO_2 limits are not scaled with OPR, more efficient engines are permitted higher NO_2 emissions. While this incentivises fuel efficiency and CO_2 reduction, it can lead to increased air quality impacts unless additional technologies are introduced (Miller 2022). New regulatory proposals aim to address this issue by introducing alternative formulations that balance the total environmental cost of different engine types.

As shown in Figure 2.7, the relationship between engine OPR and NO_x emissions (expressed as Dp/Foo, i.e., NO_x emission rate in grams of NO_x per kilonewton of rated thrust, as defined by the ICAO metric) reveals a clear historical trend toward improved emission performance. However, the figure also illustrates the increasing difficulty of achieving the mid-term and long-term ICAO CAEP targets, particularly for high-performance engines.

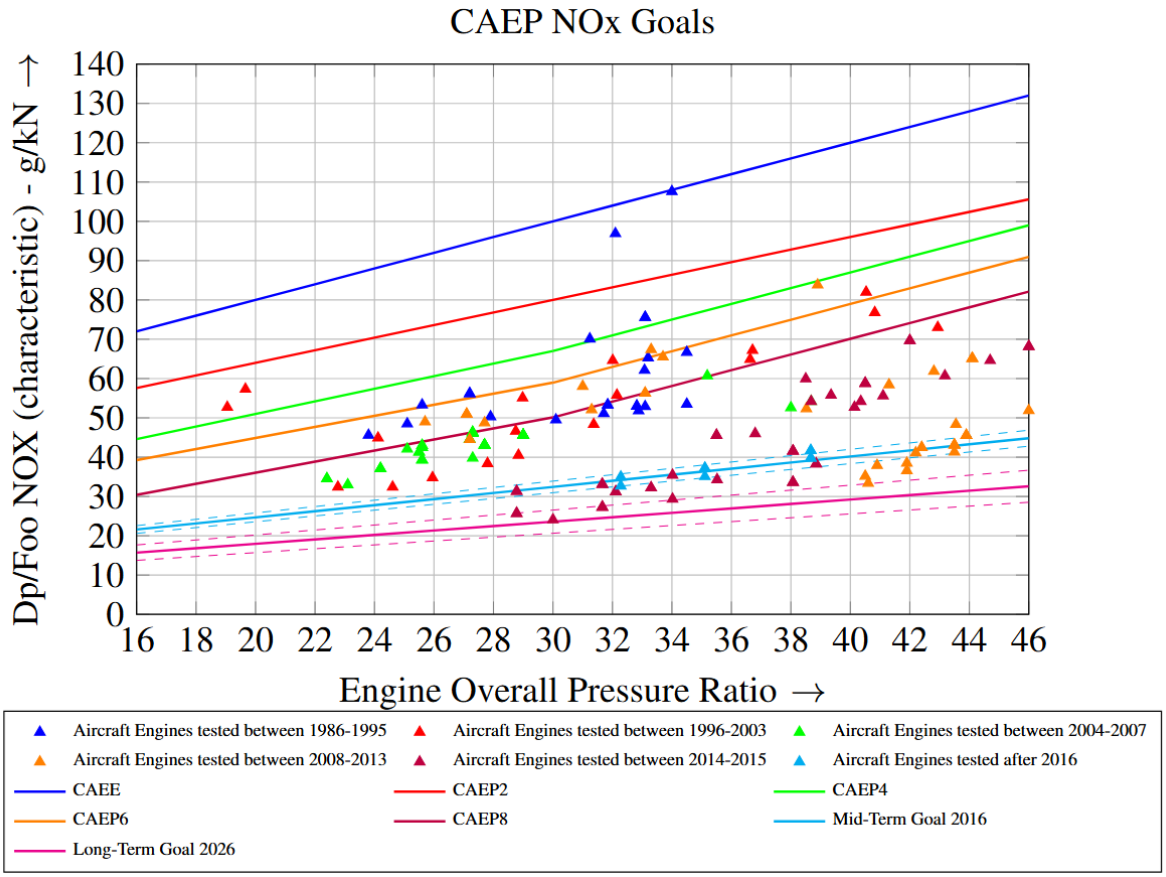

Figure 2.7: Comparison of NOx Emission Limits with Selected Passenger Aircraft Engines

In conclusion, ICAO's NO_x standards have become more stringent over time, but still reflect a compromise between efficiency and emissions. Both the regulatory limits and the long-term technology goals provide crucial reference points for evaluating the performance of aircraft engines and for guiding future innovation in sustainable aviation.

3 Methods for NO_x Emission Calculation

In order to simplify the calculation of in-flight emissions, semi-empirical fuel flow correlation methods have been developed by DLR (Deidewig 1996) and Boeing (Baughcum 1996, DuBois 2006). These methods are based on the assumption that the emission index (EI), expressed in grams of emissions per kilogram of fuel, can be estimated using engine fuel flow (W_{fuel}), ambient atmospheric conditions and flight speed.

To calculate in-flight emission indices using only fuel flow data, the method involves the following three steps, as illustrated in Figure 3.1:

1. Conversion of in-flight fuel flow (W_{fuel}) to reference conditions ($W_{\text{fuel,ref}}$).

2. Determination of the emission index at reference conditions (EI_{ref}) as a function of $W_{\text{fuel,ref}}$ using empirically derived correlations.

3. Conversion of EI_{ref} back to in-flight conditions to obtain EI.

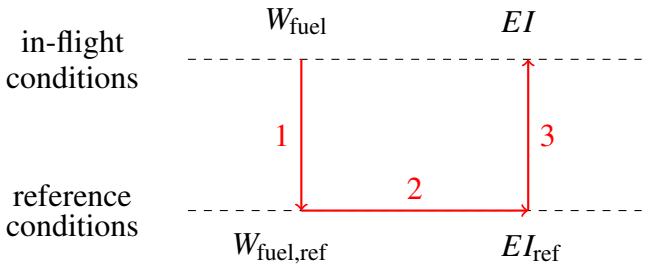

Figure 3.1: Principle of fuel flow methods

The p_3/T_3 approach, which is widely applied by engine manufacturers, estimates emissions based on the combustor inlet pressure (p_3) and temperature (T_3) (Schumann 1995). While this method offers increased accuracy, it requires access to internal engine parameters that are typically not publicly available, limiting its use outside of engine development environments (Brink 2020). Therefore, this method is only briefly mentioned in this work and is not further analyzed.

3.1 p_3/T_3 Approach

One widely recognized method for estimating NO_x emissions from aircraft engines, particularly during cruise, is the so-called p_3/T_3 approach. This method is based on the thermodynamic parameters at the entrance to the combustor, namely the total pressure and total temperature, which critically influence the formation of NO_x due to their direct relationship with flame temperature and reaction kinetics. The p_3/T_3 approach rests on the theoretical foundation that NO_x formation in gas turbine engines is primarily governed by thermal mechanisms, especially the Zeldovich mechanism. These mechanisms exhibit strong temperature dependence, where NO_x produc-

tion rates increase exponentially with rising combustor inlet temperature. As these parameters cannot be measured directly during flight, they are usually estimated using engine performance models or extrapolated from detailed engine design parameters (Harlass 2024).

The estimation of NO_x emissions using this method involves correlating the NO_x emission index (EI_{NO_x}) with normalized values of combustor inlet pressure and temperature. Empirical or semi-empirical equations derived from combustion rig experiments and engine test data are used to predict emissions under various operating conditions, including cruise. While the p_3/T_3 approach is valued for its physical accuracy and suitability for modeling cruise-phase emissions, its practical application is limited by the availability of accurate combustor inlet data. The relevant pressure and temperature values are often proprietary and not published in open literature for most commercial engine types (Brink 2020).

This method is not applied in the present analysis due to the lack of accessible and reliable data for the engines considered in this study. Instead, alternative estimation methods relying on publicly available fuel flow and performance parameters have been employed to ensure consistency and replicability.

3.2 Fuel Flow Correlation Method (DLR)

The fuel flow correlation method developed by the German Aerospace Center (DLR) offers a practical and data-driven approach for estimating NO_x emissions from aircraft engines under in-flight conditions. Unlike methods that require detailed internal engine parameters, the DLR approach uses publicly available engine certification data, specifically the correlation between fuel flow and the NO_x emission index ($EINO_x$), to extrapolate emissions for cruise and other non-standard flight phases. The methodology, including all relevant equations, is based on the work of Schaefer (2013).

The method begins by constructing a reference function that relates the NO_x emission index to the engine fuel flow rate under sea-level static conditions in the International Standard Atmosphere (ISA). This reference is based on four standardised data points from the ICAO and FOI emissions databases. These points correspond to typical thrust settings at different operating conditions: idle (7 % thrust), approach (30 %), climb-out (85 %), and take-off (100 %). A linear fit through these four points forms the basis for estimating $EINO_x$ under reference conditions.

To apply the method to actual flight conditions, a three-step procedure is used:

Step 1 involves correcting the actual engine fuel flow w_{fuel} (in kg/s) to ISA reference conditions. This is achieved using the equation:

$$w_{fuel,ref} = \frac{w_{fuel}}{\delta_{total} \cdot \sqrt{\theta_{total}}} \tag{3.1}$$

where the non-dimensional atmospheric correction factors are defined as

$$\delta_{total} = \frac{p_{total}}{101325Pa} \quad , \tag{3.2}$$

$$\theta_{total} = \frac{T_{total}}{288.15K} \tag{3.3}$$

and the stagnation (total) pressure and temperature are calculated from the ambient conditions and the flight Mach number M via:

$$p_{total} = p_{amb} \cdot \left(1 + 0.2 \cdot M^2\right)^{3.5} \tag{3.4}$$

and

$$T_{total} = T_{amb} \cdot \left(1 + 0.2 \cdot M^2\right) \quad . \tag{3.5}$$

It is important to note that the calculated fuel flow refers to a single engine, so the total aircraft fuel flow must be divided by the number of engines before applying the correction.

Step 2 uses the reduced fuel flow $w_{fuel,ref}$ to determine the corresponding NO_x emission index $EI_{NOx,ref}$, under reference conditions by interpolating the linear reference function. This function encapsulates the certified relationship between fuel flow and NO_x emissions for each engine type.

Step 3 adjusts the reference emission index for the actual atmospheric conditions at cruise altitude. This is achieved with the following correction:

$$EI_{NOx} = EI_{NOx,ref} \cdot \delta_{total}^{0.4} \cdot \theta_{total}^{3} \cdot e^{H} \quad , \tag{3.6}$$

where H is a humidity correction factor dependent on the specific humidity , calculated as:

$$H = -19.0 \cdot (\omega - 0.00634) \quad , \tag{3.7}$$

$$\omega = 10^{-3} \cdot e^{-0.0001426(h-12900)} \quad , \tag{3.8}$$

with h denoting altitude in feet. The exponential term accounts for the non-linear influence of water vapor on NO_x formation, which tends to be lower in dry, high-altitude conditions.

3.3 Fuel Flow Correlation Method (Boeing)

Boeing's Fuel Flow Method 2 (BFFM2) offers a comprehensive and empirically grounded approach for estimating gaseous emissions from aircraft engines under in-flight conditions. Unlike simpler estimation models, BFFM2 enables the calculation not only of NO_x emission indices ($EINO_x$), but also of carbon monoxide (CO) and unburned hydrocarbons (HC), based on in-flight performance parameters. This method has been referenced in U.S. aviation literature and aligns closely with ICAO certification data structures, although certain unit conventions differ and require standardization to SI units for scientific use.The methodological foundations, including the relevant equations, are also based on the work of Schaefer (2013).

Step 1 of the Boeing method mirrors the logic of the DLR approach by reducing the actual engine fuel flow W_f (in kg/s) to reference conditions, resulting in the fuel flow factor W_{ff}:

$$W_{ff} = \frac{W_f}{\delta_{amb}} \cdot \theta_{amb}^{3.8} \cdot e^{0.2 \cdot M^2} \quad , \tag{3.9}$$

where the non-dimensional ambient pressure and temperature ratios are given by:

$$\delta_{amb} = \frac{p_{amb}}{101325Pa} \quad , \tag{3.10}$$

$$\theta_{amb} = \frac{T_{amb}}{288.15K} \quad . \tag{3.11}$$

This correction accounts for ambient atmospheric conditions and Mach number effects at the current flight point.

Step 2 introduces a key modification relative to the DLR method: Boeing includes an airframe correction factor r, applied to each ICAO/FOI certification data point (see Table 3.1). This correction considers installation effects, especially bleed air extraction, and adjusts the reference fuel flow values before constructing the $EINO_x$ vs. fuel flow correlation. The reference function is then defined as a piecewise linear relationship in a log-log coordinate system, based on the adjusted ICAO data. This contrasts with the parabolic interpolation used in the DLR method, and

reflects Boeing's preference for a segmented linear approximation for greater accuracy across thrust settings.

Table 3.1: Fuel flow correction factor values (DuBois 2006)

Flight Phase	Correction Factor
Take-off	1.010
Climb-out	1.013
Approach	1.020
Idle	1.100

Step 3 recalculates the emission index for cruise or other non-reference conditions. The NO_x emission index is scaled from the reference value using atmospheric correction factors:

$$EI_{NOx} = EI_{NOx,ref} \cdot \sqrt{\frac{\delta_{total}^{1.02}}{\theta_{total}^{3.3}}} \cdot e^{H} \quad . \tag{3.12}$$

Here, δ_{total} and θ_{total} are defined analogously to previous methods, using stagnation pressure and temperature. The humidity correction term H is computed using:

$$H = -19.0 \cdot (\omega - 0.00634) \quad , \tag{3.13}$$

with specific humidity ω derived via:

$$\omega = \frac{0.62197058 \cdot \phi \cdot P_V}{P_{amb} - \phi \cdot P_V} \quad , \tag{3.14}$$

where ϕ is the relative humidity and P_V is the saturation vapor pressure, calculated from ambient temperature T_{amb} through:

$$P_V = 0.014504 \cdot 10^{\beta} \tag{3.15}$$

and β is defined as:

$$\begin{aligned}\beta = {} & 7.90298 \cdot (1-\tau) + 3.00571 + 5.02808 \cdot log(\tau) \\ & + \left(1.3816 \cdot 10^{-7}\right) \cdot \left[1 - 10^{11.344 \cdot (1-1/\tau)}\right] \\ & + \left(8.1328 \cdot 10^{-3}\right) \cdot \left[10^{3.49149 \cdot (1-\tau)} - 1\right] \quad .\end{aligned} \tag{3.16}$$

4 Identification of the Most Used Passenger Aircraft Engines

4.1 Criteria for Engine Selection

The selection of aircraft engines for this study was based on a structured, data-informed methodology to identify the most operationally relevant engines in global passenger aviation. As a starting point, this work builds upon the thesis by Kühn (2023), Fuel Consumption of the 50 Most Used Passenger Aircraft, which provides a comprehensive list of the most frequently operated aircraft types worldwide based on the World Airliner Census (2020). Building on this list, delivery data from the four major aircraft manufacturers, Airbus, Boeing, Embraer and ATR, were evaluated to identify the specific engine types installed on these aircraft. From this, a dataset of 26,402 total engine deliveries was compiled, reflecting real-world deployment volumes across the commercial passenger fleet.

Each engine model was then categorized into one of 50 primary engine families, with further differentiation into a total of 207 specific engine variants. These subcategories include variations in thrust rating, performance features, and technical specifications, such as the CFM56-7B family, which comprises variants like the CFM56-7B18, CFM56-7B18/3 and CFM56-7B20. This granularity enables a more precise analysis of emissions characteristics while maintaining comparability at the family level. To ensure data reliability and compatibility with emission standards, all identified engine types were cross-referenced with the ICAO Aircraft Engine Emissions Databank (EEDB). Only engines listed in the EEDB with available certification data were included in the final analysis. This ensures that NO_x emission estimates in this study are based on validated, industry-standard reference data.

The final dataset includes engines from five major manufacturers, with the following market shares based on delivery volumes:

- CFM International: 48 %
- Pratt & Whitney: 19 %
- International Aero Engines (IAE): 14 %
- Rolls-Royce: 10 %
- General Electric Company: 9 %

These figures are consistent with industry trends and are illustrated in Figure 4.1, which depicts the proportional distribution of engine deliveries by manufacturer. The dominance of CFM International reflects the widespread use of its CFM56 and LEAP engine series, particularly on narrow-body aircraft such as the Airbus A320 and Boeing 737 families.

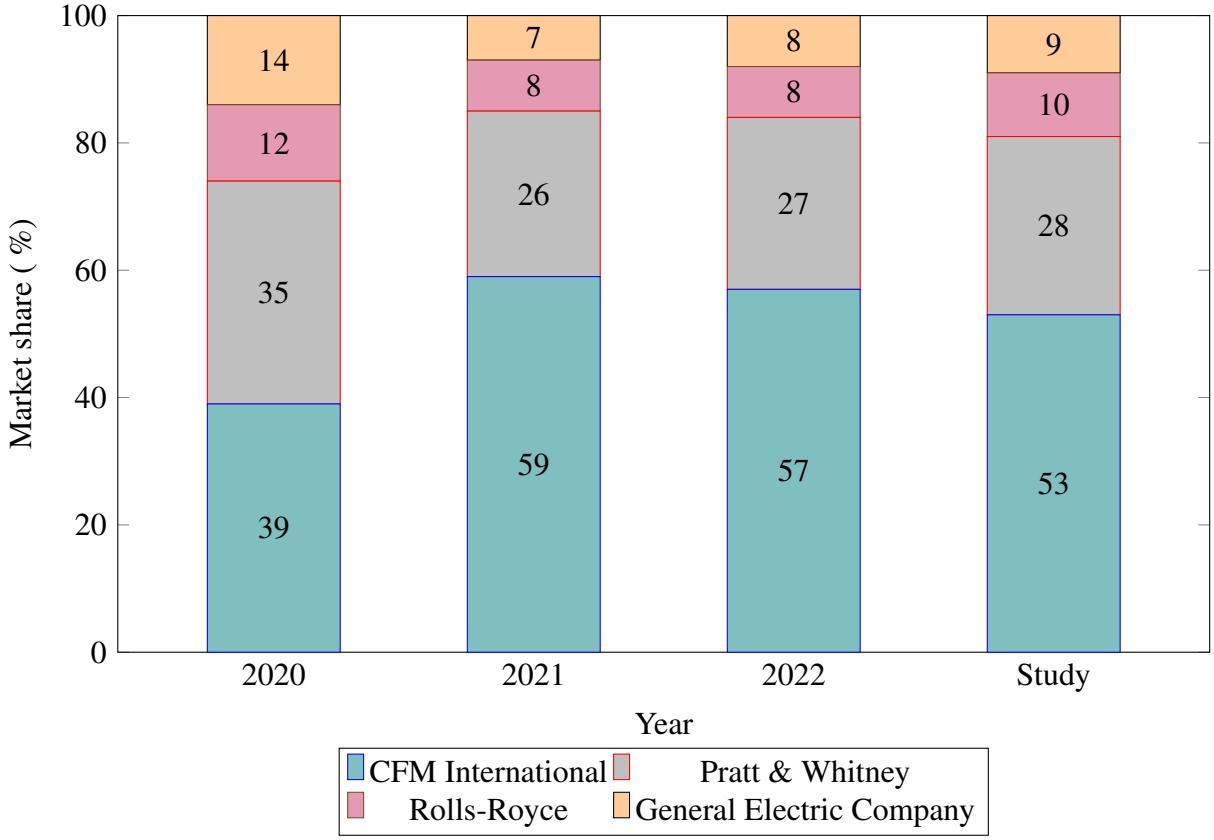

Figure 4.1: Market shares of engine manufacturers 2020-2022 (Statista 2024) and own study

This selection approach ensures that the 50 engine families studied in this work represent the majority of engines in service today, as well as those with the most significant environmental impact. This provides a representative basis for evaluating NO_x emissions in global passenger aviation. Table 4.1 lists the aircraft and engine models considered in this study, including details such as the total number of deliveries, engine models and their respective manufacturers.

Table 4.1: Aircraft models and associated engines

Airplane model	Total number	Engine model	Manufacturer
Boeing 737-800	4989	CFM56-7B	CFM International
A320ceo	4192	CFM56-5A	CFM International
		V2527-A5	International Aero Engines
A320neo	2074	PW1100G	Pratt & Whitney
		LEAP-1A	CFM International
A321ceo	1705	CFM56-5B5	CFM International
		V2533-A5	International Aero Engines
Boeing 737 Max	1654	LEAP-1B	CFM International
A321neo	1511	LEAP-1A	CFM International
		PW1100G	Pratt & Whitney
A319ceo	1257	CFM56-5B5	CFM International
		CFM56-5B7	CFM International
		V2522-A5	International Aero Engines
		V2524-A5	International Aero Engines
		V2527M-A5	International Aero Engines
Boeing MD-80	1191	JT8D-209	Pratt & Whitney
		JT8D-217A	Pratt & Whitney

Continuation of the Table 4.1

Airplane model	Total number	Engine model	Manufacturer
		JT8D-219	Pratt & Whitney
		JT8D-217C	Pratt & Whitney
Boeing 737-700	1128	CFM56-7B	CFM International
Boeing 737-300	1113	CFM56-3	CFM International
Boeing 757-200	913	PW2000	Pratt & Whitney
		RB211-535	Rolls-Royce plc
Boeing 747-400	884	PW4062	Pratt & Whitney
		RB211-524	Rolls-Royce plc
		CF6-80C2B5F	General Electric Company
Boeing 777-300ER	832	GE90-115B	General Electric Company
Embraer E175	768	CF34-8E5	General Electric Company
A330-300	727	CF6-80E1A2	General Electric Company
		PW4168	Pratt & Whitney
		PW4164	Pratt & Whitney
		Trent 768	Rolls-Royce plc
		Trent 772	Rolls-Royce plc
Boeing 787-9	639	GEnx	General Electric Company
		Trent 1000	Rolls-Royce plc
Embraer E190	568	CF34-10E	General Electric Company
A330-200	560	CF6-80E1A4	General Electric Company
		PW4168	Pratt & Whitney
		Trent 772	Rolls-Royce plc
A350-900	533	Trent XWB	Rolls-Royce plc
Boeing 737-400*	486	CFM56-3	CFM International
A380*	446	Trent 970	Rolls-Royce plc
		Trent 972	Rolls-Royce plc
		GP7270	Engine Alliance
Boeing 777-200ER	422	PW4090	Pratt & Whitney
		Trent 895	Rolls-Royce plc
		GE90-94B	General Electric Company
Boeing 787-8	397	GEnx	General Electric Company
		Trent 1000	Rolls-Royce plc
Boeing 737-500	389	CFM56-3	CFM International
A220-300	301	PW1519G	Pratt & Whitney
		PW1521G	Pratt & Whitney
		PW1524G	Pratt & Whitney
		PW1525G	Pratt & Whitney
A300	211	CF6-50C2	General Electric Company
		CF6-80C2	General Electric Company
		PW4158	Pratt & Whitney
		PW JT9D-59A	Pratt & Whitney
A340-200/300*	200	CFM56-5C2	CFM International
Embraer E170	191	CF34-8E5	General Electric Company
A340-500/600*	186	Trent 553	Rolls-Royce plc
		Trent 556	Rolls-Royce plc
Embraer E195	172	CF34-10E	General Electric Company
Boeing 717-200	155	BR700-715A1-30	Rolls-Royce Deutschland
		BR700-715C1-30	Rolls-Royce Deutschland
A330-900	137	Trent7000	Rolls-Royce plc
Embraer E195-E2	110	PW1919G	Pratt & Whitney
		PW1921G	Pratt & Whitney

Continuation of the Table 4.1

Airplane model	Total number	Engine model	Manufacturer
		PW1922G	Pratt & Whitney
		PW1923G	Pratt & Whitney
Boeing 767-300	104	PW JT9D-7R4E	Pratt & Whitney
		PW 4052	Pratt & Whitney
		CF6-80C2-B2	General Electric Company
		RB211-524	Rolls-Royce plc
A350-1000	89	Trent XWB	Rolls-Royce plc
Boeing 777-200	88	PW4077	Pratt & Whitney
		Trent 877	Rolls-Royce plc
		GE90-77B	General Electric Company
A319neo	22	LEAP-1A	CFM International
		PW1100G	Pratt & Whitney
A330-800	7	Trent7000	Rolls-Royce plc

4.2 List of the 50 Most Used Engines

Based on the methodology described in Section 4.1, the final selection includes 50 engine families, representing the majority of engines installed on the most frequently operated passenger aircraft worldwide. These engines were selected by grouping delivery data from major aircraft manufacturers according to corresponding engine models. Subvariants were grouped under broader engine families to ensure comparability and clarity in the analysis. The resulting list covers 26,402 deliveries in total, with individual engine families ranging from over 5,000 units (such as the CFM56-7B) to more specialised types with lower delivery numbers (for example, the CF6-80C2 or PW4077). The ranking reflects actual fleet importance and provides a solid foundation for evaluating NO_x emissions across a representative selection of the commercial aviation industry. The engines included span a broad spectrum of applications, from narrow-body aircraft (e.g., CFM56, V2500, LEAP) to wide-body long-haul platforms (e.g., GE90, Trent 1000, PW4000 series), as well as regional jets (e.g., CF34, BR700) and earlier-generation types (e.g., JT8D). The list also includes engines from both current-generation high-bypass turbofans and legacy models that remain in widespread service. A detailed table summarizing the engine families and their corresponding delivery counts is provided in Table 4.2. This table serves as the foundation for the emission analyses in the following sections, where NO_x emissions are calculated and statistically evaluated across various flight phases.

Table 4.2: Ranking of engine models according to the total number of engines

Ranking	Eng. Model	Eng. Sum
1	CFM56-7B	5323
2	V2527-A5	2096
3	CFM56-5A	2096
4	LEAP-1A	1803
5	PW1100G	1803
6	LEAP-1B	1654
7	CFM56-5B5	1113
8	V2533-A5	852

Continuation of the Table 4.2

Ranking	Eng. Model	Eng. Sum
9	GEnx	675
10	RB211-535	533
11	CFM56-3	496
12	PW2000	380
13	Trent 1000	361
14	PW4062	352
15	Trent 772	343
16	PW4168	343
17	CF6-80C2B5F	320
18	JT8D-209	297
19	JT8D-217A	297
20	JT8D-217C	297
21	JT8D-219	297
22	CFM56-5B7	251
23	V2522-A5	251
24	V2524-A5	251
25	V2527M-A5	251
26	CF34-8E5	239
27	RB211-524	238
28	Trent XWB	222
29	GE90-115B	208
30	CF6-80E1A4	198
31	CF34-10E	185
32	Trent 895	168
33	GE90-94B	161
34	Trent 972	148
35	Trent 970	148
36	GP7270	148
37	PW4164	145
38	Trent 768	145
39	CF6-80E1A2	145
40	Trent 553	93
41	PW4090	93
42	Trent 556	93
43	PW1524G	91
44	PW1525G	91
45	PW1521G	91
46	PW1519G	91
47	BR700-715C1-30	77
48	BR700-715A1-30	77
49	PW4077	63
50	CF6-80C2	55

5 NO_x Emissions of Selected Aircraft Engines

5.1 NO_x Emissions in the LTO Cycle

The LTO cycle, as defined by ICAO, consists of four operational phases that occur when an aircraft is near the ground: idle, take-off, climb-out and approach. Each phase is associated with a specific engine thrust setting and standardized time in mode, ensuring comparable emissions measurements across engine types, as shown in Table 5.1.

Table 5.1: LTO engine emissions cycle as outlined in ICAO Annex 16 Volume II and Bahr (1992)

Mode	Engine power	Time in Mode
Take-off	100 %	0.7 min
Climb-out	85 %	2.2 min
Approach	30 %	4.0 min
Idle (taxi)	7 %	26.0 min

NO_x emissions during the LTO cycle are particularly important due to their direct impact on local air quality in the vicinity of airports. These emissions mostly come from the engine's high-temperature combustion processes and vary with engine power settings.

This analysis uses data from the ICAO Aircraft Engine Emissions Databank, which provides certified emission values for the four LTO modes. Emissions are reported as the mass of NO_x emitted per engine per LTO cycle and are calculated based on standardized thrust settings and mode durations defined by ICAO.

Table 5.2 provides a detailed overview of NO_x emissions for selected aircraft engines during the standardised LTO cycle, as defined by ICAO guidelines. It presents both the NO_x emission indices, expressed in grams per kilogram of fuel burned (g/kg), and the corresponding total NO_x mass emissions in grams (g). The table includes the 50 most used aircraft engines, as well as all variants of these engine types in the Databank, providing comprehensive coverage of emission characteristics in this category. A small number of engines were tested multiple times, with some tests being repeated for research purposes or following engine improvements, which explains the different NOx LTO test results. All available test results are reported accordingly.

Table 5.2: NO_x emission indices EI_{Nox} (g/kg) and total mass of NO_x emissions (g) during the LTO cycle of the selected aircraft engines

Eng. ID	$EI_{Nox,\ T/O}$	$EI_{Nox,\ C/O}$	$EI_{Nox,\ App}$	$EI_{Nox,\ Idle}$	$NO_{X,\ Total}$
CFM56-7B20	20.50	17.40	9.50	4.30	3829
CFM56-7B20/2	13.25	10.81	9.39	3.75	2802
CFM56-7B20/3	15.61	13.53	7.98	3.77	2987
CFM56-7B22	23.10	19.00	10.00	4.50	4560
CFM56-7B22/2	15.08	12.16	6.37	3.94	3091
CFM56-7B22/3	17.40	14.67	8.35	3.95	3540

Continuation of the Table 5.2

Eng. ID	$EI_{Nox, T/O}$	$EI_{Nox, C/O}$	$EI_{Nox, App}$	$EI_{Nox, Idle}$	$NO_{X, Total}$
CFM56-7B24	25.30	20.50	10.10	4.40	5149
CFM56-7B24/2	16.63	13.23	6.72	4.08	3534
CFM56-7B24/3	18.93	15.60	8.60	4.09	3995
CFM56-7B26	28.80	22.50	10.80	4.70	6149
CFM56-7B26/2	19.20	14.77	7.26	4.27	4233
CFM56-7B26/3	21.79	17.08	8.93	4.27	4763
CFM56-7B26/3	22.90	17.68	9.37	4.22	4923
CFM56-7B27	30.90	23.70	11.00	4.80	6719
CFM56-7B27/2	20.81	15.59	7.53	4.36	4648
CFM56-7B27/3	23.94	17.89	9.09	4.36	5232
CFM56-7B20E	15.61	13.50	8.00	3.80	2987
CFM56-7B22E	17.40	14.67	8.35	3.95	3538
CFM56-7B22E/B1	17.40	14.67	8.35	3.95	3538
CFM56-7B24E	18.93	15.60	8.60	4.09	3996
CFM56-7B24E/B1	18.93	15.60	8.60	4.09	3996
CFM56-7B26E	21.79	17.08	8.93	4.27	4762
CFM56-7B26E/B1	21.79	17.08	8.93	4.27	4762
CFM56-7B26E/B2	21.79	17.08	8.93	4.27	4762
CFM56-7B26E/F	21.79	17.08	8.93	4.27	4762
CFM56-7B26E/B2F	21.79	17.08	8.93	4.27	4762
CFM56-7B27E	23.94	17.89	9.09	4.36	5231
CFM56-7B27E/B1	23.94	17.89	9.09	4.36	5231
CFM56-7B27E/B3	23.94	17.89	9.09	4.36	5231
CFM56-7B27AE	23.94	17.89	9.09	4.36	5231
CFM56-7B27E/F	23.94	17.89	9.09	4.36	5231
CFM56-7B27E/B1F	23.94	17.89	9.09	4.36	5231
V2527-A5	26.50	22.30	8.90	4.70	5382
V2527-A5 Up. Pa.	23.18	19.36	9.74	5.19	5102
V2527-A5E Up. Pa.	23.18	19.36	9.74	5.19	5102
V2527-A5M Up. Pa.	23.18	19.36	9.74	5.19	5102
CFM56-5A3	26.40	21.10	8.30	4.10	5110
CFM56-5A4	22.64	19.11	8.51	4.04	3851
CFM56-5A5	24.79	19.98	8.94	4.29	4367
LEAP-1A24/24E1/23	17.59	9.41	8.02	4.45	2341
LEAP-1A26/26E1	30.80	13.38	8.75	4.61	3535
LEAP-1A26CJ	30.80	13.38	8.75	4.61	3535
LEAP-1A29	49.48	21.03	9.27	4.72	5396
LEAP-1A29CJ	49.48	21.03	9.27	4.72	5396
LEAP-1A35A	59.74	32.35	9.95	4.85	7795
PW1127G1-JM	17.76	14.18	8.85	6.55	3244
PW1127G-JM	17.76	14.18	8.85	6.55	3244
PW1130G-JM	21.16	16.33	8.99	6.78	3969
PW1133G1-JM	25.23	18.92	9.14	6.98	4864
PW1133G-JM	25.23	18.92	9.14	6.98	4864
PW1124G1-JM	16.47	13.85	8.92	4.72	2626
PW1124G-JM	16.47	13.85	8.92	4.72	2626
PW1127G1-JM	18.82	15.30	9.07	4.84	3096
PW1127GA-JM	18.82	15.30	9.07	4.84	3096
PW1127G-JM	18.82	15.30	9.07	4.84	3096
PW1129G-JM	20.98	16.84	9.19	4.98	3571
PW1130G-JM	25.46	19.84	9.40	5.31	4736

Continuation of the Table 5.2

Eng. ID	$EI_{Nox,\ T/O}$	$EI_{Nox,\ C/O}$	$EI_{Nox,\ App}$	$EI_{Nox,\ Idle}$	$NO_{X,\ Total}$
PW1133GA-JM	25.46	19.84	9.40	5.31	4736
PW1133G-JM	25.46	19.84	9.40	5.31	4736
PW1124G1-JM	18.21	15.39	10.42	5.01	2912
PW1124G-JM	18.21	15.39	10.42	5.01	2912
PW1127G1-JM	20.81	16.95	10.59	5.20	3437
PW1127GA-JM	20.81	16.95	10.59	5.20	3437
PW1127G-JM	20.81	16.95	10.59	5.20	3437
PW1129G-JM	23.36	18.61	10.69	5.38	3975
PW1130G-JM	28.88	22.01	10.79	5.74	5284
PW1133GA-JM	28.88	22.01	10.79	5.74	5284
PW1133G-JM	28.88	22.01	10.79	5.74	5284
LEAP-1B25	48.90	20.35	11.10	4.57	5417
LEAP-1B27	55.26	23.26	11.59	4.59	6326
LEAP-1B28B2C	55.26	23.26	11.59	4.59	6326
LEAP-1B28BBJ1	64.36	29.59	11.92	4.68	7837
LEAP-1B28BBJ2	55.26	23.26	11.59	4.59	6326
LEAP-1B28	64.36	29.59	11.92	4.68	7837
CFM56-5B5/3	16.42	14.01	8.03	3.81	3047
V2533-A5 Up. Pa.	35.43	25.65	11.24	5.60	8377
GEnx-1B64	24.82	14.61	9.03	4.24	8576
GEnx-1B67	28.56	16.26	9.29	4.30	9759
GEnx-1B70	34.06	18.48	9.63	4.37	11457
GEnx-2B67	31.20	17.94	9.58	4.43	10978
GEnx-1B64/P1	25.74	15.36	9.11	4.37	9049
GEnx-1B67/P1	29.34	17.04	9.39	4.43	10244
GEnx-1B70/P1	34.61	19.30	9.73	4.50	11953
GEnx-1B70/72/P1	34.61	19.30	9.73	4.50	11953
GEnx-1B70/75/P1	34.61	19.30	9.73	4.50	11953
GEnx-1B74/75/P1	44.96	23.36	10.30	4.61	15268
GEnx-2B67B	31.20	17.94	9.58	4.43	10978
GEnx-1B64/P2	27.12	16.85	10.39	4.69	9747
GEnx-1B67/P2	30.32	18.57	10.67	4.76	10951
GEnx-1B70/72/P2	34.77	20.87	11.02	4.85	12629
GEnx-1B70/75/P2	34.77	20.87	11.02	4.85	12629
GEnx-1B70/P2	34.77	20.87	11.02	4.85	12629
GEnx-1B74/75/P2	42.71	24.90	11.56	4.99	15707
GEnx-1B76/P2	46.90	26.78	11.78	5.04	17251
GEnx-1B76A/P2	46.90	26.78	11.78	5.04	17251
GEnx-2B67/P	34.21	21.10	11.11	4.92	12509
RB211-535C	33.71	24.89	6.37	3.44	9277
RB211-535E4	44.88	32.06	6.78	3.46	11714
RB211-535E4	22.31	17.56	8.38	4.40	7492
RB211-535E4B	54.46	36.82	7.35	3.52	14791
RB211-535E4B	25.88	19.30	8.65	4.58	8927
CFM56-3-B1	17.70	15.50	8.30	3.90	3595
CFM56-3B-2	19.40	16.70	8.70	4.10	4213
CFM56-3C-1	20.70	17.80	9.10	4.30	4810
CFM56-3C-1 (Rerated)	16.60	14.70	8.00	3.80	3210
PW2037	29.41	23.96	9.77	4.10	8120
PW2040	35.04	26.62	10.49	4.37	9989
Trent 1000-L2	52.65	39.86	13.67	5.74	20735

Continuation of the Table 5.2

Eng. ID	**$EI_{Nox,\ T/O}$**	**$EI_{Nox,\ C/O}$**	**$EI_{Nox,\ App}$**	**$EI_{Nox,\ Idle}$**	**$NO_{X,\ Total}$**
Trent 1000-K2	58.04	43.07	14.06	5.91	23531
Trent 1000-J2	58.04	43.07	14.06	5.91	23531
Trent 1000-H2	40.46	31.49	12.56	5.21	14299
Trent 1000-G2	49.57	37.80	13.41	5.62	19058
Trent 1000-D2	52.65	39.86	13.67	5.74	20735
Trent 1000-C2	52.65	39.86	13.67	5.74	20735
Trent 1000-A2	46.11	35.48	13.11	5.48	17288
Trent 1000-AE3	48.25	36.92	13.66	5.53	18221
Trent 1000-CE3	55.28	41.46	14.26	5.79	22034
Trent 1000-D3	55.28	41.46	14.26	5.79	22034
Trent 1000-G3	51.93	39.30	13.98	5.67	20196
Trent 1000-H3	42.14	32.83	13.04	5.29	15026
Trent 1000-J3	60.68	44.92	14.68	5.97	25064
Trent 1000-K3	60.68	44.92	14.68	5.97	25064
PW4062	34.36	25.98	12.17	3.78	14555
Trent 772	43.60	32.66	10.68	5.74	21462
Trent 772	35.56	26.82	10.42	4.66	17668
PW4168	42.39	33.91	14.66	4.15	19704
PW4168	26.90	20.20	12.10	5.20	13936
PW4168-1D	30.15	22.31	12.39	4.08	14812
PW4168A	42.39	33.91	14.66	4.15	19704
PW4168A	26.90	20.20	12.10	5.20	13936
PW4168A-1D	30.15	22.31	12.39	4.08	14812
CF6-80C2B5F	28.58	21.76	12.74	4.91	13142
JT8D-209	22.80	19.00	8.80	3.50	5075
JT8D-217A	17.54	13.54	7.66	4.57	4582
JT8D-217C	16.49	13.02	7.65	4.05	4216
JT8D-219	27.00	20.80	9.13	3.60	6106
JT8D-219	18.72	13.73	7.65	4.16	4604
CFM56-5B7/P	28.00	23.20	10.00	4.30	5641
CFM56-5B7/3	21.57	17.23	8.85	4.22	4511
V2522-A5	24.50	20.80	8.70	4.50	4720
V2522-A5 Up. Pa.	21.34	18.33	9.32	5.09	4563
V2524-A5	26.20	22.00	9.00	4.70	5278
V2524-A5 Up. Pa.	22.96	19.25	9.69	5.18	5039
V2527M-A5	26.50	22.30	8.90	4.70	5382
CF34-8E5A1	15.81	13.15	11.06	4.70	2419
RB211-524G	58.71	40.54	9.56	4.63	21075
RB211-524G-T	28.43	21.80	9.68	4.00	12513
RB211-524H	65.84	46.31	10.26	4.78	24501
RB211-524H-T	31.19	23.19	9.91	4.16	13995
Trent XWB-97	56.91	40.17	12.69	4.81	28456
Trent XWB-75	36.23	28.29	10.13	4.06	14512
Trent XWB-84	45.24	34.20	11.12	4.41	19903
Trent XWB-97	66.05	48.51	14.86	5.64	33539
GE90-115B	51.07	36.44	16.17	5.51	34113
CF6-80E1A4	43.15	30.30	10.13	4.62	18055
CF6-80E1A4	31.28	23.54	12.66	4.77	15027
CF34-10E2A1	17.98	15.26	7.64	3.56	2742
CF34-10E5	18.66	15.54	8.08	3.51	2836

Continuation of the Table 5.2

Eng. ID	$EI_{Nox, T/O}$	$EI_{Nox, C/O}$	$EI_{Nox, App}$	$EI_{Nox, Idle}$	$NO_{X, Total}$
CF34-10E5	17.78	14.97	7.59	3.55	2757
CF34-10E5	18.51	15.62	7.76	3.59	2871
CF34-10E5A1	20.83	16.93	8.43	3.67	3328
CF34-10E5A1	19.68	16.22	7.94	3.69	3214
CF34-10E5A1	20.45	16.88	8.14	3.72	3341
CF34-10E6	18.66	15.54	8.08	3.51	2836
CF34-10E6	17.78	14.97	7.59	3.55	2757
CF34-10E6	18.51	15.62	7.76	3.59	2871
CF34-10E6A1	20.83	16.93	8.43	3.67	3328
CF34-10E6A1	19.68	16.22	7.94	3.69	3214
CF34-10E6A1	20.45	16.88	8.14	3.72	3341
CF34-10E7	20.83	16.93	8.43	3.67	3328
CF34-10E7	19.68	16.22	7.94	3.69	3214
CF34-10E7	20.45	16.88	8.14	3.72	3341
CF34-10E7-B	19.68	16.22	7.94	3.69	3214
Trent 895	47.79	34.29	11.39	5.11	28029
GE90-94B	56.41	41.74	17.38	6.09	30617
GE90-94B	51.33	40.63	15.81	5.55	28540
Trent 972-84	39.78	30.36	12.23	5.51	17699
Trent 972E-84	39.78	30.36	12.23	5.51	17699
Trent 970B-84	41.34	31.30	12.37	5.57	18591
Trent 970-84	38.29	29.42	12.09	5.44	16826
GP7270	41.73	31.37	12.90	5.24	17713
PW4164	38.57	31.66	14.10	4.03	17232
PW4164	23.87	18.66	11.88	4.99	12150
PW4164-1D	26.31	20.97	12.10	3.79	12895
Trent 768	39.11	30.01	10.34	5.60	18672
Trent 768	31.25	24.66	10.01	4.52	15658
Trent 768	32.01	24.90	10.12	4.46	15414
CF6-80E1A2	39.29	28.02	9.91	4.53	16203
CF6-80E1A2	28.72	22.01	12.66	4.88	13796
Trent 553-61	40.55	30.98	11.37	5.96	14444
PW4090	57.52	41.17	12.74	4.48	31121
Trent 556-61	44.91	32.76	11.78	6.19	16113
Trent 556-61	44.77	33.25	11.68	6.09	16167
PW1524G	28.10	21.20	11.10	6.10	4125
PW1524G	26.00	20.50	10.40	6.00	3903
PW1525G	28.10	21.20	11.10	6.10	4125
PW1525G	26.00	20.50	10.40	6.00	3903
PW1521G	23.20	18.50	10.90	5.60	3250
PW1521G	22.10	18.10	10.10	5.60	3139
PW1521GA	22.10	18.10	10.10	5.60	3139
PW1519G	20.20	16.70	10.70	5.30	2739
PW1519G	19.60	16.60	9.80	5.30	2656
BR700-715C1-30	31.39	22.41	11.55	5.72	5314
BR700-715C1-30	27.92	20.05	9.23	4.28	4588
BR700-715A1-30	23.97	18.65	11.19	5.37	4002
BR700-715A1-30	20.97	16.43	8.75	3.95	3340
PW4077	39.80	32.50	11.30	4.20	19299
PW4077D	44.68	34.05	11.63	3.81	21799

Continuation of the Table 5.2

Eng. ID	$EI_{Nox, T/O}$	$EI_{Nox, C/O}$	$EI_{Nox, App}$	$EI_{Nox, Idle}$	$NO_{X, Total}$
CF6-80C2A1	32.22	24.85	9.76	3.99	12382
CF6-80C2A1	26.55	20.45	12.43	4.68	11514
CF6-80C2A2	27.93	20.69	9.44	3.95	9728
CF6-80C2A2	22.35	18.37	11.86	4.49	9339
CF6-80C2A3	34.50	25.46	9.93	3.92	13074
CF6-80C2A3	27.68	21.05	12.48	4.72	12074
CF6-80C2A5	34.38	22.86	9.11	3.79	12735
CF6-80C2A5	28.57	21.69	12.53	4.76	12640
CF6-80C2A5F	28.11	21.27	12.64	4.90	12796
CF6-80C2A8	33.50	22.00	9.00	3.70	11797
CF6-80C2A8	26.42	20.45	12.43	4.68	11491
CF6-80C2B1	28.11	21.26	8.83	3.73	10400
CF6-80C2B1	24.93	19.68	12.32	4.60	10719
CF6-80C2B1F	27.73	21.07	9.00	3.78	10528
CF6-80C2B2	23.89	18.65	8.77	3.70	8796
CF6-80C2B2	22.02	18.25	11.79	4.45	9169
CF6-80C2B2F	23.56	18.32	8.54	3.64	8361
CF6-80C2B2F	21.55	18.09	11.80	4.52	9192
CF6-80C2B4	29.20	21.80	8.90	3.67	11211
CF6-80C2B4	25.93	20.17	12.37	4.68	11226
CF6-80C2B4F	28.72	21.32	8.88	3.71	10635
CF6-80C2B4F	25.08	19.72	12.47	4.73	11137
CF6-80C2B6	30.81	22.94	9.11	3.79	12362
CF6-80C2B6	28.57	21.69	12.53	4.76	12640
CF6-80C2B6F	32.16	23.09	9.06	3.75	12134
CF6-80C2B7F	32.16	23.09	9.06	3.75	12134
CF6-80C2B7F	27.38	21.05	12.63	4.81	12420
CF6-80C2B8F	26.85	20.84	12.42	4.59	12213
CF6-80C2B8FA	26.90	20.85	12.63	4.83	12400
CF6-80C2D1F	32.65	24.02	9.16	3.80	12714
CF6-80C2D1F	28.12	21.30	12.66	4.85	12724
CF6-80C2B1F	24.94	19.72	12.47	4.73	11113
CF6-80C2B5F	28.58	21.76	12.74	4.91	13142
CF6-80C2B6F	27.38	21.05	12.63	4.81	12420

Based on the total NO_x emissions per engine model, the five best-performing (i.e., lowest-emitting) and five worst-performing (i.e., highest-emitting) engines in the dataset are as follows:

Table 5.3: Top 5 lowest NO_x emitting engines during the LTO cycle

Engine Identification	NO_x Total (g)	Thrust (kN)	Entry into Service
CF34-8E5A1	1930	62.5	2002
LEAP-1A24/24E1/23	2341	106.8	2016
CF34-8E5	2419	59.7	2002
CF34-8E5A2	2480	64.5	2002
PW1122G-JM	2572	107.8	2014

Table 5.4: Top 5 highest NO_x emitting engines during the LTO cycle

Engine Identification	NO_x Total (g)	Thrust (kN)	Entry into Service
GE90-115B	34113	513.9	2003
Trent XWB-97	33539	436.7	2016
Trent 1000-J3/K3	25064	350.9	2017
Trent 1000-D3	22034	334.7	2017
Trent 772 (Phase 5)	21462	320.3	2014

Several significant trends and conclusions can be drawn from the available data. First, there is a pronounced positive correlation between rated engine thrust and total NO_x emissions as seen in Tables 5.3 and 5.4 . Larger engines with more thrust, which are typically designed for large airplanes and long-haul operations, inherently produce higher levels of NO_x during the LTO cycle. Higher thrust levels require more fuel, which leads to greater NO_x emissions. Therefore, engine size is a key driver of total pollutant output.

Emission contributions across the LTO phases vary significantly:

- **Take-off** (100 % thrust) and **climb-out** (85 % thrust) are responsible for approximately **77 %** of total NO_x emissions. These high-power settings lead to elevated combustion temperatures, which promote thermal NO formation.
- **Approach** occurs at 30 % thrust and contributes roughly **16 %** of total emissions.
- **Taxiing**, although operating at only 7 % thrust, accounts for about **7 %** of total NO_x emissions due to its relatively long duration on the ground.

5.2 NO_x Emissions During Cruise

The NO_x emissions during cruise phase were calculated based on the corrected fuel flow and altitude-specific emission indices. The engine fuel flow values during cruise were taken from the work of Mattausch (2024), where the values were calculated using the BFFM2 model. To ensure comparability and consistency, the given engine fuel flow values ($\dot{m}_{\text{fuel}}$, in kg/s) were corrected to ISA reference conditions. This correction is necessary because engine performance and emissions can vary noticeably depending on altitude and ambient conditions. The corrected fuel flow provides a standardized basis for evaluating emission characteristics consistently.

The engine fuel flow and all following analyses refer to a single individual engine. Consequently, for multi-engine aircraft, the total aircraft fuel flow must be divided by the number of engines to obtain per-engine values. From the corrected fuel flow, the reference NO_x emission index ($EI_{\text{NOx,ref}}$) was determined using the established reference function that relates the emission index to fuel flow under reference conditions.

As the final step, the reference emission index was re-corrected to the actual cruise conditions

(altitude-dependent), including effects of temperature, pressure, and humidity, to reflect the NO_x emissions at cruise more accurately. The cruise conditions used in this study are listed in Table 5.5. Commercial aircraft typically cruise at altitudes between 30,000 feet and 42,000 feet (Epic Flight Academy 2024). Therefore, an altitude of 36,000 ft was selected as a representative cruise level. The corresponding ambient temperature and static pressure were derived from the ICAO Standard Atmosphere (Deutscher Wetterdienst 2025). The relative humidity was taken from Scholz (2024), based on a diagram showing the "Minimum Relative Humidity for Persistent Contrails". The Mach number was adopted from Mattausch (2024).

Table 5.5: Cruise flight conditions used for NO_x emission analysis

Parameter	**Value**
Mach number	0.78
Altitude	36,000 ft
Static ambient pressure p_{amb}	22,632 Pa
Static ambient temperature T_{amb}	216.65 K
Relative humidity	0.6

Figure 5.1 compares the NO_x emission index under cruise conditions as calculated by two different methods: the DLR method and the Boeing Fuel Flow Method (BFFM). The values are given in grams per kilogram of fuel (g/kg), with the DLR results on the y-axis and the BFFM results on the x-axis. The data points generally align along a 1:1 diagonal, indicating that both models produce comparable results in most cases. There are slight deviations from the line, with some engines showing a tendency for the DLR method to give slightly higher NO_x values under cruise conditions. However, these deviations are minor and do not suggest that either model systematically over- or underestimates. The results are consistent with findings from previous studies and confirm that the DLR model provides cruise NO_x predictions in a similar range to the established BFFM method. The closeness of the results suggests that both models capture the essential physics governing NO_x formation during high-altitude, steady-state engine operation.

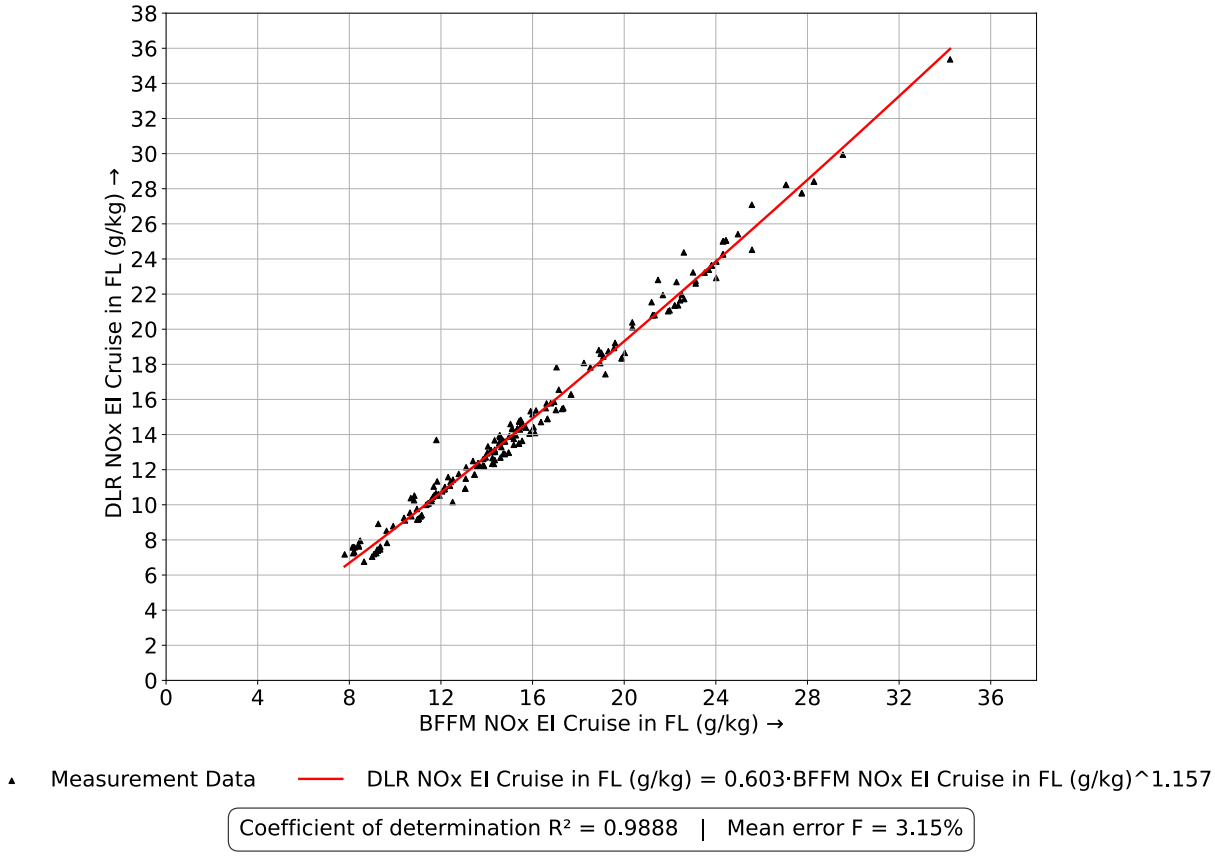

Figure 5.1: Comparison of NO_x emission index in cruise calculated with the DLR method (y-axis) and the BFFM method (x-axis).

Table 5.6 presents emission indices for nitrogen oxides (EI_{NOx}) during cruise flight, expressed in grams of NO_x per kilogram of burned fuel, for the engines mentioned in Table 4.2 and their subvariants. These values were calculated using two established methods: the DLR method and the BFFM2 model. While both methods yield consistent overall trends, individual discrepancies of up to approximately 2.7 g/kg are observed in some engine variants.

Table 5.6: NO_x emission indices EI_{Nox} (g/kg) during cruise of the selected aircraft engines, calculated using the DLR method and BFFM2

Engine	Eng. ID	$EI_{Nox,\ Cr,\ DLR}$	$EI_{Nox,\ Cr,\ BFFM2}$
CFM56-7B	CFM56-7B20	13.01	14.30
	CFM56-7B20/2	7.83	9.64
	CFM56-7B20/3	10.01	11.36
	CFM56-7B22	13.29	14.64
	CFM56-7B22/2	8.52	9.63
	CFM56-7B22/3	10.08	11.44
	CFM56-7B24	13.61	14.80
	CFM56-7B24/2	8.78	9.92
	CFM56-7B24/3	10.21	11.57
	CFM56-7B26	13.99	15.20
	CFM56-7B26/2	9.25	10.39
	CFM56-7B26/3	10.58	11.89
	CFM56-7B26/3	11.09	12.39
	CFM56-7B27	14.29	15.45

Continuation of Table 5.6

Engine	Eng. ID	$EI_{Nox, Cr, DLR}$	$EI_{Nox, Cr, BFFM2}$
	CFM56-7B27/2	9.55	10.65
	CFM56-7B27/3	12.36	13.62
	CFM56-7B20E	9.99	11.35
	CFM56-7B22E	10.08	11.44
	CFM56-7B22E/B1	10.08	11.45
	CFM56-7B24E	10.21	11.57
	CFM56-7B24E/B1	10.21	11.57
	CFM56-7B26E	10.58	11.89
	CFM56-7B26E/B1	10.59	11.90
	CFM56-7B26E/B2	10.58	11.89
	CFM56-7B26E/F	10.58	11.89
	CFM56-7B26E/B2F	10.58	11.89
	CFM56-7B27E	10.90	12.15
	CFM56-7B27E/B1	12.36	13.62
	CFM56-7B27E/B3	10.90	12.15
	CFM56-7B27AE	10.91	12.15
	CFM56-7B27E/F	10.90	12.15
	CFM56-7B27E/B1F	12.36	13.62
V2527-A5	V2527-A5	14.77	15.43
	V2527-A5 Up. Pa.	12.71	13.94
	V2527-A5E Up. Pa.	12.71	13.94
	V2527-A5M Up. Pa.	12.71	13.94
CFM56-5A	CFM56-5A3	15.37	16.15
	CFM56-5A4	14.61	15.54
	CFM56-5A5	14.59	15.57
LEAP-1A	LEAP-1A24/24E1/23	10.52	11.94
	LEAP-1A26/26E1	15.33	15.91
	LEAP-1A26CJ	16.55	17.14
	LEAP-1A29	25.00	24.31
	LEAP-1A29CJ	25.02	24.33
	LEAP-1A35A	35.37	34.23
PW11	PW1127G1-JM	10.92	13.06
	PW1127G-JM	10.92	13.06
	PW1130G-JM	14.09	16.11
	PW1133G1-JM	15.46	17.29
	PW1133G-JM	15.46	17.29
	PW1124G1-JM	11.72	13.46
	PW1124G-JM	11.72	13.47
	PW1127G1-JM	12.21	13.87
	PW1127GA-JM	12.21	13.88
	PW1127G-JM	12.21	13.87
	PW1129G-JM	12.66	14.25
	PW1130G-JM	16.28	17.68
	PW1133GA-JM	16.27	17.68
	PW1133G-JM	16.28	17.68
	PW1124G1-JM	12.96	14.95
	PW1124G-JM	12.97	14.96
	PW1127G1-JM	13.48	15.40
	PW1127GA-JM	13.49	15.41
	PW1127G-JM	13.48	15.40
	PW1129G-JM	14.05	15.87

Continuation of Table 5.6

Engine	Eng. ID	$EI_{Nox, Cr, DLR}$	$EI_{Nox, Cr, BFFM2}$
	PW1130G-JM	18.35	19.89
	PW1133GA-JM	18.35	19.89
	PW1133G-JM	18.35	19.89
LEAP-1B	LEAP-1B25	23.24	23.00
	LEAP-1B27	25.05	24.44
	LEAP-1B28B2C	25.05	24.44
	LEAP-1B28BBJ1	28.22	27.06
	LEAP-1B28BBJ2	25.05	24.44
	LEAP-1B28	28.22	27.06
CFM56-5B5	CFM56-5B5/3	10.25	11.57
V2533-A5	V2533-A5 Up. Pa.	18.07	18.95
GEnx	GEnx-1B64	11.02	12.17
	GEnx-1B67	12.14	13.10
	GEnx-1B70	13.67	14.34
	GEnx-2B67	13.86	14.59
	GEnx-1B64/P1	11.43	12.52
	GEnx-1B67/P1	12.49	13.40
	GEnx-1B70/P1	13.94	14.57
	GEnx-1B70/72/P1	13.94	14.57
	GEnx-1B70/75/P1	13.94	14.57
	GEnx-1B74/75/P1	18.81	18.89
	GEnx-2B67B	13.86	14.59
	GEnx-1B64/P2	12.22	13.58
	GEnx-1B67/P2	13.14	14.35
	GEnx-1B70/72/P2	14.33	15.34
	GEnx-1B70/75/P2	14.33	15.34
	GEnx-1B70/P2	14.33	15.34
	GEnx-1B74/75/P2	18.44	19.09
	GEnx-1B76/P2	20.80	21.25
	GEnx-1B76A/P2	20.80	21.25
	GEnx-2B67/P	15.51	16.57
RB211-535	RB211-535C	17.84	17.05
	RB211-535E4	22.81	21.48
	RB211-535E4	11.31	12.42
	RB211-535E4B	24.37	22.60
	RB211-535E4B	11.76	12.78
CFM56-3	CFM56-3-B1	10.55	11.71
	CFM56-3B-2	10.46	11.66
	CFM56-3C-1	10.33	11.60
	CFM56-3C-1 (Rerated)	10.66	11.78
PW20	PW2037	17.83	18.52
	PW2040	18.75	19.31
Trent 1000	Trent 1000-L2	23.63	23.81
	Trent 1000-K2	27.75	27.75
	Trent 1000-J2	27.75	27.75
	Trent 1000-H2	21.96	22.52
	Trent 1000-G2	23.22	23.51
	Trent 1000-D2	23.63	23.81
	Trent 1000-C2	23.63	23.81
	Trent 1000-A2	22.76	23.12
	Trent 1000-AE3	23.39	23.69

Continuation of Table 5.6

Engine	**Eng. ID**	**$EI_{Nox, Cr, DLR}$**	**$EI_{Nox, Cr, BFFM2}$**
	Trent 1000-CE3	24.27	24.31
	Trent 1000-D3	24.27	24.31
	Trent 1000-G3	23.85	24.02
	Trent 1000-H3	22.61	23.12
	Trent 1000-J3	28.41	28.28
	Trent 1000-K3	28.41	28.28
PW4062	PW4062	15.78	16.79
Trent 772	Trent 772	8.92	9.26
	Trent 772	7.58	8.23
PW4168	PW4168	21.72	22.62
	PW4168	12.92	14.72
	PW4168-1D	14.40	15.71
	PW4168A	21.02	21.92
	PW4168A	12.55	14.35
	PW4168A-1D	13.96	15.27
CF6-80C2B5F	CF6-80C2B5F	12.89	14.78
JT8D-209	JT8D-209	14.35	15.10
JT8D-217A	JT8D-217A	9.35	10.71
JT8D-217C	JT8D-217C	9.11	10.43
JT8D-219	JT8D-219	14.83	15.47
	JT8D-219	9.76	10.95
CFM56-5B7	CFM56-5B7/P	14.46	15.48
	CFM56-5B7/3	10.76	12.05
V2522-A5	V2522-A5	14.74	15.42
	V2522-A5 Up. Pa.	12.61	13.85
V2524-A5	V2524-A5	14.84	15.61
	V2524-A5 Up. Pa.	12.79	14.10
V2527M-A5	V2527M-A5	14.77	15.43
CF34-8E5	CF34-8E5A1	10.16	12.51
RB211-524	RB211-524G	27.09	25.57
	RB211-524G-T	13.33	14.05
	RB211-524H	13.69	11.80
	RB211-524H-T	7.18	7.80
Trent XWB	Trent XWB-97	25.41	24.97
	Trent XWB-75	20.39	20.35
	Trent XWB-84	21.54	21.20
	Trent XWB-97	29.94	29.54
GE90-115B	GE90-115B	18.65	20.02
CF6-80E1A4	CF6-80E1A4	20.11	20.36
	CF6-80E1A4	14.71	16.37
CF34-10E	CF34-10E2A1	13.50	14.54
	CF34-10E5	13.62	14.72
	CF34-10E5	12.95	14.02
	CF34-10E5	13.52	14.56
	CF34-10E5A1	13.90	14.99
	CF34-10E5A1	13.11	14.18
	CF34-10E5A1	13.66	14.70
	CF34-10E6	13.62	14.72
	CF34-10E6	12.95	14.02
	CF34-10E6	13.52	14.56
	CF34-10E6A1	13.90	14.99

Continuation of Table 5.6

Engine	**Eng. ID**	**$EI_{Nox, Cr, DLR}$**	**$EI_{Nox, Cr, BFFM2}$**
	CF34-10E6A1	13.11	14.18
	CF34-10E6A1	13.66	14.70
	CF34-10E7	13.90	14.99
	CF34-10E7	13.11	14.18
	CF34-10E7	13.66	14.70
	CF34-10E7-B	13.11	14.18
Trent 895	Trent 895	18.08	18.24
GE90-94B	GE90-94B	24.52	25.58
	GE90-94B	22.92	24.02
Trent 972	Trent 972-84	21.35	22.21
	Trent 972E-84	21.35	22.20
Trent 970	Trent 970B-84	21.65	22.44
	Trent 970-84	21.08	21.98
GP7270	GP7270	22.39	23.00
PW4164	PW4164	21.36	22.35
	PW4164	12.34	14.24
	PW4164-1D	13.76	15.18
Trent 768	Trent 768	18.93	19.56
	Trent 768	15.15	16.00
	Trent 768	15.78	16.61
CF6-80E1A2	CF6-80E1A2	19.22	19.60
	CF6-80E1A2	14.09	15.90
Trent 553	Trent 553-61	14.60	15.04
PW4090	PW4090	22.69	22.28
Trent 556	Trent 556-61	18.60	18.98
	Trent 556-61	18.66	19.00
PW1524G	PW1524G	15.40	17.02
	PW1524G	14.42	16.04
PW1525G	PW1525G	12.24	13.83
	PW1525G	11.49	13.08
PW1521G	PW1521G	15.51	17.34
	PW1521G	14.89	16.65
	PW1521GA	14.89	16.65
PW1519G	PW1519G	13.64	15.54
	PW1519G	13.42	15.18
BR700-715C1-30	BR700-715C1-30	13.01	14.36
	BR700-715C1-30	11.58	12.31
BR700-715A1-30	BR700-715A1-30	17.44	19.18
	BR700-715A1-30	15.86	16.95
PW4077	PW4077	20.80	21.33
	PW4077D	21.95	21.69
CF6-80C2	CF6-80C2A1	11.04	11.68
	CF6-80C2A1	9.21	11.03
	CF6-80C2A2	7.63	8.42
	CF6-80C2A2	6.76	8.65
	CF6-80C2A3	11.33	11.83
	CF6-80C2A3	9.34	11.11
	CF6-80C2A5	10.38	10.68
	CF6-80C2A5	9.41	11.16
	CF6-80C2A5F	9.17	10.97
	CF6-80C2A8	10.52	10.84

Continuation of Table 5.6

Engine	Eng. ID	$EI_{Nox, Cr, DLR}$	$EI_{Nox, Cr, BFFM2}$
	CF6-80C2A8	9.20	11.03
	CF6-80C2B1	14.80	15.50
	CF6-80C2B1	12.69	14.60
	CF6-80C2B1F	14.31	15.12
	CF6-80C2B2	7.24	8.17
	CF6-80C2B2	7.19	9.08
	CF6-80C2B2F	7.32	8.21
	CF6-80C2B2F	7.05	9.00
	CF6-80C2B4	7.59	8.18
	CF6-80C2B4	7.45	9.28
	CF6-80C2B4F	7.73	8.40
	CF6-80C2B4F	7.25	9.18
	CF6-80C2B6	7.58	8.13
	CF6-80C2B6	7.62	9.35
	CF6-80C2B6F	7.95	8.48
	CF6-80C2B7F	7.95	8.47
	CF6-80C2B7F	7.39	9.24
	CF6-80C2B8F	7.45	9.22
	CF6-80C2B8FA	7.46	9.35
	CF6-80C2D1F	10.26	10.83
	CF6-80C2D1F	9.15	10.99
	CF6-80C2B1F	12.33	14.31
	CF6-80C2B5F	12.89	14.78
	CF6-80C2B6F	7.39	9.24

The majority of engines show differences between the two models of around 0.5 ... 1.5 g/kg, with the BFFM2 method calculating a higher emission index at cruise. The PW1130G-JM shows the maximum absolute difference, with the BFFM2 value (19.89 g/kg) being 3.61 g/kg higher than the DLR estimate (16.28 g/kg).

Table 5.7: Lowest NO_x emission indices during cruise

Engine	$EI_{NOx, DLR}$	$EI_{NOx, BFFM2}$	Pressure Ratio	Entry into Service
CF6-80C2A2	6.76	8.65	28.0	1985
RB211-524H-T	7.18	7.80	34.0	—
CF6-80C2B2F	7.05	9.00	27.5	1985
CF6-80C2B2	7.19	9.08	27.7	1985
CF6-80C2B4	7.25	9.18	30.4	1985

Table 5.8: Highest NO_x emission indices during cruise

Engine	$EI_{NOx,\ DLR}$	$EI_{NOx,\ BFFM2}$	Pressure Ratio	Entry into Service
LEAP-1A35A	35.37	34.23	38.5	2016
Trent 1000-J3	28.41	28.28	47.8	2017
Trent 1000-K3	28.41	28.28	47.8	2017
LEAP-1A29CJ	25.02	24.33	35.5	2016
LEAP-1A29	25.00	24.31	35.5	2016

Tables 5.7 and 5.8 show a positive correlation between the overall pressure ratio and the NO_x emission index (EI_{NOx}) during cruise. Engines with higher pressure ratios, such as the LEAP-1A and Trent 1000 series, have significantly higher NO_x emission index values than older engines, such as the CF6-80C2 or RB211-524 series. This trend is consistent with the thermally-driven formation of NO_x as seen in Figure 2.3, which increases exponentially with combustion temperature, as described by the extended Zeldovich mechanism. An increase in the OPR improves fuel efficiency but also raises the combustor inlet temperature. If this is not counteracted by the design of the combustor, it leads to a significant increase in thermal NOx production (Jaravel 2023). As a result, although modern high-efficiency engines are optimised for fuel savings and CO_2 reduction, they tend to emit more NO_x per unit of fuel.

6 Statistical Analysis of NO_x Emissions

Nitrogen oxides (NO_x) emitted by aircraft engines are a major contributor to atmospheric pollution and are closely monitored because of their impact on air quality and climate change. This chapter presents a statistical analysis of NO_x emissions data derived from the ICAO Aircraft Engine Emissions Databank. The analysis aims to identify emission trends for different engine types and operating conditions, examine correlations with engine performance parameters, and evaluate regression-based models for predicting NO_x formation.

6.1 Comparison of NO_x Emissions with Legal Limits

Over the past few decades, the aviation industry has faced increasing regulatory pressure to reduce NO_x emissions from aircraft engines. In response, several international standards have been developed under ICAO's Committee on Aviation Environmental Protection (CAEP) that define emission limits as a function of overall engine OPR. These limits have been progressively tightened through successive phases of CAEP, reflecting growing environmental awareness and technological advances in engine design. In order to assess compliance and the evolution of NO_x emissions over time, a comparison is made between the measured Dp/Foo NO_x characteristics of various passenger aircraft engines and the applicable CAEP standards. Figure 6.1 provides a visual summary of this comparison. The vertical axis represents the NO_x emission characteristic (Dp/Foo) in g/kN, while the horizontal axis shows the total OPR. Each triangle represents an individual engine, color-coded by test period from 1986 to post-2016.

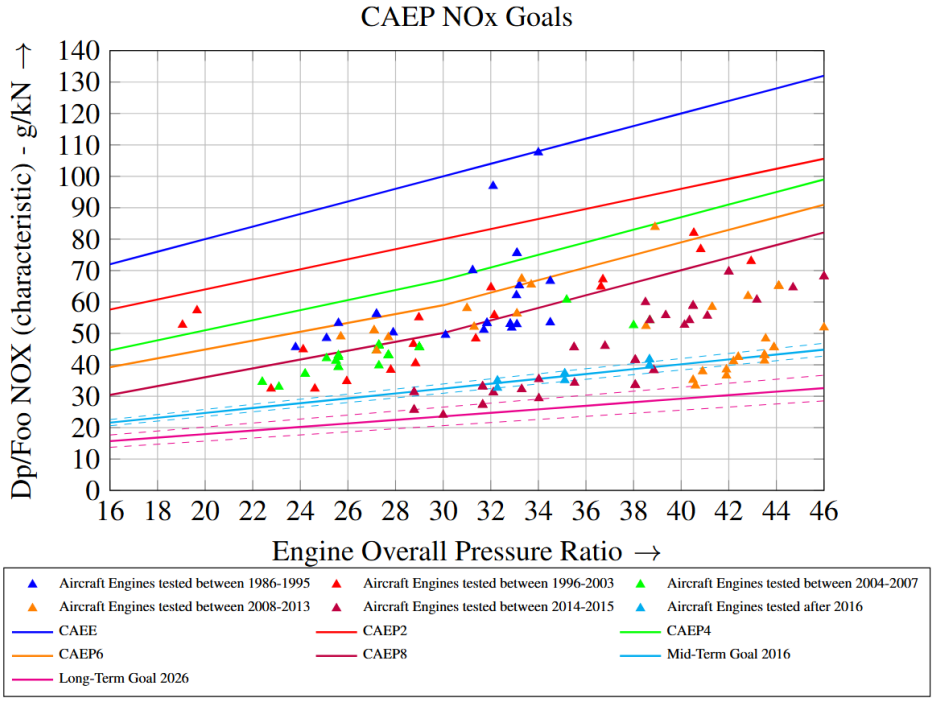

Figure 6.1: Comparison of NO_x emission limits (CAEP standards) with selected passenger aircraft engines tested between 1986 and post-2016.

The plotted CAEP lines (CAEP2 to CAEP8) and future environmental targets (mid- and long-

term targets) show how emission limits have evolved. A general trend emerges: engines with higher compression ratios tend to emit more NO_x, which is thermodynamically expected due to higher combustion temperatures. However, newer engines, especially those tested after 2008, show significantly reduced NO_x levels due to improved combustor designs such as Double Annular Combustor (DAC), Twin Annular Premixing Swirler (TAPS) II and TALON-X. Older engines, particularly those developed before the 2000s, often approach or exceed earlier CAEP limits, confirming the impact of technological innovation driven by regulatory evolution. The close proximity of many newer engines to mid- and long-term emissions targets also demonstrates the industry's readiness to meet future environmental benchmarks.

While regulatory compliance is clearly visible at the macro level, the underlying physical drivers of NO_x formation, such as OPR, fuel flow, and thrust, require more detailed investigation. Understanding these relationships is essential not only for emissions certification, but also for the development of accurate predictive models and the design of next-generation low-emission powertrains.

The following section therefore shifts the focus from a regulatory comparison to a parameter-driven analysis of NO_x formation. By examining the correlations between emissions and key engine variables, a more fundamental understanding of NO_x behavior is developed.

6.2 Relationship Between NO_x Emissions and Aircraft Parameters

Understanding the relationship between NO_x emissions and aircraft engine parameters is essential for both emissions prediction and low-emission engine design. In this section, statistical relationships between NO_x emissions and key engine and operational parameters, such as engine OPR, fuel flow and thrust, will be investigated using data from the ICAO Aircraft Engine Emissions Database. The analysis aims to identify how specific engine characteristics influence NO_x formation, thereby supporting the formulation of predictive models and regulatory strategies.

Figure 6.2 illustrates the relationship between the NO_x emission index at take-off (measured in g/kg of fuel) and the OPR of various aircraft engines, using data obtained from the ICAO Aircraft Engine Emissions Databank. An power function regression model was used to represent the general trend of NO_x formation with increasing OPR. Although the regression curve captures a general upward trend, the statistical indicators reveal significant limitations. The coefficient of determination R^2 is relatively low, indicating that the model explains only a small portion of the variability in the data. In addition, the MAPE is high, indicating significant deviations between predicted and actual values. Together, these metrics indicate a low predictive reliability of the fitted model.

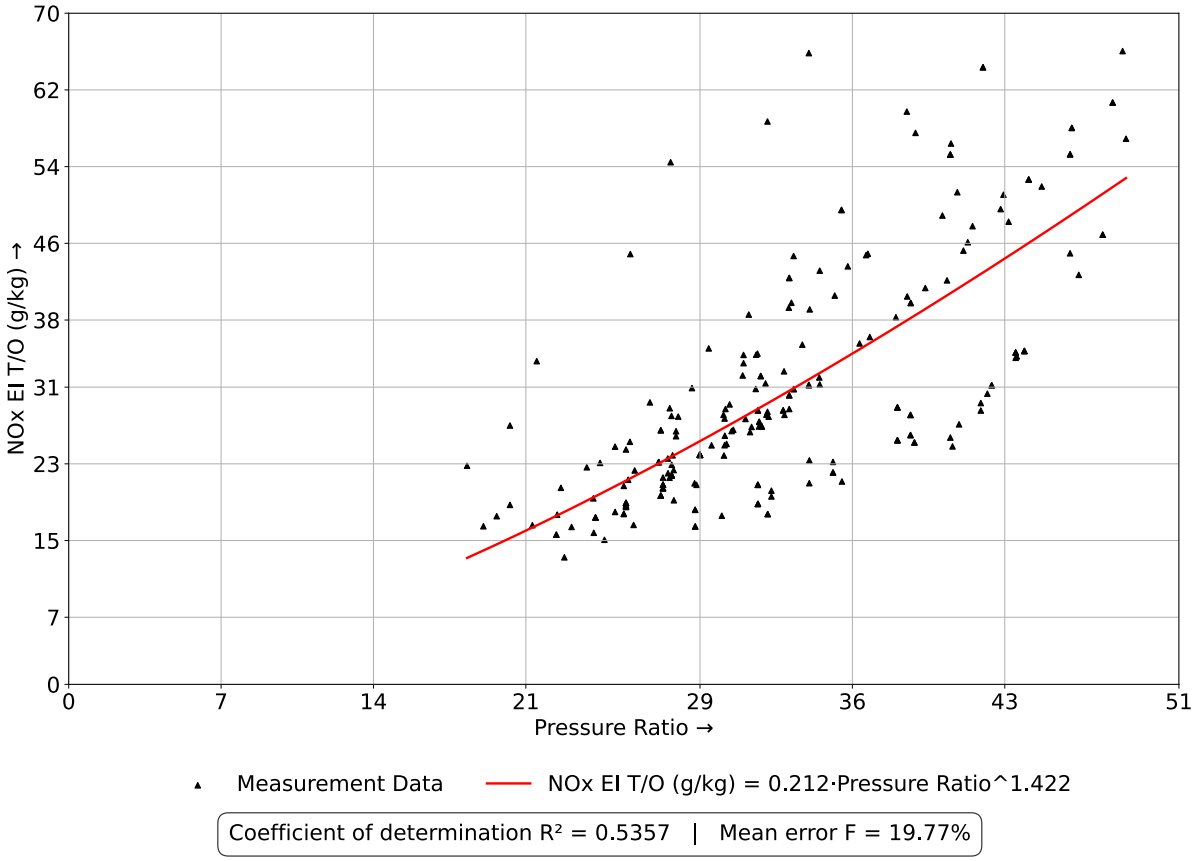

Figure 6.2: NO_x emission index at take-off (g NO_x per kg of fuel) as a function of Overall Pressure Ratio (OPR) for all engine configurations, with power-law regression fit.

This weak model performance implies that a simple power function is insufficient to describe the complex mechanisms governing NO_x emissions at take-off for a wide range of engine designs. A likely reason for this limitation is the inclusion of engines with fundamentally different combustor technologies within the same data set. These technologies may differ significantly in their NO_x formation behavior due to differences in flame temperature control, staged combustion, or lean-burn strategies. As a result, aggregating all engine types into a single graph introduces high variability and reduces the ability of the model to provide accurate generalizations.

In addition, the visual distribution of the data points reveals the presence of several apparent trends or "bands," with clusters of engines following different trajectories. This observation supports the hypothesis that engines with different combustion chamber technologies, such as conventional diffused flame, lean burn or staged combustion, have fundamentally different NO_x formation characteristics. The presence of such clusters suggests that the dataset contains heterogeneous engine types, each with specific emission behaviors. Consequently, a single-variable exponential model is insufficient and a more robust multivariate or classification-based approach is required.

Figure 6.3 shows the NO_x emissions index at take-off versus total OPR for a series of CFM International CFM56 turbofan engines. The dataset includes all publicly available CFM56 engine variants listed in the ICAO Aircraft Engine Emissions Databank.

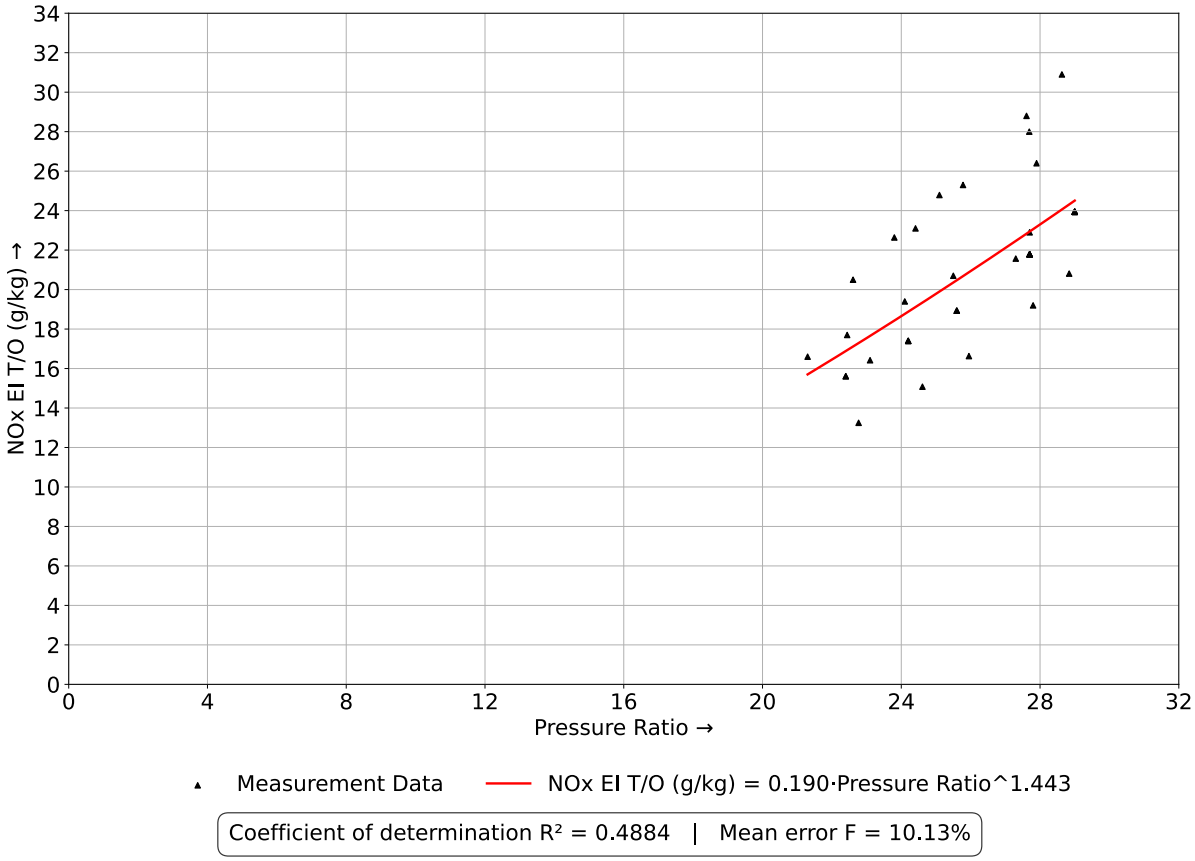

Figure 6.3: NO_x emission index at take-off (g NO_x per kg of fuel) as a function of OPR for CFM56 engine variants, based on ICAO data.

The plot reveals the presence of multiple distinct emission trajectories or "paths" within the data, suggesting that engines equipped with different combustor types follow separate emission characteristics as a function of OPR. This visual clustering further supports the hypothesis that combustor design plays a significant role in NO_x generation, and that grouping all configurations within a single model may blur meaningful distinctions. This collection of engines includes a range of combustion technologies, namely Single Annular Combustior (SAC), DAC (Double Annular Combustior), technology insert and model variants designated "E", each representing different stages of combustion technology evolution. The diversity of these designs results in notable differences in NO_x formation behavior.

Figure 6.4 focuses exclusively on CFM56 engines equipped with a DAC, isolating this specific technology from the broader data set. In contrast to the heterogeneous distribution observed in the previous figure, the data here show a much clearer exponential trend.

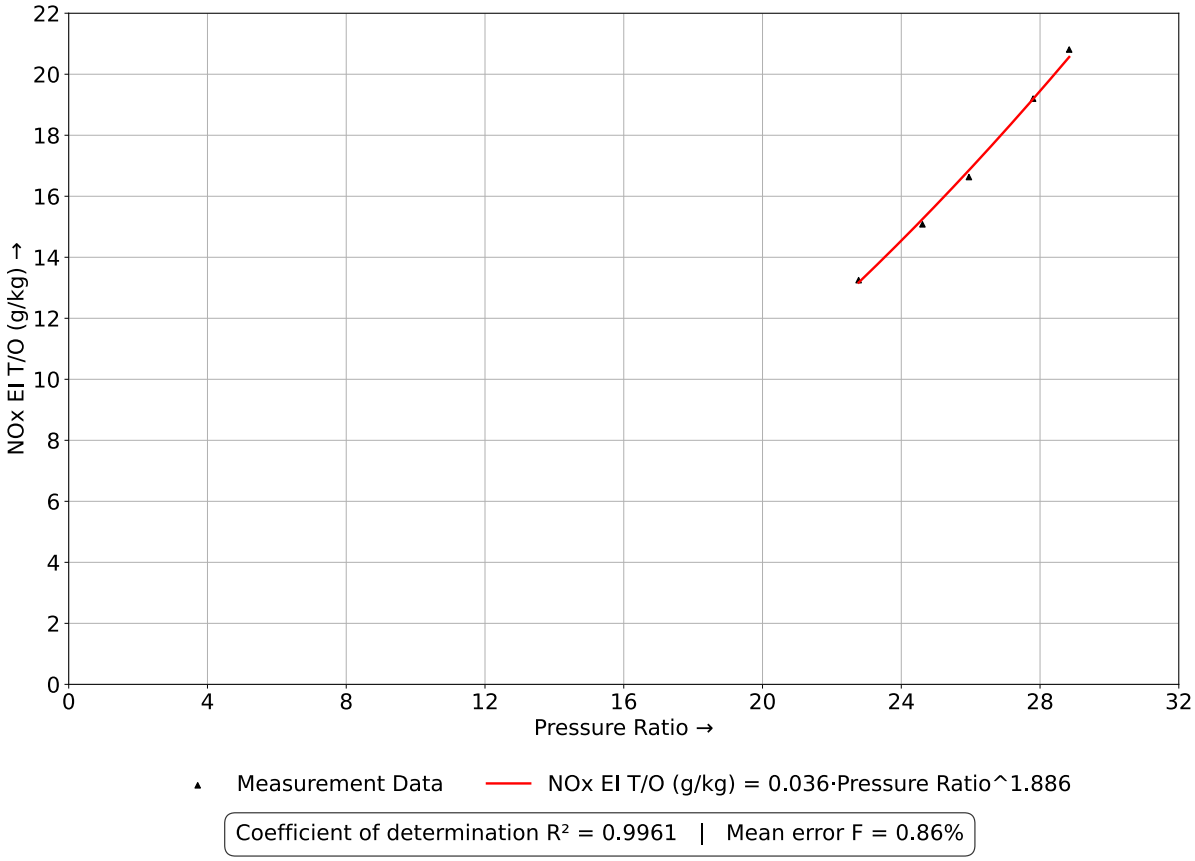

Figure 6.4: NO_x emission index at take-off (g NO_x per kg of fuel) as a function of OPR for CFM56 engines with DAC combustor configuration.

The regression fit applied to the DAC-only data set shows significantly improved model performance, as visually indicated by the reduced scatter and more coherent alignment of data points along the regression curve. This suggests that engines with the same combustor technology have more uniform NO_x formation characteristics with respect to the OPR. This result reinforces the earlier hypothesis that combining engines with different combustor designs into a single model introduces noise and reduces predictive accuracy. By narrowing the focus to a single combustor type, the influence of OPR on NO_x emissions becomes more discernible and statistically reliable. Such findings underscore the importance of stratifying emissions data by technology category when conducting regression-based analyses.

To further support the hypothesis that combustor technology significantly influences NO_x emission behavior, Figure 6.5 to Figure 6.8 presents four separate regression plots, each representing CFM56 engines with different technological configurations: SAC (Single Annular Combustor), TI, the "E" Enhanced variant, and engines with no specific combustor description. The "SAC" engines are equipped with a SAC, a standard configuration found on many earlier engine variants. The "DAC" engines, discussed in the previous section, feature a Dual Annular Combustor designed to reduce emissions through staged combustion. The TI engines include a modified High Pressure Compressor (HPC), an optimized SAC and an improved High Pressure Turbine (HPT). Finally, the "E" (Enhanced) variants feature a modified HPT and Low Pressure Turbine (LPT), focusing on efficiency and performance improvements rather than combustor redesign.

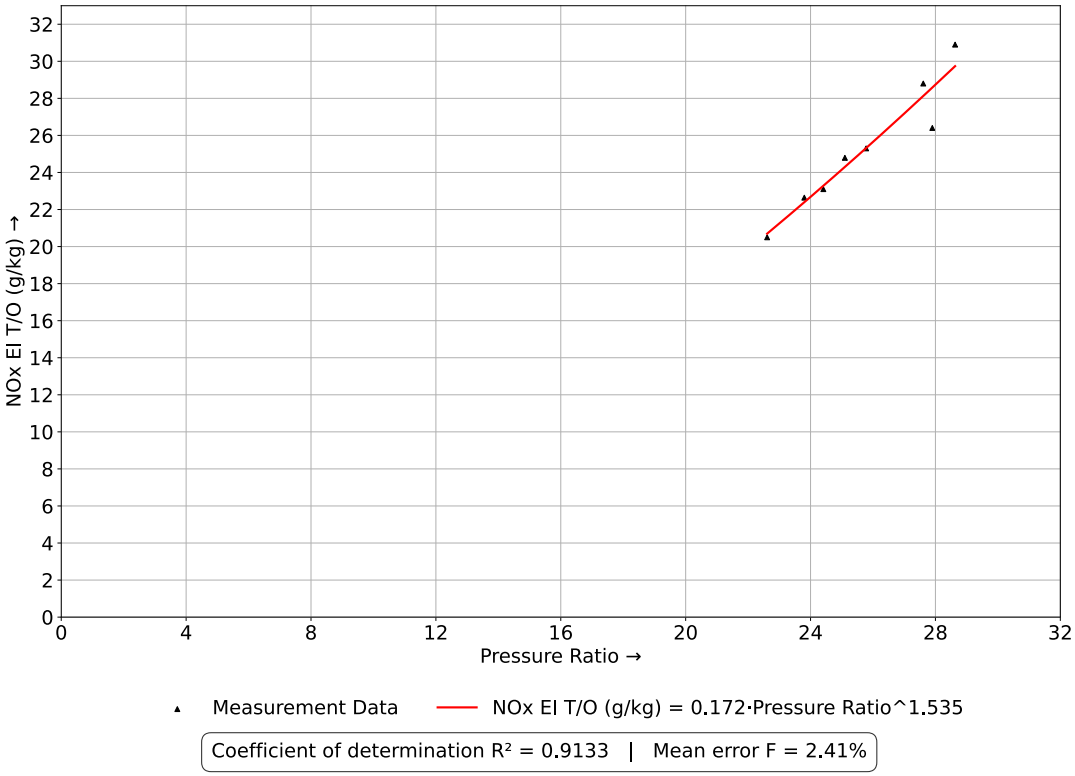

Figure 6.5: NO_x emission index at take-off (g NO_x per kg of fuel) as a function of OPR for CFM56 engines with SAC combustor configuration.

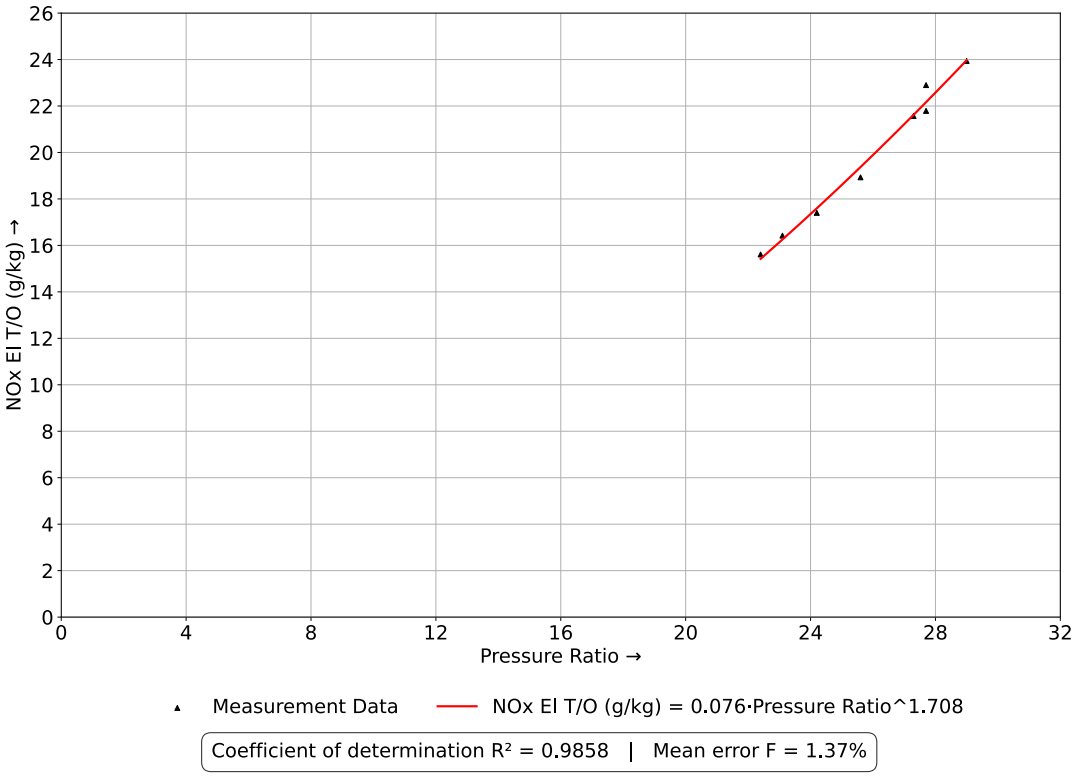

Figure 6.6: NO_x emission index at take-off (g NO_x per kg of fuel) as a function of OPR for CFM56 engines with TI combustor configuration.

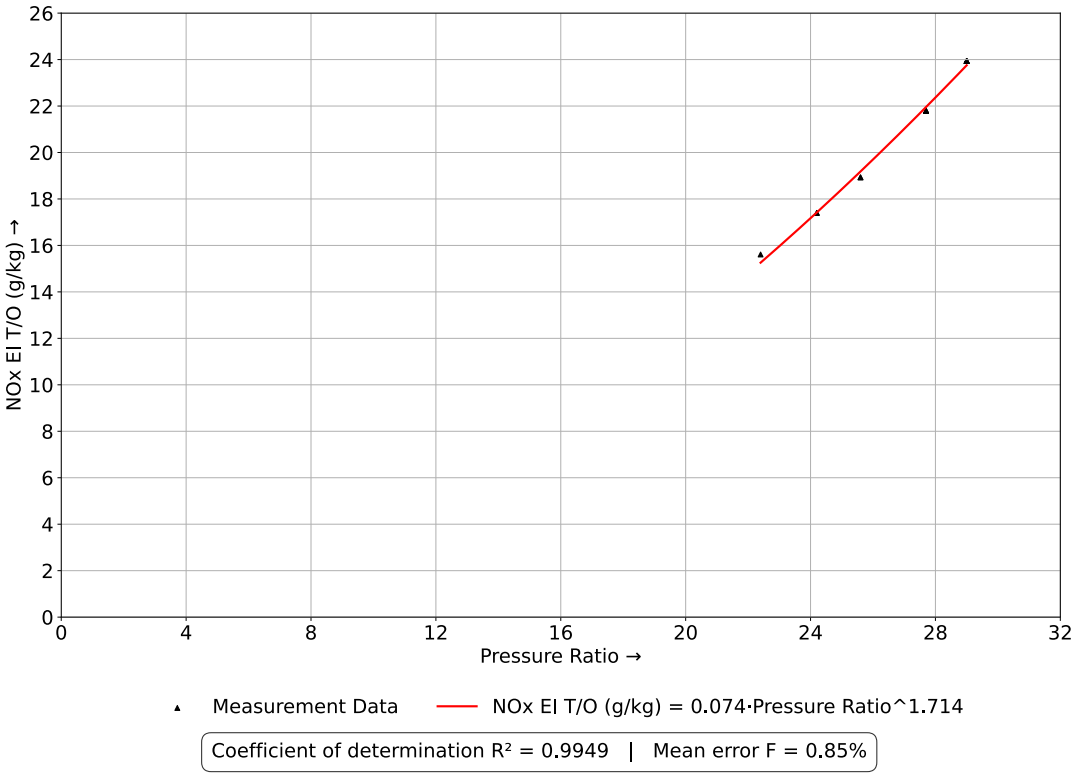

Figure 6.7: NO_x emission index at take-off (g NO_x per kg of fuel) as a function of OPR for CFM56 Enhanced (E) engine variants.

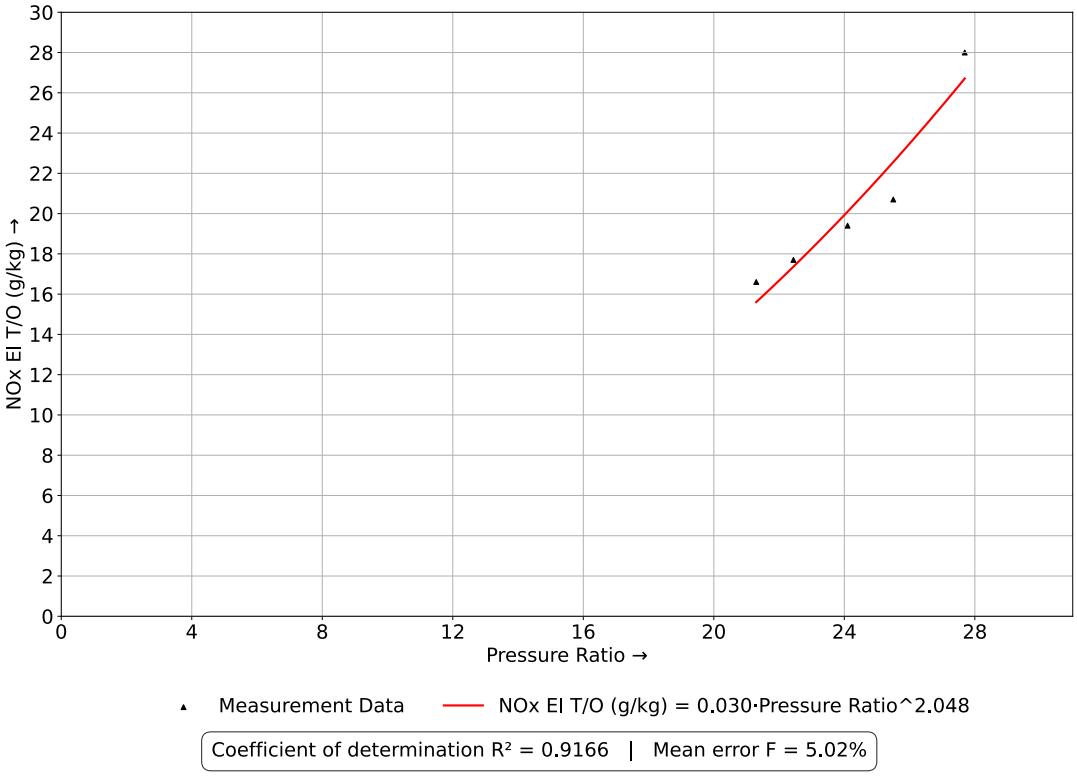

Figure 6.8: NO_x emission index at take-off (g NO_x per kg of fuel) as a function of OPR for CFM56 engine variants without specified combustor type.

Each plot shows the NO_x emission index at take-off as a function of the total OPR. In all

four cases, a dedicated power regression was applied to the respective subset of engines. As seen in the DAC example, the regression quality improves significantly when only engines with the same or similar combustor technology are included. The reduced data scatter and the visibly stronger curve fit in these subplots provide further support for the hypothesis that emissions are highly technology dependent. These results show that separating the data by combustor type reveals clear differences in NO_x emission behavior that cannot be captured by a single, combined model. The more consistent regression curves in each group suggest that combustor technology strongly influences how NO_x is formed. In the next sections of this thesis, this distinction will be used in all further regression analyses. The insights gained from this technology-based approach will help interpret and evaluate the results of all subsequent models.

The figures show that, across the range of OPR, engines using DAC technology have the lowest NO_x emission index at take-off. This trend is further quantified in Table 6.1, which summarizes the corresponding values at a representative pressure ratio of 24. For example, DAC engines emit approximately 14.43 g of NO_x per kg of fuel. The TI and Enhanced (E) combustor variants display very similar emission characteristics, with NO_x emission indices of 17.31 g/kg and 17.18 g/kg, respectively. Engines with SAC technology exhibit the highest NO_x value at this point, at around 22.60 g/kg, while engines without a specified combustor type produce 20.13 g/kg. However, SAC engines demonstrate a reduction in NO_x emissions beyond an OPR of approximately 30 and eventually outperform engines without a specified combustor type in this range.

Table 6.1: NO_x emission index at take-off for different combustor technologies at OPR = 24

Combustor Type	**$EI_{NO_x,TO}$ (g/kg fuel) at OPR = 24**	**Equation**
DAC	14.43	$EI_{NO_x,TO} = 0.036 \cdot \pi_{OPR}^{1.886}$
E	17.18	$EI_{NO_x,TO} = 0.074 \cdot \pi_{OPR}^{1.714}$
TI	17.31	$EI_{NO_x,TO} = 0.076 \cdot \pi_{OPR}^{1.708}$
Unspec. combustor	20.13	$EI_{NO_x,TO} = 0.030 \cdot \pi_{OPR}^{2.048}$
SAC	22.60	$EI_{NO_x,TO} = 0.172 \cdot \pi_{OPR}^{1.535}$

Figure 6.9 shows the relationship between total OPR and rated thrust (in kN) for the CFM56 engine variants mentioned above. The data show a nearly linear relationship between these two parameters, indicating that as thrust increases, the corresponding OPR increases in a consistent manner. This linear trend suggests that higher-thrust variants of the CFM56 family are generally equipped with more advanced compressors capable of achieving higher OPRs. This design approach is typical in turbofan engine development, where higher compression allows for more efficient combustion and consequently higher thrust. The clear and continuous nature of this relationship underscores the strong link between thermodynamic performance and engine size within the same engine family.

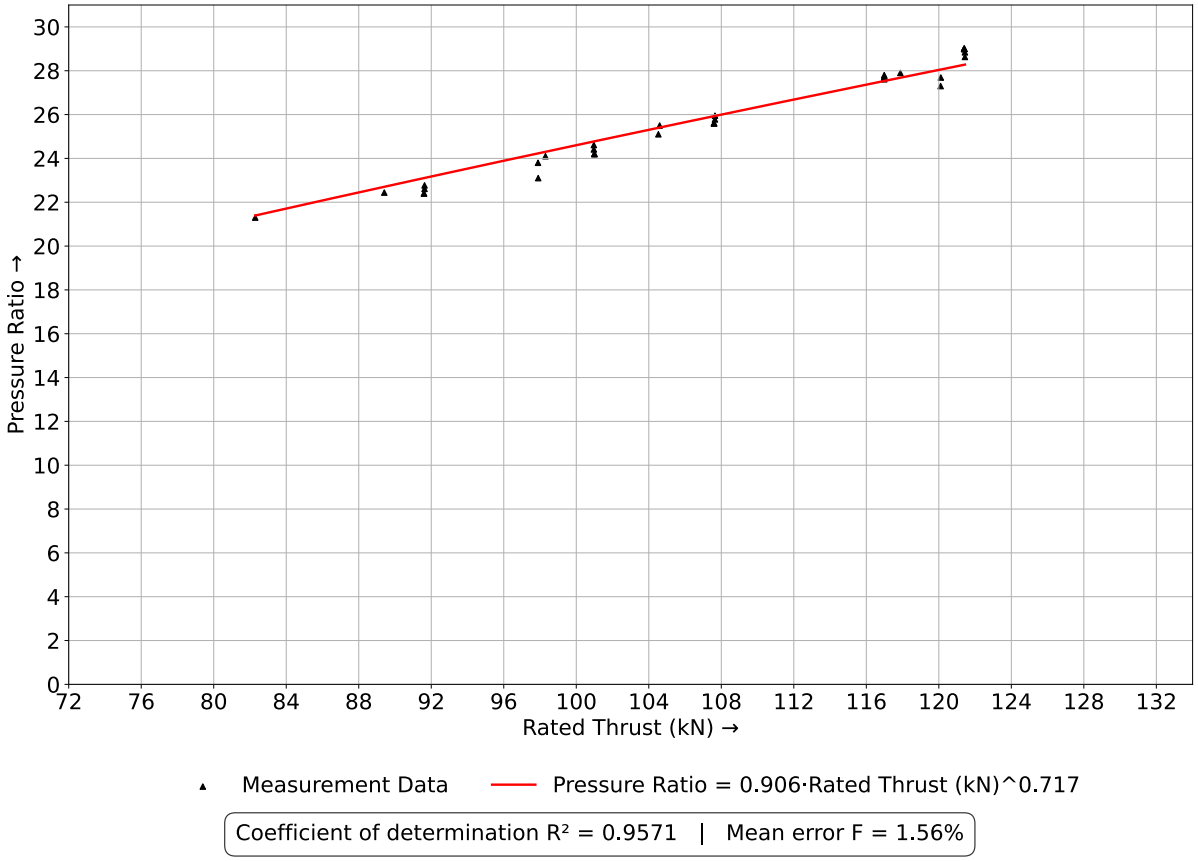

Figure 6.9: OPR in relation to rated thrust for CFM56 engine variants.

Figure 6.10 shows the correlation between the Take-off NO_x emission index and the rated thrust (in kN) for CFM56 "E" series engines. A clear quadratic trend is evident, indicating that NO_x emissions increase more than proportionally with thrust. This pattern can be explained by considering the previously observed relationship between thrust and OPR (see Figure 6.9). As thrust increases, engines operate at higher OPRs, resulting in higher combustion temperatures and increased NO_x formation rates. The quadratic shape of the curve reflects the combined effect of increasing fuel flow and more intense thermodynamic conditions in the combustor.

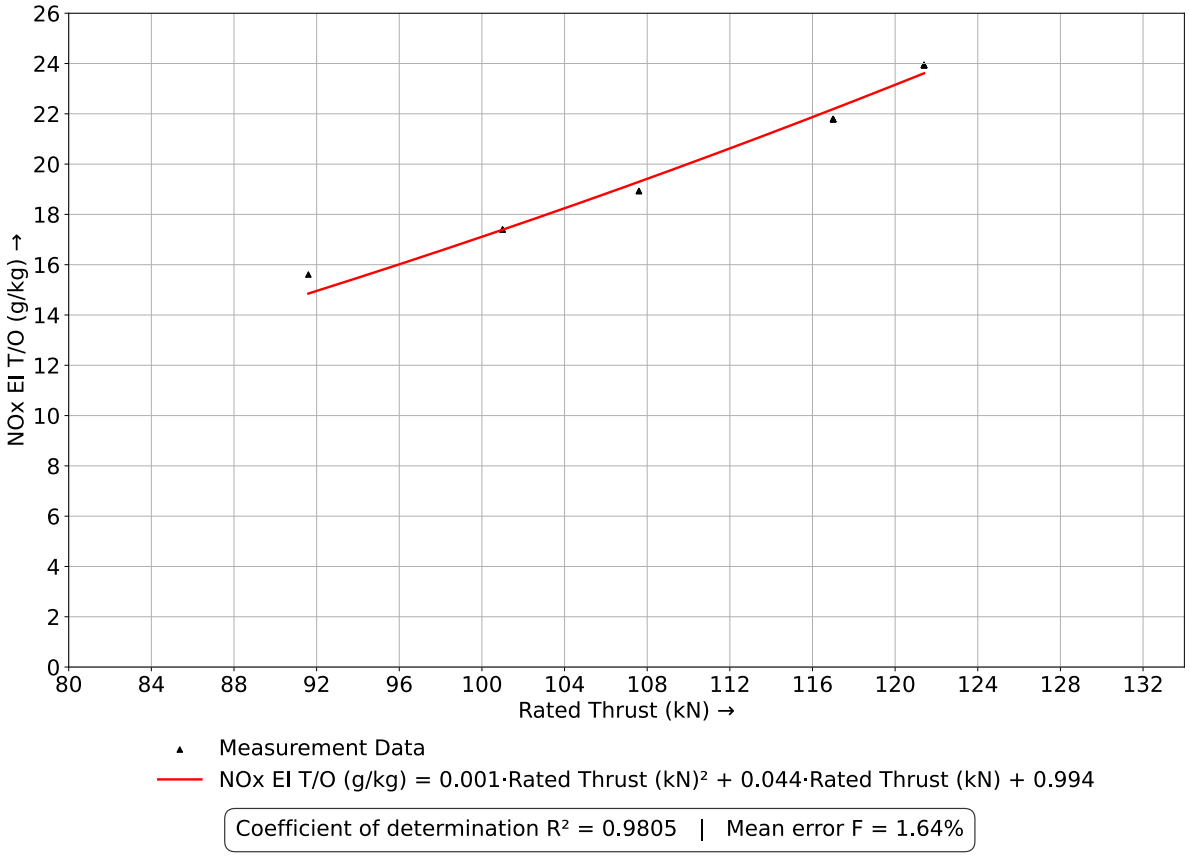

Figure 6.10: NO_x emission index at take-off in relation to rated thrust for CFM56 E-variant engines.

In summary, this analysis shows that NO_x emission behavior at take-off is strongly influenced by design-specific factors, such as combustor configuration, and performance-related parameters, such as OPR and thrust.

Beyond take-off, NO_x emissions during other flight phases, particularly cruise, are also relevant for environmental impact assessments. While this chapter focuses on take-off conditions due to their regulatory importance and data availability, supplementary analyses were performed for NO_x emissions during cruise and across the full LTO cycle. Figure 6.11 shows the total NO_x emissions over the entire LTO cycle as a function of the OPR for various CFM56 engine variants. The LTO values represent the cumulative mass of NO_x produced during the standardized ICAO operational phases (idle, approach, climb-out, and take-off), offering a more comprehensive picture of real-world airport-level emissions.

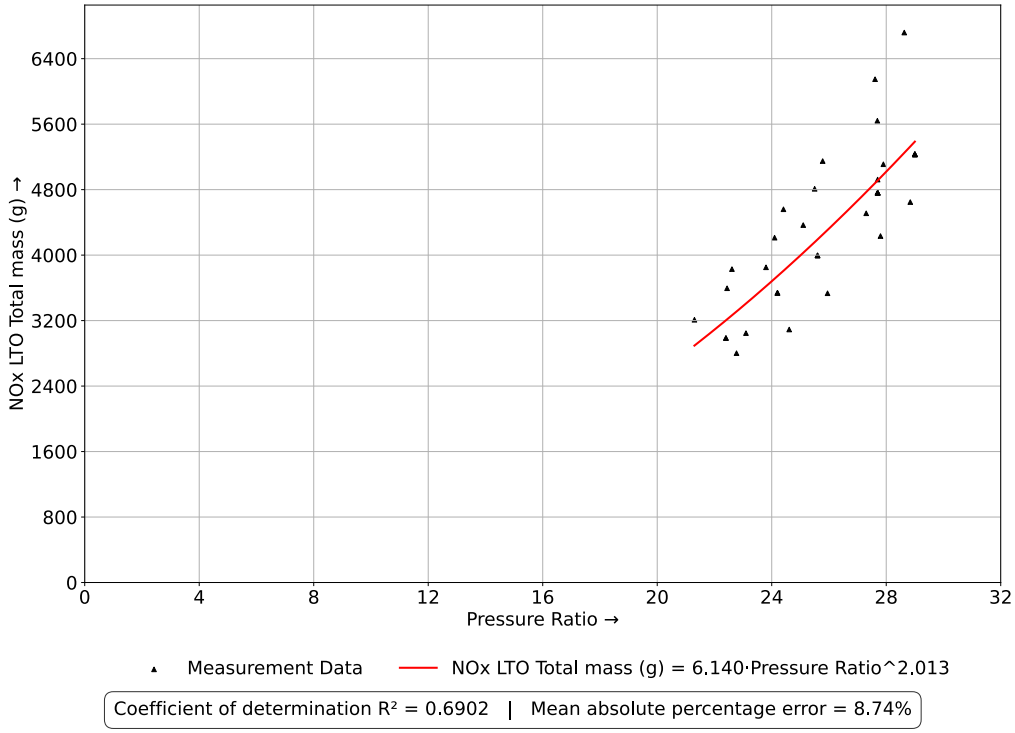

Figure 6.11: Total NO_x mass over the full LTO cycle in relation to OPR for CFM56 engines.

The data reveal a clear positive correlation between OPR and total NO_x emissions across the LTO cycle. This trend is consistent with earlier findings based on take-off emissions and supports the general thermodynamic understanding that higher OPRs typically lead to higher combustion temperatures and increased NO_x formation. However, the LTO-based perspective integrates engine performance across multiple power settings, providing a more balanced view of emissions performance than take-off data alone. The distribution also reveals clustering effects, indicating that combustor type and engine subvariant continue to play significant roles. Nevertheless, using aggregated LTO data helps mitigate phase-specific variability and provides a meaningful basis for comparing the overall environmental impact of engines. This finding reinforces the utility of OPR as a robust predictor of NO_x emissions, even beyond single operating conditions.

Figure 6.12 illustrates the relationship between the total NO_x mass emitted over the entire LTO cycle and the rated thrust (in kN) for CFM56 engines. Similar to the previous diagram, the values represent the cumulative NO_x emissions across all ICAO-defined LTO phases, thereby reflecting the complete near-ground emission behavior of the engines.

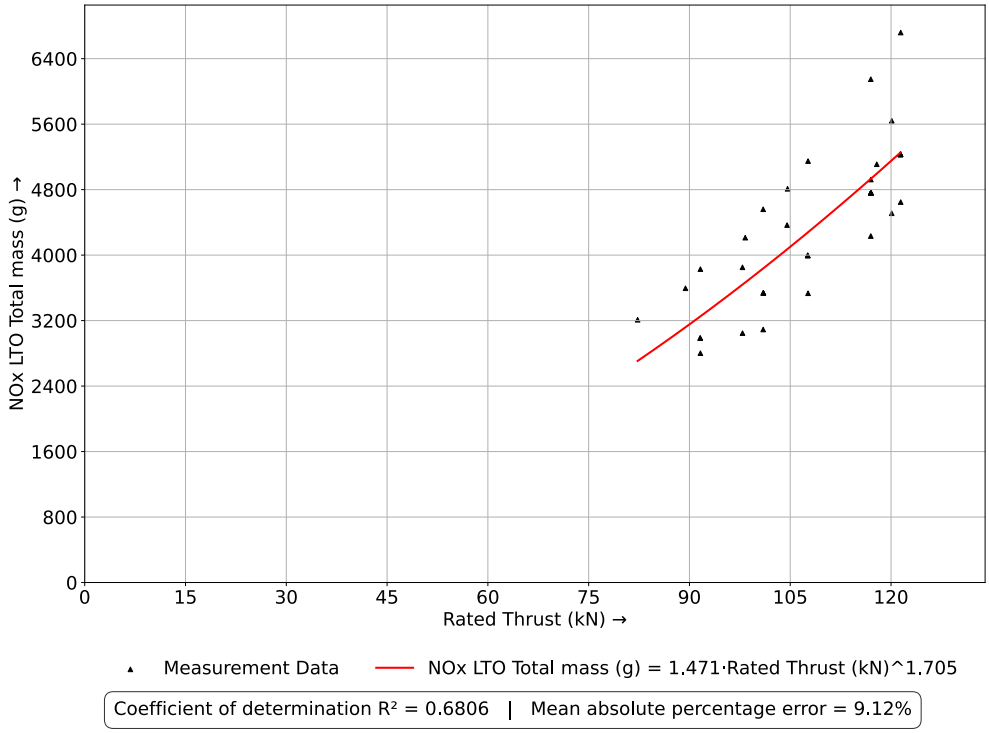

Figure 6.12: Total NO_x mass over the full LTO cycle in relation to rated thrust for CFM56 engines.

The plot reveals a strong upward trend, indicating that engines with higher rated thrust produce significantly more NO_x emissions over the full LTO cycle. This observation aligns with physical expectations, as higher-thrust engines generally consume more fuel and exhibit higher thermal loads, both of which are primary contributors to NO_x formation. Interestingly, the increase in NO_x appears to be more than linear, suggesting that emission growth accelerates with increasing engine size or thrust class. This behavior may stem from the combined effects of increased fuel flow, higher OPRs, and greater engine core dimensions, all of which intensify combustion conditions. These findings underscore the importance of considering thrust class when comparing or regulating aircraft engine emissions.

To further investigate the influence of combustor design on overall NO_x production, the total NO_xmass emitted over the full LTO cycle was plotted against the OPR for different CFM56 subgroups, each representing a distinct combustor technology. Figures 6.13 through 6.16 show separate regressions for the SAC, Dual Annular Combustor (DAC), Enhanced (E), and TI variants.

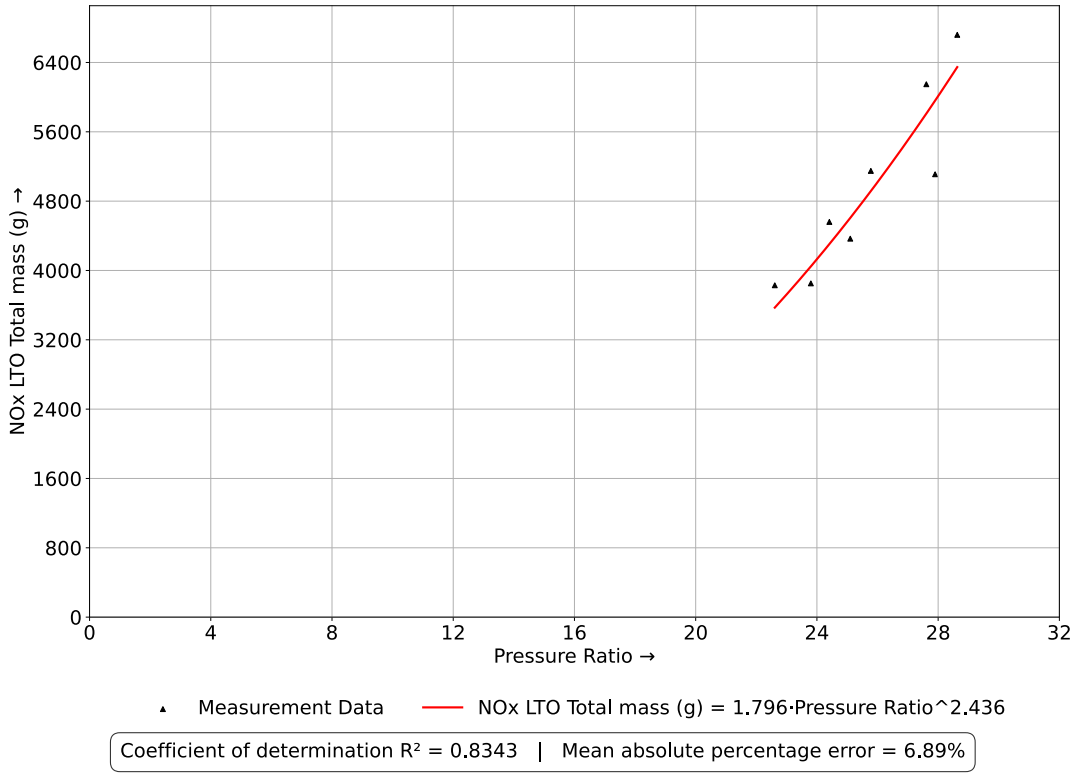

Figure 6.13: Total NO_x mass over the LTO cycle in relation to OPR for CFM56 engines with SAC combustor.

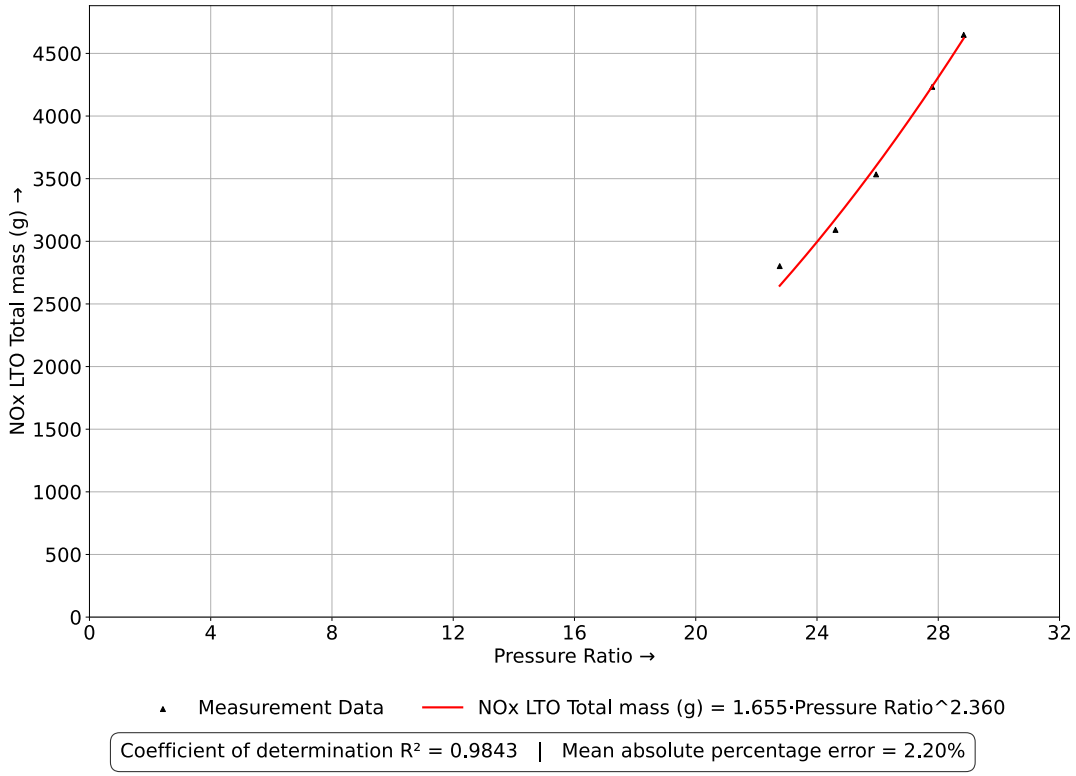

Figure 6.14: Total NO_x mass over the LTO cycle in relation to OPR for CFM56 engines with DAC combustor.

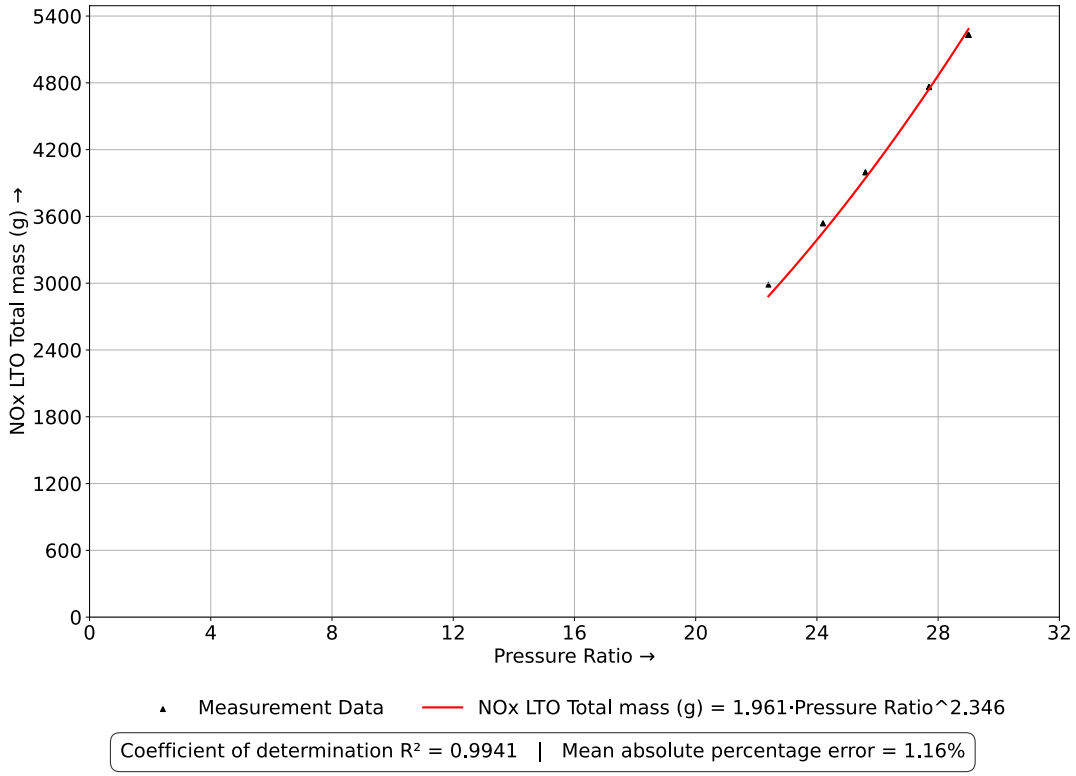

Figure 6.15: Total NO_x mass over the LTO cycle in relation to OPR for CFM56 engines with Enhanced (E) configuration.

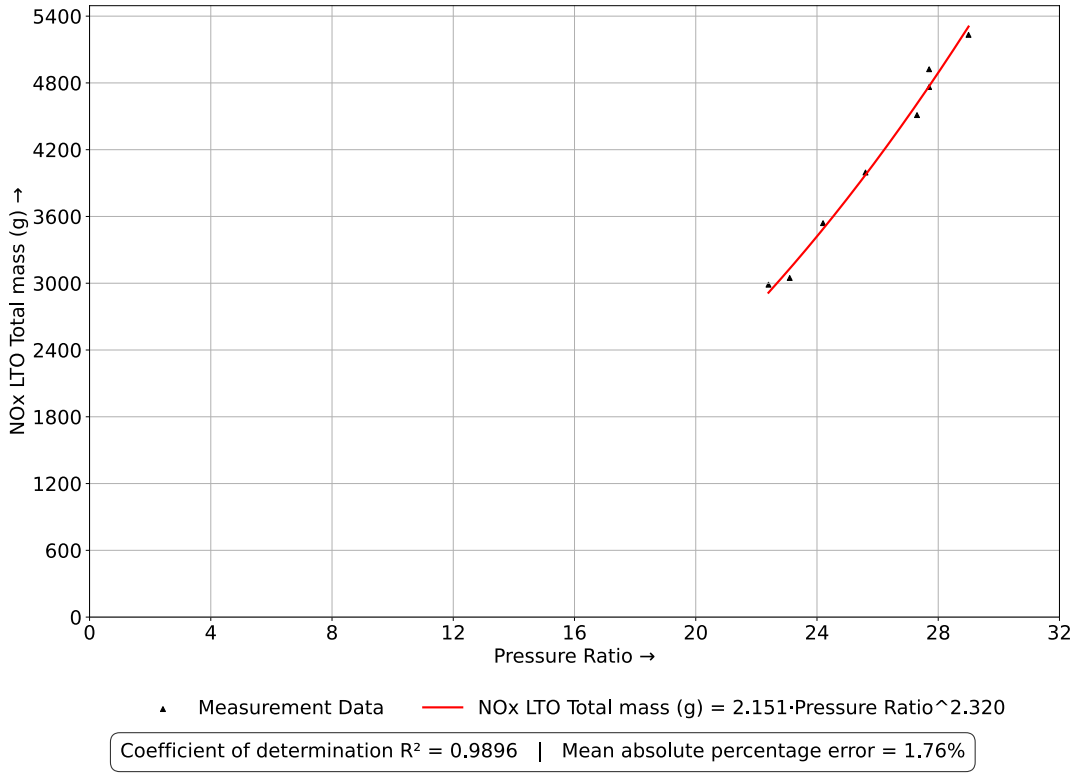

Figure 6.16: Total NO_x mass over the LTO cycle in relation to OPR for CFM56 engines with TI configuration.

An increasing trend of LTO NO_x emissions with higher OPRs is clearly visible across all sub-types. However, the magnitude and slope of the increase differ among combustor types. SAC engines show a moderate but steady increase, while DAC and TI variants exhibit steeper rises, consistent with their design focus on reducing emissions under specific operating conditions, such as take-off, but less so across the full LTO cycle. The Enhanced (E) variants, although optimized for efficiency, still present considerable NO_x output at higher OPRs. This suggests that improvements in fuel burn do not necessarily correlate with lower NO_x in all phases of operation. These differences highlight the importance of distinguishing between combustor technologies when analyzing emission behavior. Even when the engines share the same core architecture (as in the CFM56 family), the variation in NO_x formation across configurations is significant. Therefore, technology-specific modeling is essential for accurately characterizing emissions performance in regulatory or design contexts.

To conclude the analysis of NO_x emissions over the LTO cycle, Figure 6.17 presents a combined evaluation of all 50 engines and their respective sub-variants, without stratification by combustor type. This comprehensive view enables direct comparison with earlier, more specific analyses and illustrates the effect of engine diversity on model quality.

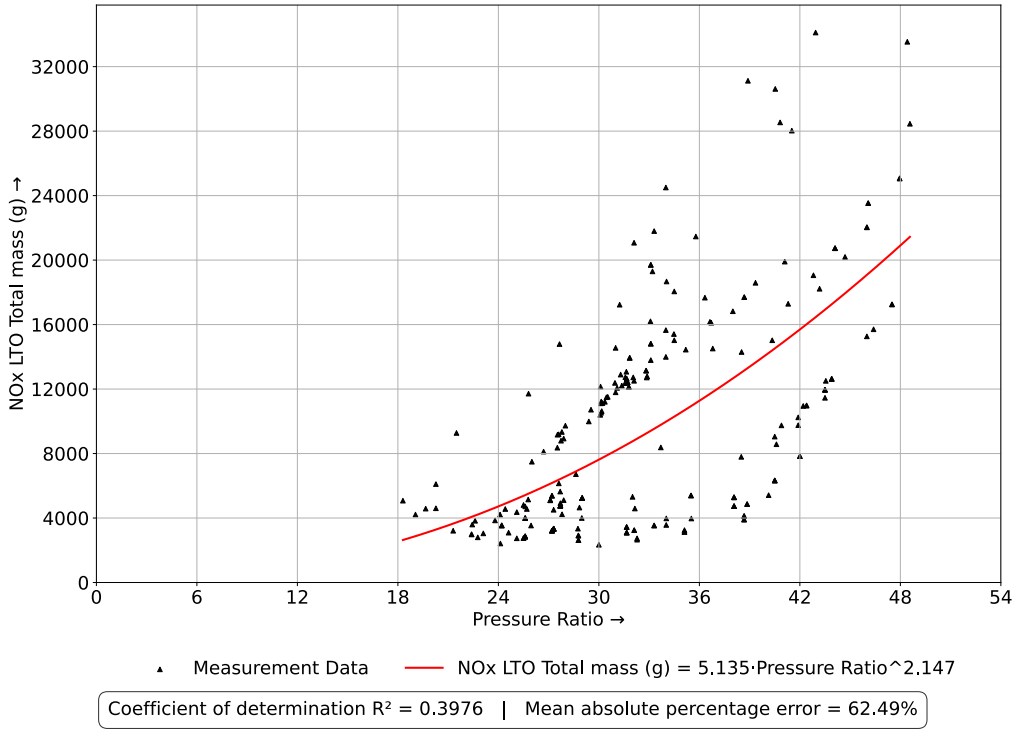

Figure 6.17: Total NO_x mass over the LTO cycle in relation to OPR for all 50 engine configurations.

Figure 6.18 builds on the correlation analysis presented in Figure 6.17 by introducing a classification of NO_x emissions based on combustor technology. Each data point is colour-coded according to the combustor technology employed (e.g. TAPS II, LEC or SAC), and individual trendlines have been fitted for each group. This refined analysis highlights the importance of considering technological context when modelling or predicting NO_x emissions, as purely pressure-based regressions are insufficient for accurate assessments.

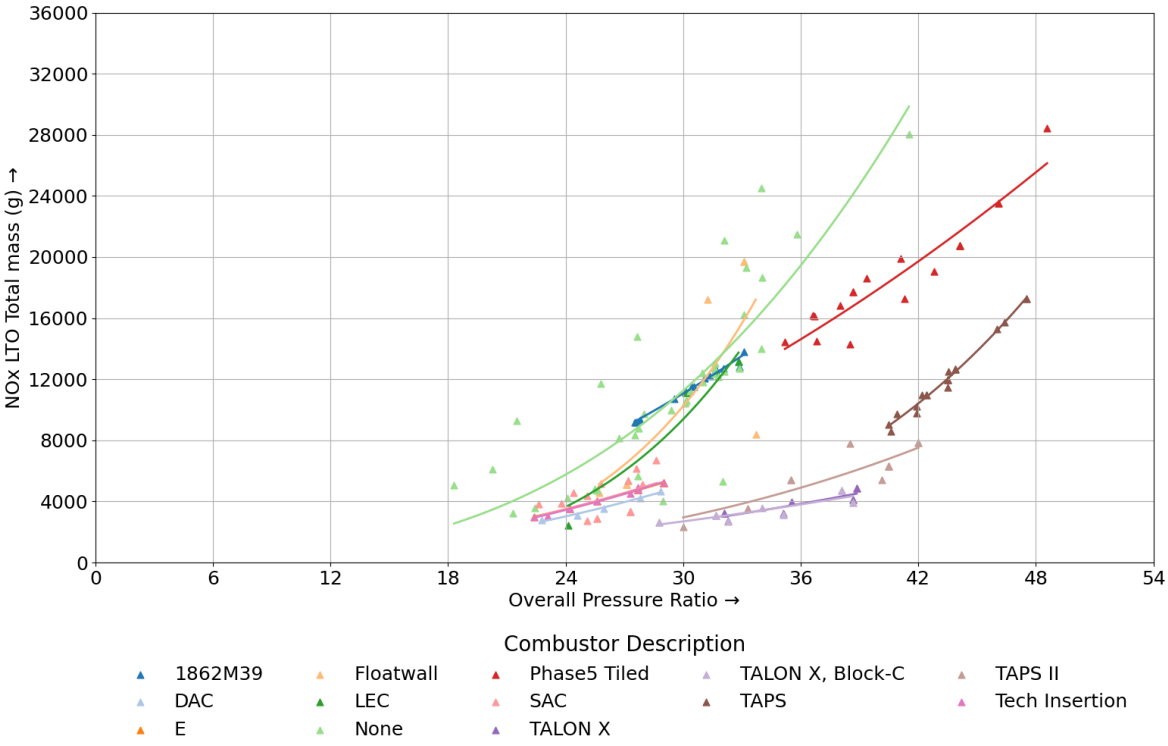

Figure 6.18: Differentiated representation of NO_x mass over the LTO cycle as a function of OPR, categorized by combustor technology.

Even when engines operate at similar OPR values, the measured NO_x emissions can differ significantly. This suggests that the type of combustor used has a significant impact on emission levels. Modern low-emission technologies such as TAPS, TAPS II or LEC produce considerably less NO_x than older or conventional designs such as Phase5 Tiled. The 'none' category has no special combustor description and can also be considered conventional. Table 6.2 shows the regression equation for the analysed combustors in Figure 6.18. It should be noted that not all combustor variants were analysed due to insufficient data points for a reasonable regression.

Table 6.2: Power-law regression equations for total NO_x mass emissions of different combustor types as a function of OPR

Combustor Type	**Equation**	R^2	MAPE (%)
1862M39	$NO_{x,\mathrm{LTO}} = 8.4138 \cdot \pi_{\mathrm{OPR}}{}^{2.1115}$	0.9794	1.00
DAC	$NO_{x,\mathrm{LTO}} = 2.0706 \cdot \pi_{\mathrm{OPR}}{}^{2.2920}$	0.9851	2.27
E	$NO_{x,\mathrm{LTO}} = 3.5853 \cdot \pi_{\mathrm{OPR}}{}^{2.1641}$	0.9997	0.23
Floatwall	$NO_{x,\mathrm{LTO}} = 0.0027 \cdot \pi_{\mathrm{OPR}}{}^{4.4585}$	0.5961	33.55
LEC	$NO_{x,\mathrm{LTO}} = 0.0051 \cdot \pi_{\mathrm{OPR}}{}^{4.2434}$	0.9388	16.21
None	$NO_{x,\mathrm{LTO}} = 0.4131 \cdot \pi_{\mathrm{OPR}}{}^{3.0026}$	0.6975	27.25
Phase5 Tiled	$NO_{x,\mathrm{LTO}} = 13.918 \cdot \pi_{\mathrm{OPR}}{}^{1.9412}$	0.8874	5.69
SAC	$NO_{x,\mathrm{LTO}} = 2.7534 \cdot \pi_{\mathrm{OPR}}{}^{2.2485}$	0.2084	25.85
TALON X	$NO_{x,\mathrm{LTO}} = 2.0353 \cdot \pi_{\mathrm{OPR}}{}^{2.1049}$	0.8034	8.27
TALON X, Block-C	$NO_{x,\mathrm{LTO}} = 4.3019 \cdot \pi_{\mathrm{OPR}}{}^{1.8930}$	0.7531	9.21
TAPS	$NO_{x,\mathrm{LTO}} = 0.0021 \cdot \pi_{\mathrm{OPR}}{}^{4.1307}$	0.9875	1.89
TAPS II	$NO_{x,\mathrm{LTO}} = 0.2323 \cdot \pi_{\mathrm{OPR}}{}^{2.7783}$	0.7880	12.62
Tech Insertion	$NO_{x,\mathrm{LTO}} = 2.4790 \cdot \pi_{\mathrm{OPR}}{}^{2.2764}$	0.9899	1.62

In addition to OPR, total fuel consumption during the LTO cycle is a relevant predictor of NO_x emissions. Figure 6.19 shows a power-law relationship between NO_x mass and LTO fuel use, described by:

$$NO_{x,\mathrm{LTO}} = 0.237 \cdot m_{\mathrm{f,LTO}}{}^{1.627} \tag{6.1}$$

This fit has a coefficient of determination of $R^2 = 0.8823$ and a MAPE of 17.75 %. The exponent greater than 1 indicates a more than proportional increase in NO_x with fuel consumption. This supports using fuel burn as a proxy for emissions when detailed engine data are unavailable.

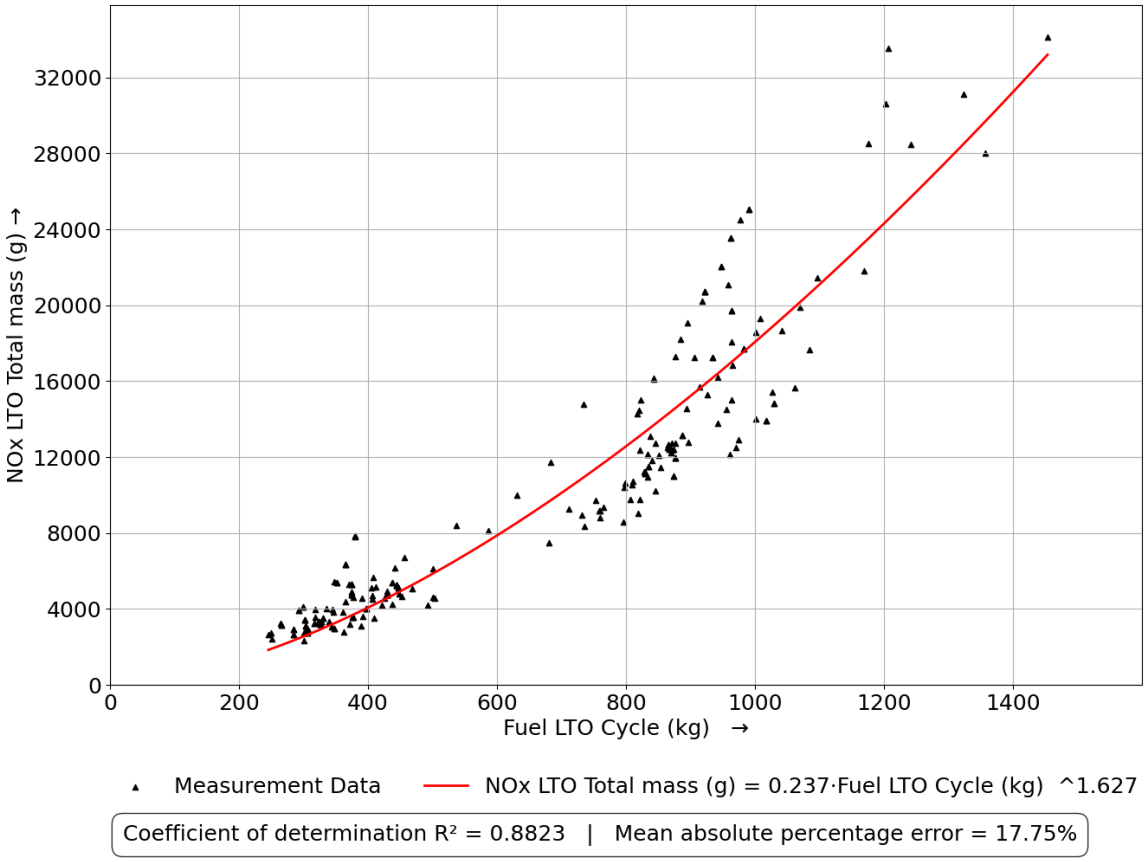

Figure 6.19: Total NO_x mass over the LTO cycle in relation to fuel consumption per cycle for all 50 engine configurations.

Further analyses and additional graphical models related to NO_x emissions, including those concerning cruise conditions, are provided in the appendix. To maintain the focus and scope of the present section, these complementary materials are not discussed in detail here.

Table 6.3 presents the best performing regression models for estimating NO_x emissions during the LTO cycle across a range of combustor technologies. Each model is expressed as a power law function of one or more operational parameters such as fuel flow rate at cruise ($\dot{m}_{f,Cr}$), LTO fuel mass ($m_{f,LTO}$) or overall pressure ratio (π_{OPR}), selected based on their physical relevance and statistical performance. The models were chosen according to the highest coefficient of determination (R^2) and the lowest MAPE.

Tables 6.4 and 6.5 present the best performing regression models for estimating the NO_x emission index at take-off and cruise. In both cases, the models are selected based on their coefficient of determination (R^2) and MAPE.

Table 6.3: Top regression models for estimating NO_x emissions during the LTO cycle across different combustor types, selected by highest R^2 and lowest MAPE.

Combustor Type	**Equation**	R^2	MAPE (%)
1862M39	$NO_{x,LTO} = 26210 \cdot \dot{m}_{f,Cr}{}^{1.56}$	0.9900	0.91
DAC	$NO_{x,LTO} = 0.0017 \cdot m_{f,LTO}{}^{2.424}$	0.9878	2.04
E	$NO_{x,LTO} = 31720 \cdot \dot{m}_{f,Cr}{}^{1.539}$	0.9998	0.23
Floatwall	$NO_{x,LTO} = 32660 \cdot \dot{m}_{f,Cr}{}^{1.333}$	0.9985	2.28
LEC	$NO_{x,LTO} = 22780 \cdot \dot{m}_{f,Cr}{}^{1.275}$	0.9984	1.93
None	$NO_{x,LTO} = 0.2779 \cdot m_{f,LTO}{}^{1.599}$	0.8642	13.49
Phase5 Tiled	$NO_{x,LTO} = 13.92 \cdot \pi_{OPR}{}^{1.941}$	0.8874	5.69
SAC	$NO_{x,LTO} = 0.0298 \cdot m_{f,LTO}{}^{2.005}$	0.9752	2.86
TALON X	$NO_{x,LTO} = 2.035 \cdot \pi_{OPR}{}^{2.105}$	0.8034	8.27
TALON X, Block-C	$NO_{x,LTO} = 26750 \cdot \dot{m}_{f,Cr}{}^{1.244}$	0.8231	8.69
TAPS	$NO_{x,LTO} = 0.0021 \cdot \pi_{OPR}{}^{4.131}$	0.9875	1.89
TAPS II	$NO_{x,LTO} = 3.0889 \cdot 10^{-10} \cdot m_{f,LTO}{}^{5.196}$	0.9902	2.46
Tech Insertion	$NO_{x,LTO} = 32180 \cdot \dot{m}_{f,Cr}{}^{1.54}$	0.9912	1.63

Table 6.4: Top regression models for predicting the NO_x emission index at take-off ($EI_{NO_x,TO}$) across combustor technologies, selected by highest R^2 and lowest MAPE.

Combustor Type	**Equation**	R^2	MAPE (%)
1862M39	$EI_{NO_x,TO} = 46.93 \cdot \dot{m}_{f,Cr}{}^{1.114}$	0.9116	2.13
DAC	$EI_{NO_x,TO} = 0.0127 \cdot \pi_{OPR}{}^{2.208}$	0.9992	1.78
E	$EI_{NO_x,TO} = 0.0672 \cdot \pi_{OPR}{}^{1.743}$	0.9951	0.83
Floatwall	$EI_{NO_x,TO} = 55.46 \cdot \dot{m}_{f,Cr}{}^{0.618}$	0.9381	5.72
LEC	$EI_{NO_x,TO} = 33.56 \cdot \dot{m}_{f,Cr}{}^{0.427}$	0.9651	2.72
None	$EI_{NO_x,TO} = 0.5811 \cdot \pi_{OPR}{}^{1.191}$	0.3109	18.38
Phase5 Tiled	$EI_{NO_x,TO} = 0.1123 \cdot \pi_{OPR}{}^{1.622}$	0.8793	4.73
SAC	$EI_{NO_x,TO} = 0.0258 \cdot m_{f,LTO}{}^{1.150}$	0.9180	3.70
TALON X	$EI_{NO_x,TO} = 0.0236 \cdot \pi_{OPR}{}^{1.922}$	0.8730	5.65
TALON X, Block-C	$EI_{NO_x,TO} = 0.0787 \cdot \pi_{OPR}{}^{1.587}$	0.9983	0.63
TALON X, Block-D	$EI_{NO_x,TO} = 177.1 \cdot \dot{m}_{f,Cr}{}^{1.294}$	0.9981	0.79
TAPS	$EI_{NO_x,TO} = 2.266 \cdot \dot{m}_{f,Cr}{}^{2.934}$	0.9845	1.90
TAPS II	$EI_{NO_x,TO} = 3954 \cdot \dot{m}_{f,Cr}{}^{3.027}$	0.9574	6.36
Tech Insertion	$EI_{NO_x,TO} = 0.0761 \cdot \pi_{OPR}{}^{1.708}$	0.9858	1.37

Table 6.5: Top regression models for estimating the NO_x emission index at cruise ($EI_{NO_x,Cr}$) across combustor technologies, selected by highest R^2 and lowest MAPE.

Combustor Type	**Equation**	R^2	MAPE (%)
1862M39	$EI_{NO_x,Cr} = 0.0001 \cdot {T_{TO}}^{2.061}$	0.2434	13.07
DAC	$EI_{NO_x,Cr} = 17.72 \cdot {\dot{m}_{f,Cr}}^{0.523}$	0.9997	0.54
E	$EI_{NO_x,Cr} = 0.2618 \cdot {m_{f,LTO}}^{0.615}$	0.4667	3.25
Floatwall	$EI_{NO_x,Cr} = 24.83 \cdot {\dot{m}_{f,Cr}}^{0.439}$	0.9308	5.33
LEC	$EI_{NO_x,Cr} = 10.46 \cdot {\dot{m}_{f,Cr}}^{0.088}$	0.0559	17.07
None	$EI_{NO_x,Cr} = 13.33 \cdot {\dot{m}_{f,Cr}}^{-0.012}$	0.0002	35.17
Phase5 Tiled	$EI_{NO_x,Cr} = 0.1370 \cdot {\pi_{OPR}}^{1.370}$	0.8328	5.20
SAC	$EI_{NO_x,Cr} = 6.236 \cdot {T_{TO}}^{0.176}$	0.3951	2.76
TALON X	$EI_{NO_x,Cr} = 0.3185 \cdot {\pi_{OPR}}^{1.052}$	0.4177	9.11
TALON X, Block-C	$EI_{NO_x,Cr} = 0.6064 \cdot {\pi_{OPR}}^{0.880}$	0.4764	7.00
TALON X, Block-D	$EI_{NO_x,Cr} = 81.25 \cdot {\dot{m}_{f,Cr}}^{1.072}$	0.9280	3.84
TAPS	$EI_{NO_x,Cr} = 67.33 \cdot {\dot{m}_{f,Cr}}^{2.986}$	0.9460	3.54
TAPS II	$EI_{NO_x,Cr} = 1079 \cdot {\dot{m}_{f,Cr}}^{2.627}$	0.8482	8.51
Tech Insertion	$EI_{NO_x,Cr} = 0.0710 \cdot {\pi_{OPR}}^{1.479}$	0.9847	4.34

The performance of the presented regression models should be interpreted in the context of how the data is distributed across different types of combustor. The number of data points available for model fitting varies widely. From a minimum of five for the LEC combustor to a maximum of 40 for engines with no specified combustor technology (none). Other combustor types have between six and 26 data points, including DAC (6), TALON-X (9), Tech Insertion (8), 1862M39 (17), E (16), Floatwall (10), SAC (15), TAPS (20), Phase5 Tiled (26), TALON-X Block C (14), TALON-X Block D (9) and TAPS-II (12).

6.3 Regression Analysis of NO_x Emission Dependencies

This section uses regression models to quantify the dependencies between NO_x emissions and influencing factors such as OPR, rated thrust, fuel flow and combustor technology. This provides deeper insights into predictive modeling and the physical mechanisms of NO_x formation.

Figure 6.20 presents a multivariate regression analysis of CFM56 engines. OPR and rated thrust are used as independent variables to model the NO_x emission index at take-off. The left side of the figure shows the actual data points in three-dimensional space. The right side illustrates the fitted regression surface based on the power-law equation.

$$\mathrm{EI}_{\mathrm{NO_x,TO}} = 0.762 \cdot {\pi_{\mathrm{OPR}}}^{0.577} \cdot {T_{\mathrm{TO}}}^{0.307} \tag{6.2}$$

The model shows an overall upward trend: higher OPRs and greater thrust levels lead to increased NO_x formation.

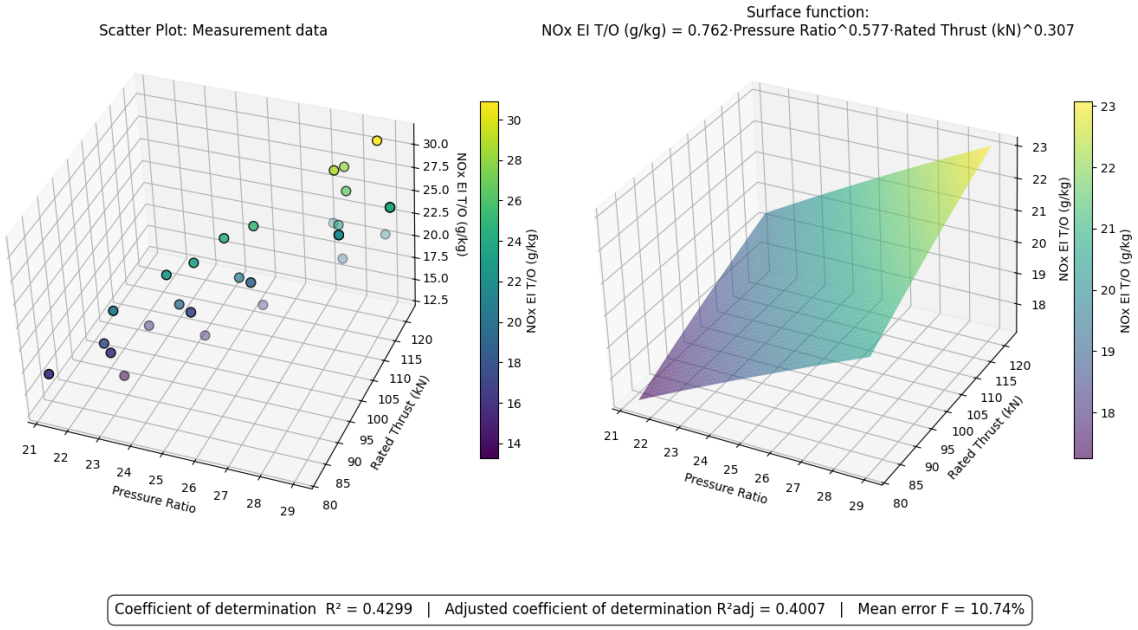

Figure 6.20: Multivariate power-law regression model for NO_x emission index at take-off for CFM56 engines, using OPR and rated thrust as independent variables.

This behavior aligns with thermodynamic expectations because elevated pressure and power output are usually linked to higher combustion temperatures and fuel flow rates, which are critical drivers of NO_x production. Although the model captures the overall trend, its statistical performance is moderate. The coefficient of determination ($R^2 = 0.4299$) and the adjusted coefficient ($R^2_{\mathrm{adj}} = 0.4007$) indicate that less than half of the variance in the data is explained by the regression. With a MAPE of 10.74 %, the model's predictive accuracy is limited, especially for engines with complex emission behavior. Nevertheless, this multivariate approach is clearly an improvement over simple, single-variable regressions because it more accurately reflects the multiple dependencies involved in NO_x formation. A visual comparison of the measured data

with the fitted surface confirms that incorporating both the OPR and the thrust enhances the realism of the model.

To complement the take-off based regression, Figure 6.21 presents a multivariate model that relates total NO_x emissions over the full LTO cycle to OPR and rated thrust. Again, only CFM56 engines are considered. The regression is expressed by the following equation:

$$NO_{x,\mathrm{LTO}} = 1.931 \cdot {\pi_{\mathrm{OPR}}}^{0.403} \cdot {T_{\mathrm{TO}}}^{1.366} \tag{6.3}$$

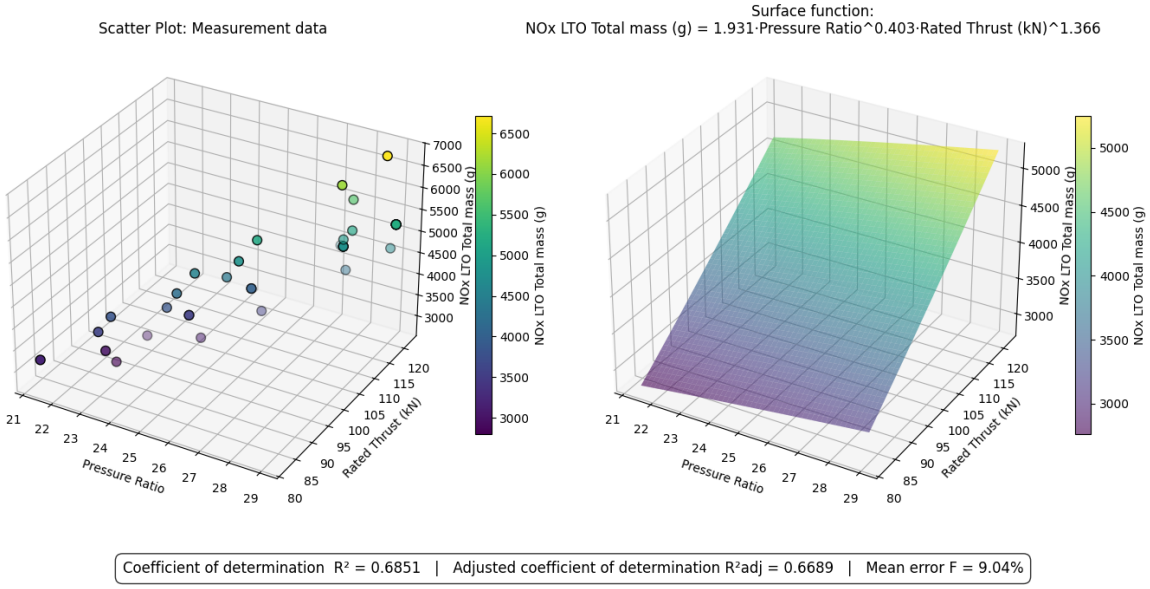

Figure 6.21: Multivariate regression model for total NO_x mass emitted during the LTO cycle as a function of OPR and rated thrust for CFM56 engines.

This model provides a more comprehensive estimate of emissions by incorporating all engine operating modes during the LTO cycle. The exponent on thrust is notably higher than in the take-off model, indicating a stronger dependency of total NO_x mass on engine power output over the entire cycle. The statistical fit ($R^2 = 0.6851$, $R^2_{\mathrm{adj}} = 0.6689$, and a mean error of 9.04%) suggests a moderate-to-strong explanatory power. This supports the conclusion that thrust, in conjunction with OPR, remains a key determinant of NO_x output not only during take-off but across all operating phases of the LTO cycle.

A second multivariate regression model analyzes the NO_x emission index at take-off as a function of OPR and fuel flow at take-off, replacing thrust as an independent variable. Figure 6.22 shows the resulting data distribution and regression surface for CFM56 engines. The fitted model follows a power-law form.

$$\mathrm{EI}_{\mathrm{NO_x,TO}} = 0.206 \cdot {\pi_{\mathrm{OPR}}}^{1.419} \cdot {\dot{m}_{\mathrm{f,TO}}}^{0.000} \tag{6.4}$$

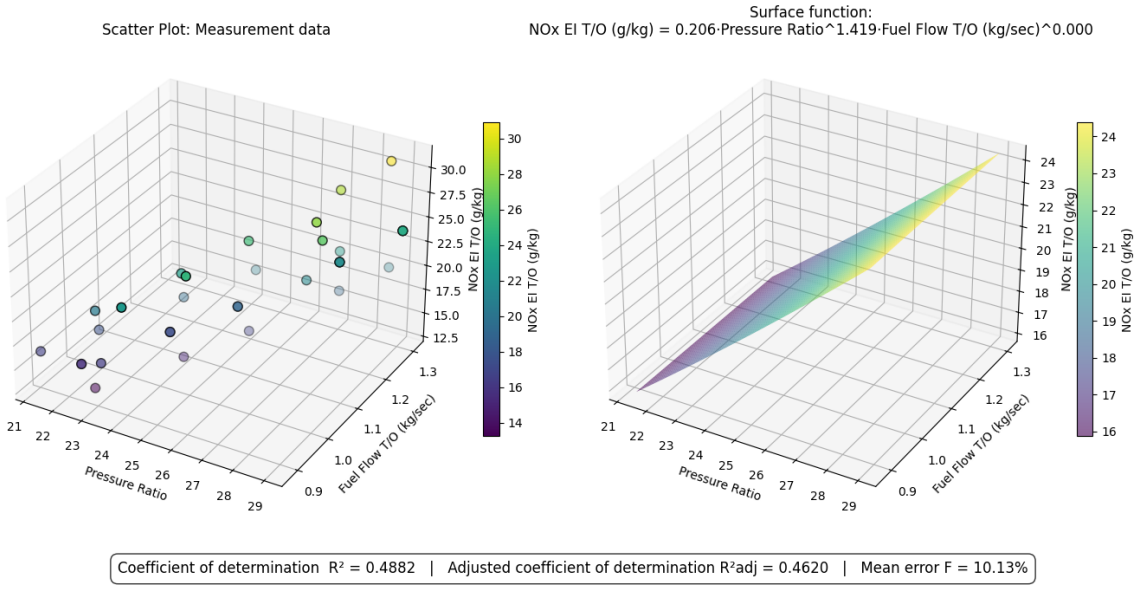

Figure 6.22: Multivariate power-law regression model for NO_x emission index at take-off using OPR and fuel flow at take-off for CFM56 engines.

Notably, the exponent of the fuel flow variable is nearly zero, suggesting that fuel flow does not provide additional explanatory power in this model. This reflects the strong correlation between OPR and fuel flow in the CFM56 dataset. Consequently, the model primarily attributes variability in emissions to OPR. However, this comes at the cost of predictive quality: the unadjusted $R^2 = 0.2620$, the adjusted $R^2_{\text{adj}} = 0.2241$, and the mean error is 10.65 %. These values are significantly lower than those of previous models. To verify whether this effect holds under different flight phases, a corresponding model for climb-out conditions was generated (Figure 6.23). The results show a similar pattern: the influence of fuel flow remains negligible, and OPR is the dominant factor.

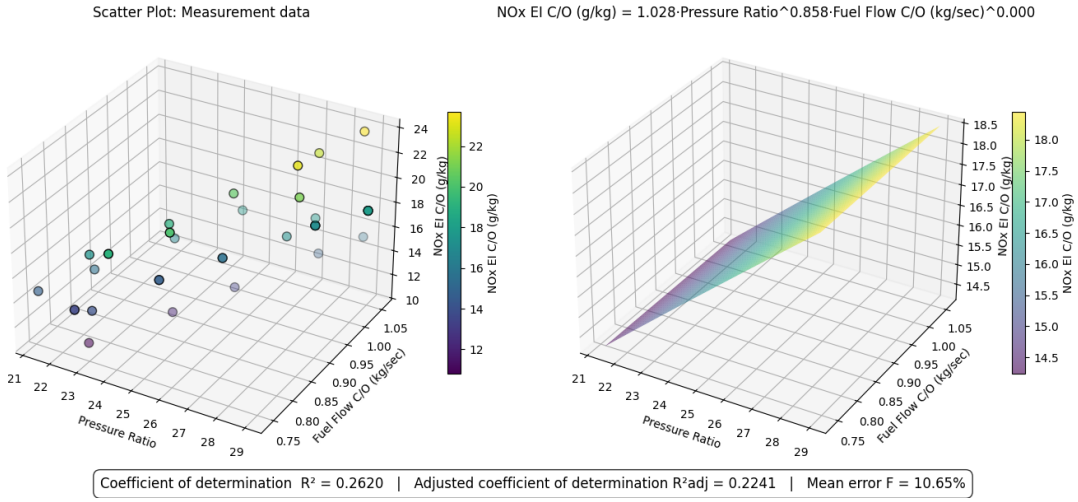

Figure 6.23: Regression model for NO_x EI during climb-out using OPR and fuel flow for CFM56 engines.

The following equation relates the NO_x emission index at take-off to OPR and the fuel flow rate during climb-out:

$$EI_{\text{NO}_x,\text{TO}} = 0.206 \cdot \pi_{\text{OPR}}{}^{1.419} \cdot \dot{m}_{\text{f,CO}}{}^{0.000} \tag{6.5}$$

However, when extending the dataset to include all engine types in our sample (Figure 6.24), a different picture emerges. The variance in engine architecture and design leads to a breakdown of the OPR-fuel flow correlation. In this broader dataset, both variables meaningfully contribute to the emission model, and fuel flow is no longer redundant. This underscores the importance of dataset composition and internal correlations when interpreting multivariate regression results.

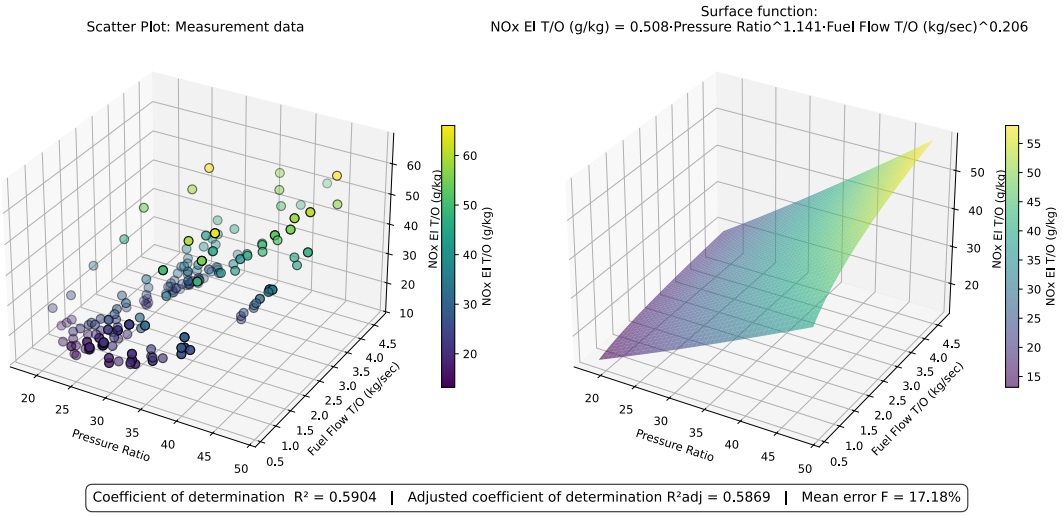

Figure 6.24: Regression model for NO_x EI at take-off including all engine types in the dataset. In contrast to the CFM56-only model, both OPR and fuel flow significantly influence emissions.

The following equation describes the NO_x emission index at take-off as a function of OPR and fuel flow rate:

$$EI_{NO_x,TO} = 0.508 \cdot \pi_{OPR}{}^{1.141} \cdot \dot{m}_{f,TO}{}^{0.206} \tag{6.6}$$

The following focused regression analysis uses only the CFM56 "E" variants. These engines share consistent design elements, enabling a more homogeneous evaluation of NO_x emission behavior under take-off conditions. Figure 6.25 shows the regression surface derived from OPR and rated thrust as predictors of the NO_x emission index at take-off. The resulting power-law model is defined as follows:

$$\mathrm{EI}_{NO_x,TO} = 0.806 \cdot \pi_{OPR}{}^{0.969} \cdot T_{TO}{}^{0.016} \tag{6.7}$$

The results clearly demonstrate that the OPR is the dominant influencing variable, with an exponent close to one indicating a nearly linear relationship. In contrast, the influence of rated thrust appears negligible, as evidenced by its low exponent of 0.016. However, it is important to note that the number of data points in this subset is relatively limited. Additionally, the range of rated thrust values is only from approximately 90 kN to 120 kN. This limited variation may explain why thrust has little statistical weight in the regression; the model cannot capture broader trends beyond this range. Thus, while OPR evidently drives NO_x formation in this subset, the limited data range may underrepresent the true role of thrust across the full CFM56 engine family.

The model fit is considerably stronger than previous regressions that included heterogeneous combustor types. The coefficient of determination is $R^2 = 0.8221$, with an adjusted value of $R^2_{\text{adj}} = 0.7948$, and a low mean error of 4.72 %. These results confirm that restricting the analysis to a single combustor configuration improves statistical clarity and predictive quality.

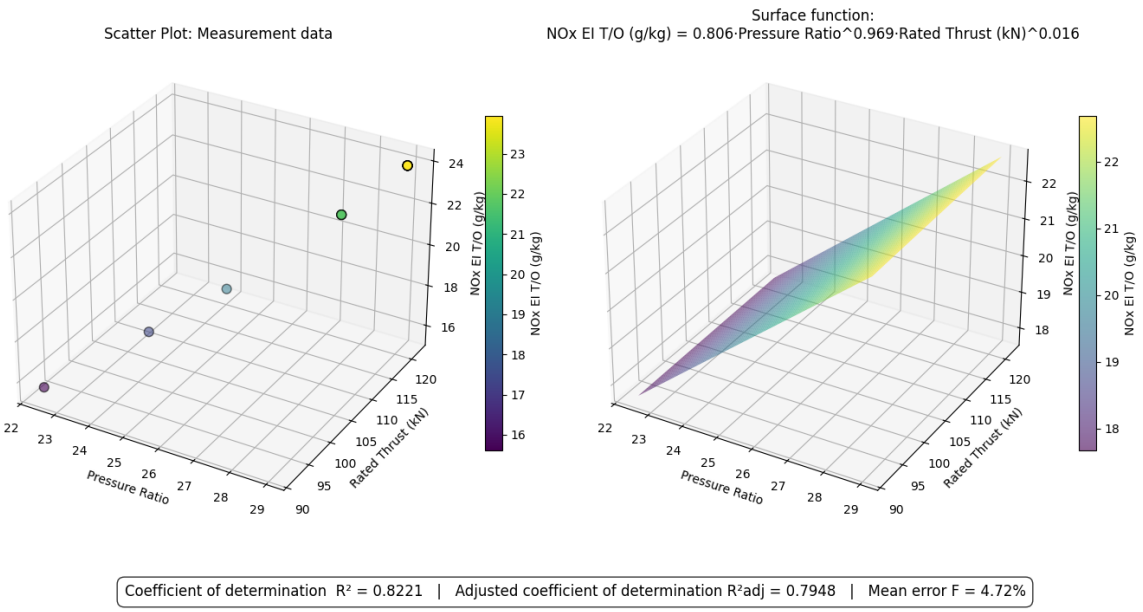

Figure 6.25: Multivariate regression model for NO_x emission index at take-off using OPR and rated thrust for CFM56 "E" variants.

To complement the previous analysis, Figure 6.26 presents a focused regression model for the total NO_x mass over the entire LTO cycle, specifically for CFM56 engines of the "E" variant. The model uses OPR and rated thrust as explanatory variables and captures emission behavior with exceptionally high accuracy.

$$\text{NO}_{x,\text{LTO}} = 0.952 \cdot {\pi_{\text{OPR}}}^{1.118} \cdot {T_{\text{TO}}}^{1.009} \tag{6.8}$$

The surface fit shows nearly linear dependence on both parameters. The coefficients suggest a slightly stronger sensitivity to the OPR, which aligns with thermodynamic expectations. Higher compression ratios typically result in elevated flame temperatures and increased NO_x formation. The statistical metrics highlight the excellent fit quality, with a coefficient of determination $R^2 = 0.9994$, an adjusted $R^2_{\text{adj}} = 0.9993$, and a mean error of only 0.36 %. These values suggest that the emission behavior of this engine configuration is highly predictable given the relevant design and performance parameters.

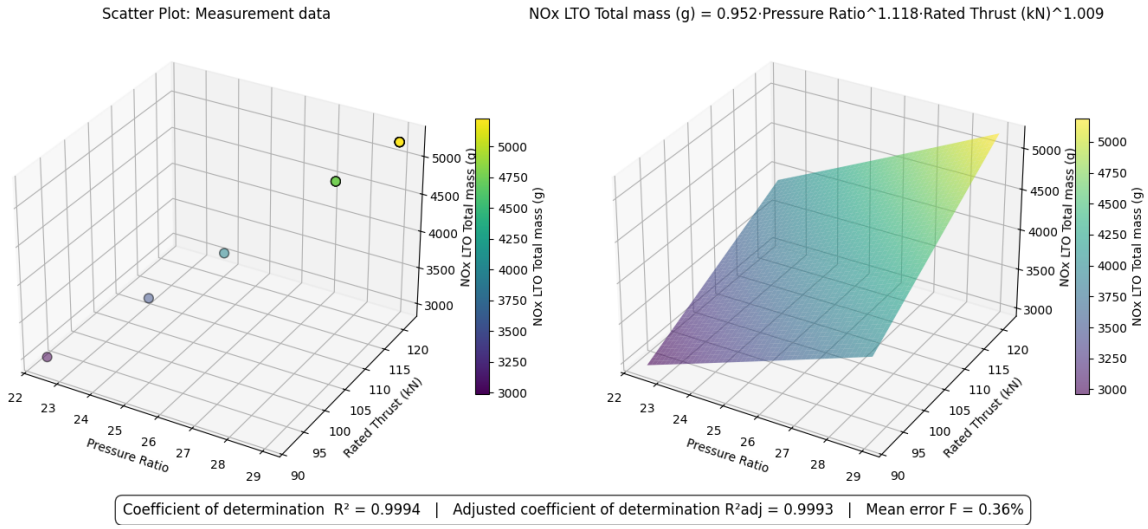

Figure 6.26: Multivariate regression model for NO_x total mass over the LTO cycle using OPR and rated thrust for CFM56 "E" variants.

Another model was generated using the full dataset, which included all 50 engines and their respective sub-variants, without filtering by specific technologies or configurations. This approach aims to reflect overall emission behavior across a wide range of commercial turbofan engines and assess the limitations of aggregated modeling. Figure 6.27 shows the regression result based on OPR and rated thrust as explanatory variables for the NO_x emission index at take-off. The fitted surface follows this expression:

$$\mathrm{EI}_{\mathrm{NO_x,TO}} = 0.774 \cdot {\pi_{\mathrm{OPR}}}^{0.718} \cdot {T_{\mathrm{TO}}}^{0.227} \tag{6.9}$$

Compared to focused models developed for specific engine families, this aggregated model's performance is significantly reduced. The coefficient of determination drops to $R^2 = 0.5478$, and the mean error increases to 19.92 %, indicating much broader data scatter. These results confirm earlier observations that the inclusion of heterogeneous engine architectures, combustor designs, and performance classes introduces a high degree of variability that cannot be adequately captured by a simple regression surface.

The 3D scatter plot on the left clearly reveals clustering and divergence patterns caused by differences in underlying engine technology. Although general trends are still visible, the wide dispersion of the data points undermines the model's predictive value. Though smooth, the regression surface only approximates the central tendency of the data and fails to account for technology-specific deviations.

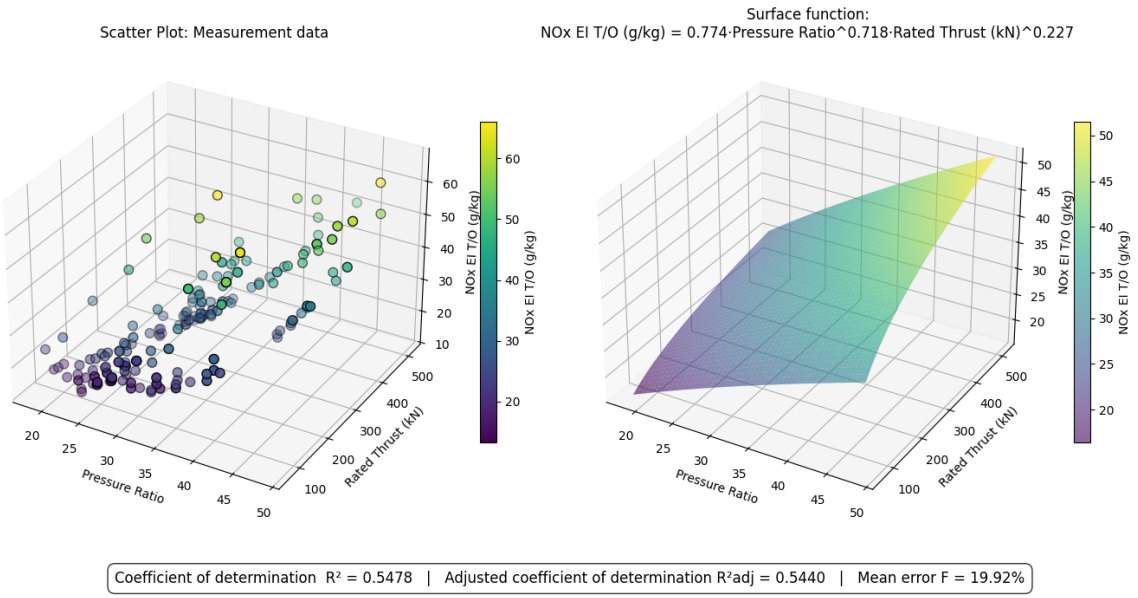

Figure 6.27: Multivariate regression surface for NO_x emissions at take-off using the complete engine dataset (no filtering).

A complementary regression model was developed to estimate the total NO_x emissions over the entire LTO cycle. Figure 6.28 shows the resulting surface based on OPR and rated thrust, using the full engine dataset without filtering by combustor type or generation.

$$NO_{x,\mathrm{LTO}} = 3.711 \cdot \pi_{\mathrm{OPR}}{}^{0.000} \cdot T_{\mathrm{TO}}{}^{1.464} \tag{6.10}$$

This result indicates that, within the aggregated dataset, rated thrust is the dominant explanatory variable for cumulative NO_x emissions during the LTO cycle. The exponent of 1.464 reflects strong nonlinear scaling with engine size. In contrast, OPR shows no statistical influence in this model, as evidenced by an exponent of zero. However, the model's explanatory power remains limited. Because the dataset includes engines of various generations, technologies, and thrust classes, the resulting regression surface does not capture the detailed emission behavior of specific engine types or LTO sub phases. Furthermore, the model lacks sensitivity to technology-specific features, such as combustor design. Therefore, while the model provides a broad overview of total NO_x mass trends across commercial passenger aircraft engines, it is unsuitable for precise emissions forecasting.

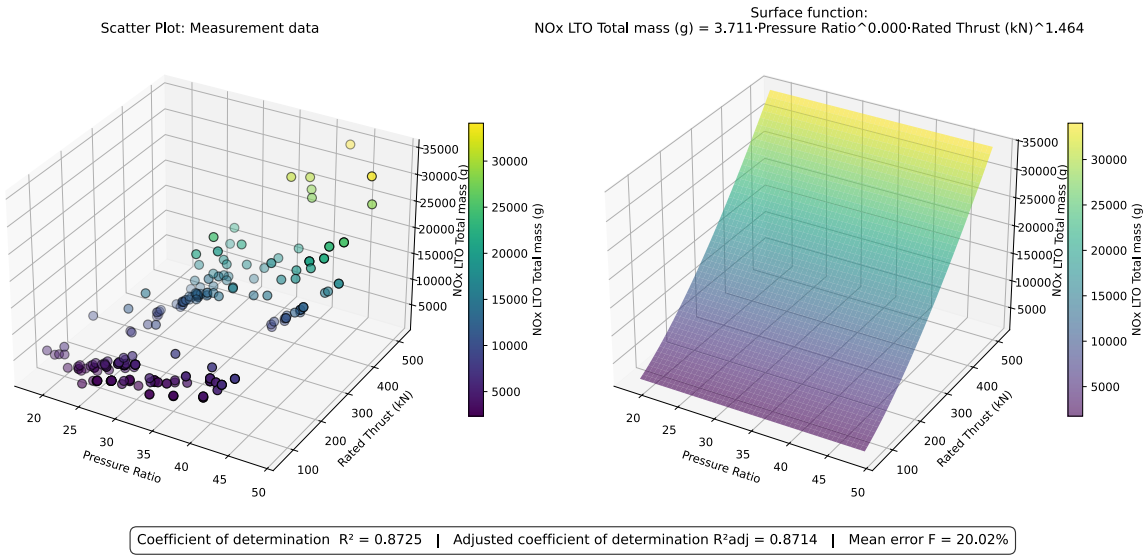

Figure 6.28: Regression surface for total NO_x mass during the LTO cycle based on rated thrust and OPR, using the full engine dataset.

An additional regression model was developed using directly measured fuel flow rates during take-off and idle to estimate the total NO_x mass over the LTO cycle. This approach aims to improve prediction accuracy by relying on parameters that more accurately represent combustion conditions.

$$NO_{x,\mathrm{LTO}} = 4904.234 \cdot \dot{m}_{\mathrm{f,TO}}{}^{1.399} \cdot \dot{m}_{\mathrm{f,IDLE}}{}^{0.169} \tag{6.11}$$

As shown in Figure 6.29, this model achieves a significantly higher coefficient of determination ($R^2 = 0.8583$) and a lower mean prediction error (19.79%) than models using OPR or thrust alone. These results highlight the value of operational parameters, such as fuel flow, in capturing the nonlinear scaling behavior of NO_x emissions.

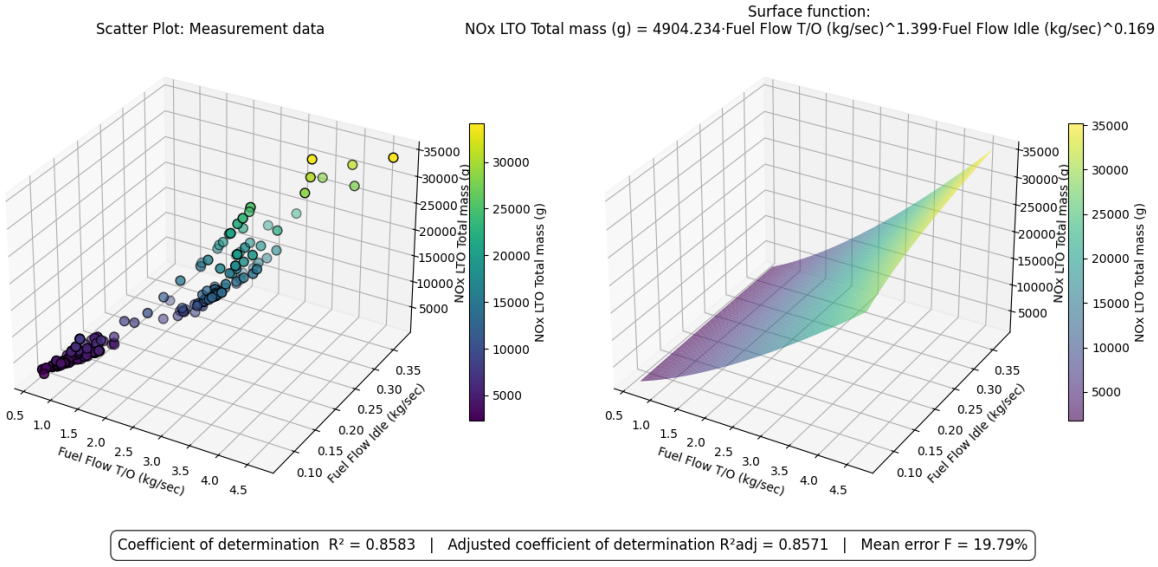

Figure 6.29: Regression surface for total NO_x mass over the LTO cycle using fuel flow rates at take-off and idle.

Tables 6.6, 6.7, and 6.8 summarise the best-fitting power-law regressions for estimating NO_x emissions from various combustor types. The models describe emissions during both the LTO cycle and cruise, using parameters such as overall pressure ratio (π_{OPR}), rated Thrust (T_{TO}), and fuel flow rates ($\dot{m}_{f,Cr}$, $m_{f,LTO}$). Each equation is accompanied by its coefficient of determination (R^2) and MAPE to indicate model quality. The results should be interpreted with caution, given the considerable variation in the number of data points between combustor types. This variability can affect the statistical robustness of the fitted models. Notably, the category where no special combustor is mentioned consistently shows poor model performance in both cruise and take-off emission regressions, with low R^2 values and relatively high MAPE. This suggests that, for engines lacking detailed combustor classification, the available input parameters may not adequately capture the relevant emission mechanisms. Interestingly, in the case of total NO_x emissions over the full LTO cycle (Table 6.6), the regressions for 'None' perform moderately better. This may indicate that, over the entire cycle, phase-specific inaccuracies average out the discrepancies to some extent. Consequently, individual combustor differences may influence total LTO emissions less than cruise or isolated operational modes.

Table 6.6: Best-fitting power-law regressions for total NO_x emissions ($NO_{x,LTO}$) by combustor type

Combustor Type	**Equation**	R^2	MAPE (%)
1862M39	$NO_{x,LTO} = 3.7359 \cdot 10^3 \cdot \pi_{OPR}{}^{0.5124} \cdot \dot{m}_{f,Cr}{}^{1.1891}$	0.9898	0.86
DAC	$NO_{x,LTO} = 1.11452 \cdot 10^5 \cdot T_{TO}{}^{-0.2181} \cdot \dot{m}_{f,Cr}{}^{1.7958}$	0.9999	1.83
E	$NO_{x,LTO} = 7.3773 \cdot 10^3 \cdot T_{TO}{}^{0.2576} \cdot \dot{m}_{f,Cr}{}^{1.3501}$	0.9998	0.17
Floatwall	$NO_{x,LTO} = 8.250824 \cdot 10^6 \cdot T_{TO}{}^{-0.9054} \cdot \dot{m}_{f,Cr}{}^{2.2656}$	0.9999	0.51
LEC	$NO_{x,LTO} = 5.854289 \cdot 10^6 \cdot T_{TO}{}^{-0.9122} \cdot \dot{m}_{f,Cr}{}^{2.2372}$	1.0000	0.07
None	$NO_{x,LTO} = 1.7435 \cdot 10^3 \cdot \pi_{OPR}{}^{0.7588} \cdot \dot{m}_{f,Cr}{}^{1.0628}$	0.8329	13.45
Phase5 Tiled	$NO_{x,LTO} = 1.5255 \cdot 10^2 \cdot \pi_{OPR}{}^{1.4032} \cdot \dot{m}_{f,Cr}{}^{0.7964}$	0.9479	3.48
SAC	$NO_{x,LTO} = 1.3616 \cdot 10^5 \cdot T_{TO}{}^{-0.2715} \cdot \dot{m}_{f,Cr}{}^{1.7839}$	0.9715	2.69
TALON X	$NO_{x,LTO} = 8.5486 \cdot 10^1 \cdot \pi_{OPR}{}^{1.3505} \cdot \dot{m}_{f,Cr}{}^{0.6410}$	0.9981	0.66
TALON X, Block-C	$NO_{x,LTO} = 2.1579 \cdot 10^2 \cdot \pi_{OPR}{}^{1.1517} \cdot \dot{m}_{f,Cr}{}^{0.7894}$	0.9958	1.11
TALON X, Block-D	$NO_{x,LTO} = 2.355 \cdot 10^{-1} \cdot \pi_{OPR}{}^{1.1977} \cdot m_{f,LTO}{}^{0.9550}$	0.9998	0.29
TAPS	$NO_{x,LTO} = 1.152 \cdot 10^{-4} \cdot \pi_{OPR}{}^{4.8218} \cdot \dot{m}_{f,Cr}{}^{-0.5309}$	0.9866	1.85
TAPS II	$NO_{x,LTO} = 8.034737 \cdot 10^6 \cdot T_{TO}{}^{-0.4695} \cdot \dot{m}_{f,Cr}{}^{3.8206}$	0.9924	2.47
Tech Insertion	$NO_{x,LTO} = 2.2889 \cdot 10^3 \cdot T_{TO}{}^{0.4694} \cdot \dot{m}_{f,Cr}{}^{1.2118}$	0.9943	0.83

Table 6.7: Best-fitting power-law regressions for cruise NO_x emissions ($NO_{x,\mathrm{Cr}}$) by combustor type

Combustor Type	**Equation**	R^2	MAPE (%)
1862M39	$EI_{\mathrm{NO_x,Cr}} = 1.3234 \cdot 10^{-7} \cdot T_{\mathrm{TO}}{}^{-3.1985} \cdot m_{\mathrm{f,LTO}}{}^{5.3117}$	0.1562	13.42
DAC	$EI_{\mathrm{NO_x,Cr}} = 4.35428 \cdot 10^{1} \cdot T_{\mathrm{TO}}{}^{-0.1466} \cdot \dot{m}_{\mathrm{f,Cr}}{}^{0.6821}$	0.9996	0.46
E	$EI_{\mathrm{NO_x,Cr}} = 1.28787 \cdot 10^{2} \cdot \pi_{\mathrm{OPR}}{}^{4.2933} \cdot T_{\mathrm{TO}}{}^{-3.5182}$	0.5542	2.45
Floatwall	$EI_{\mathrm{NO_x,Cr}} = 1.90537 \cdot 10^{1} \cdot T_{\mathrm{TO}}{}^{1.2466} \cdot m_{\mathrm{f,LTO}}{}^{-1.0178}$	0.9234	4.09
LEC	$EI_{\mathrm{NO_x,Cr}} = 3.99 \cdot 10^{-2} \cdot \pi_{\mathrm{OPR}}{}^{1.5977} \cdot T_{\mathrm{TO}}{}^{-0.2537}$	-0.8212	16.78
None	$EI_{\mathrm{NO_x,Cr}} = 8.985 \cdot 10^{-1} \cdot T_{\mathrm{TO}}{}^{-0.8187} \cdot m_{\mathrm{f,LTO}}{}^{1.0710}$	0.0167	34.96
Phase5 Tiled	$EI_{\mathrm{NO_x,Cr}} = 1.53718 \cdot 10^{1} \cdot T_{\mathrm{TO}}{}^{2.2756} \cdot m_{\mathrm{f,LTO}}{}^{-1.8677}$	0.5884	7.54
SAC	$EI_{\mathrm{NO_x,Cr}} = 2.29844 \cdot 10^{1} \cdot T_{\mathrm{TO}}{}^{0.6681} \cdot m_{\mathrm{f,LTO}}{}^{-0.6015}$	0.5977	1.88
TALON X	$EI_{\mathrm{NO_x,Cr}} = 3.922 \cdot 10^{-1} \cdot \pi_{\mathrm{OPR}}{}^{1.1292} \cdot T_{\mathrm{TO}}{}^{-0.1015}$	0.2412	8.99
TALON X, Block-C	$EI_{\mathrm{NO_x,Cr}} = 3.639 \cdot 10^{-1} \cdot \pi_{\mathrm{OPR}}{}^{0.7823} \cdot T_{\mathrm{TO}}{}^{0.1799}$	0.4305	7.13
TALON X, Block-D	$EI_{\mathrm{NO_x,Cr}} = 2.0 \cdot 10^{-3} \cdot T_{\mathrm{TO}}{}^{-1.0085} \cdot m_{\mathrm{f,LTO}}{}^{2.3881}$	0.9999	0.08
TAPS	$EI_{\mathrm{NO_x,Cr}} = 4.511 \cdot 10^{-5} \cdot \pi_{\mathrm{OPR}}{}^{5.3345} \cdot T_{\mathrm{TO}}{}^{-1.2924}$	0.9656	2.94
TAPS II	$EI_{\mathrm{NO_x,Cr}} = 1.1 \cdot 10^{-7} \cdot \pi_{\mathrm{OPR}}{}^{1.2470} \cdot T_{\mathrm{TO}}{}^{3.0294}$	0.9601	4.35
Tech Insertion	$EI_{\mathrm{NO_x,Cr}} = 4.0139 \cdot \pi_{\mathrm{OPR}}{}^{1.6395} \cdot T_{\mathrm{TO}}{}^{-0.9282}$	0.5656	3.09

Table 6.8: Best-fitting power-law regressions for NO_x emission index at take-off ($EI_{NO_x,TO}$) by combustor type

Combustor Type	**Equation**	R^2	MAPE (%)
1862M39	$EI_{NO_x,TO} = 8.84 \cdot 10^{-2} \cdot \pi_{OPR}{}^{1.6866} \cdot \dot{m}_{f,TO}{}^{0.1809}$	0.9998	0.72
DAC	$EI_{NO_x,TO} = 6.82 \cdot 10^{-2} \cdot \pi_{OPR}{}^{1.4846} \cdot \dot{m}_{f,TO}{}^{0.2859}$	0.9898	1.72
E	$EI_{NO_x,TO} = 4.657 \cdot 10^{-1} \cdot \pi_{OPR}{}^{3.2768} \cdot T_{TO}{}^{-1.4782}$	0.9998	0.14
Floatwall	$EI_{NO_x,TO} = 2.59 \cdot 10^{-2} \cdot \pi_{OPR}{}^{1.3975} \cdot m_{f,LTO}{}^{0.3629}$	0.9946	2.15
LEC	$EI_{NO_x,TO} = 7.64 \cdot 10^{-2} \cdot \pi_{OPR}{}^{1.4886} \cdot m_{f,LTO}{}^{0.1076}$	0.9988	0.33
None	$EI_{NO_x,TO} = 9.999 \cdot 10^{-1} \cdot \pi_{OPR}{}^{0.7273} \cdot T_{TO}{}^{0.1932}$	0.3007	17.22
Phase5 Tiled	$EI_{NO_x,TO} = 1.669 \cdot 10^{-1} \cdot \pi_{OPR}{}^{1.6804} \cdot m_{f,LTO}{}^{-0.0897}$	0.8714	4.56
SAC	$EI_{NO_x,TO} = 1.24 \cdot 10^{-2} \cdot \pi_{OPR}{}^{0.3671} \cdot m_{f,LTO}{}^{1.0718}$	0.9241	3.11
TALON X	$EI_{NO_x,TO} = 9.35 \cdot 10^{-2} \cdot \pi_{OPR}{}^{2.3253} \cdot m_{f,LTO}{}^{-0.4911}$	0.9960	0.75
TALON X, Block-C	$EI_{NO_x,TO} = 7.36 \cdot 10^{-2} \cdot \pi_{OPR}{}^{1.5735} \cdot T_{TO}{}^{0.0198}$	0.9982	0.60
TALON X, Block-D	$EI_{NO_x,TO} = 6.4 \cdot 10^{-3} \cdot \pi_{OPR}{}^{0.9148} \cdot m_{f,LTO}{}^{0.6490}$	0.9995	0.31
TAPS	$EI_{NO_x,TO} = 4.0 \cdot 10^{-7} \cdot \pi_{OPR}{}^{2.8310} \cdot m_{f,LTO}{}^{1.1324}$	0.9885	1.39
TAPS II	$EI_{NO_x,TO} = 3.7 \cdot 10^{-9} \cdot \pi_{OPR}{}^{0.6909} \cdot m_{f,LTO}{}^{3.6834}$	0.9449	6.46
Tech Insertion	$EI_{NO_x,TO} = 1.052 \cdot 10^{-1} \cdot \pi_{OPR}{}^{1.8265} \cdot T_{TO}{}^{-0.1184}$	0.9804	1.34

7 Summary

This study examined the relationship between NO_x emissions and engine parameters using data from the ICAO Aircraft Engine Emissions Databank. The results show that OPR, rated thrust, fuel flow and combustor technology are the main factors influencing NO_x emissions. Regression models using the full dataset showed low accuracy due to differences in engine design. These models had a low coefficient of determination (e.g., below 0.55), high prediction errors and visible data clusters. This means that NO_x behavior cannot be described well using a single general model.

When the data was divided by combustor type, the model performance improved significantly. For example, engines with DAC or the Enhanced ("E") type had much better results, with coefficient of determination R^2 values up to 0.9994 and prediction errors below 5 %. This shows that combustor technology has an effect on NO_x formation and must be considered as a separate category in modeling.

Multivariable models showed that OPR is the most important continuous predictor of NO_x at take-off when not considering classification in combustor technology. Thrust and fuel flow contribute less in some engine families due to limited variation or multicollinearity. In homogeneous groups, combining OPR and thrust improves prediction.

In addition to the modelling element, the study makes a passing reference to an emerging trade-off in environmental performance. Namely, that low-NO_x combustors, whilst reducing NO_x-induced climate effects, have the potential to increase soot emissions and contrail formation.

8 Conclusions and Recommendations

Initial regression models applied to the complete dataset showed poor predictive performance due to high design variability. In contrast, models based on combustor type achieved better results, with adjusted coefficient of determination values above 0.99 in the most homogeneous groups. These findings demonstrate that combustor technology is a key categorical variable and must be explicitly included in any reliable modeling approach.

OPR emerged as the most influential continuous variable. In certain subgroups, such as the CFM56 "E" engines, OPR alone was sufficient to model NO_x emissions with high accuracy. In other cases, the inclusion of a second variable, typically rated thrust, led to substantial improvements in fit quality, visible in higher exponents and lower prediction errors. However, beyond two variables, the benefit of adding further predictors remains an open question.

In addition to these findings, the study highlights a newly recognised trade-off in emissions optimisation. While low-NO_x combustor designs effectively reduce ozone-related climate effects, they often increase soot emissions. This soot promotes the formation of persistent contrails, which significantly contribute to radiative forcing, especially under night-time and cold-humid atmospheric conditions. Therefore, improving NO_x performance alone may inadvertently worsen other climate effects.

Based on the results, the following recommendations are made for future work:

1. **Investigate the Use of a Third Predictor:** Future studies should test whether including a third parameter (e.g., fuel flow or bypass ratio) improves the predictive accuracy of NO_x models beyond OPR and thrust.

2. **Extend Multivariate Modeling:** More advanced regression techniques may help capture non-linear dependencies and reduce overfitting, especially when applied within defined engine groups.

3. **Explore the Use of p_3/T_3-Based Modeling Approaches:** If more detailed combustor information becomes available (e.g., combustor inlet temperature or pressure), future studies could apply semi-empirical methods such as the P_3/T_3 approach. This would allow for more physically grounded NO_x predictions beyond purely statistical regression models.

List of References

AGARD, 1980. *Multilingual Aeronautical Dictionary*. Neuilly, France: Advisory Group for Aerospace Research and Development (AGARD/NATO).
Available from: http://MAD.Profscholz.de
Archived at: https://bit.ly/AGARD-1980

BAHR, D. W., 1992. *Aircraft Turbine Engine NOx Emission Limits: Status and Trends*. In: Volume 2: Aircraft Engine; Marine; Microturbines and Small Turbomachinery. Cologne, Germany: American Society of Mechanical Engineers, V002T02A036.
Available from: https://asmedigitalcollection.asme.org/GT/proceedings/GT1992/78941/Cologne,%20Germany/242253
Archived at: https://perma.cc/96VX-G8JA

BENOSA, Guillem, ZHU, Shupeng, MAC KINNON, Michael, & DABDUB, Donald, 2018. *Air quality impacts of implementing emission reduction strategies at southern California airports*. In: *Atmospheric Environment*, vol. 185, pp. 121–127.
Available from: https://linkinghub.elsevier.com/retrieve/pii/S1352231018302796 (Closed Access)

BIRCH, N.T., 2000. *2020 vision: the prospects for large civil aircraft propulsion*. In: *The Aeronautical Journal*, vol. 104, no. 1038, pp. 347–352.
Available from: https://www.cambridge.org/core/product/identifier/S0001924000063971/type/journal_article (Closed Access)

Cambridge University Press, 2023. *Aircraft*. In: *Cambridge Dictionary*.
Available from: https://dictionary.cambridge.org/dictionary/english/aircraft

CIRIUM, 2020. *World Airliner Census 2020*.
Available from: https://bit.ly/3hkGFsB
Archived at: https://perma.cc/W36D-L4X5

CROCKER, David, & COLLIN, Peter, 2005. *Dictionary of Aviation*.
Available from: https://bit.ly/crocker-2005
Archived at: https://perma.cc/X9TG-DJKN

DEIDEWIG, F., RÖSSLER, H.-J., & SCHÄFER, W., 1996. *Methods to Assess Aircraft Engine Emissions in Flight*. In: ICAS Proceedings 1996, Volume 1, ICAS–96–4.1.2.
Available from: https://www.icas.org/icas_archive
Archived at: https://perma.cc/SSS9-YDVS

DEUTSCHER WETTERDIENST (DWD), 2025. *Standardatmosphäre*.
Available from: https://www.dwd.de/DE/service/lexikon/begriffe/S/Standardatmosphaere_pdf.pdf?__blob=publicationFile&v=3

Archived at: https://perma.cc/SQ8A-MBV8

DUBOIS, Doug, & PAYNTER, Gerald C., 2006. *"Fuel Flow Method2" for Estimating Aircraft Emissions*. SAE Technical Paper 2006-01-1987. Society of Automotive Engineers.
Available from: https://www.sae.org/publications/technical-papers/content/2006-01-1987/ (Closed Access)

EASA, 2023. *European Aviation Environmental Report 2023* [PDF]. European Union Aviation Safety Agency.
Available from: https://www.easa.europa.eu/pl/downloads/45576/en
Archived at: https://perma.cc/RTD6-QUDJ

EASA, 2025. *ICAO Aircraft Engine Emissions Databank*. European Union Aviation Safety Agency.
Available from: https://www.easa.europa.eu/en/domains/environment/icao-aircraft-engine-emissions-databank
Archived at: https://perma.cc/8N3R-MVQ4

EKICI, Selcuk, & SEVINC, Hasan, 2022. *Understanding a commercial airline company: A case study on emissions and air quality costs*. In: *International Journal of Environmental Science and Technology*, vol. 19, no. 6, pp. 5139–5154.
Available from: https://doi.org/10.1007/s13762-021-03471-3 (Closed Access)

EPIC FLIGHT ACADEMY, 2024. *How High Do Planes Fly?*
Available from: https://epicflightacademy.com/how-high-do-planes-fly
Archived at: https://perma.cc/7EJY-WE38

EUROCONTROL, 2025. *LTO – Landing and Take-Off Cycle*.
Available from: https://ansperformance.eu/acronym/lto/
Archived at: https://perma.cc/Y7C6-3LYG

GREWE, Volker, DAMERIS, Martin, FICHTER, Christine, & SAUSEN, Robert, 2002a. *Impact of aircraft NO_x emissions. Part 1: Interactively coupled climate-chemistry simulations and sensitivities to climate-chemistry feedback, lightning and model resolution*. In: *Meteorologische Zeitschrift*, vol. 11, no. 3, pp. 177–186.
Available from: https://doi.org/10.1127/0941-2948/2002/0011-0177
Archived at: https://perma.cc/36GZ-625C

GREWE, Volker, DAMERIS, Martin, FICHTER, Christine, & LEE, David S., 2002b. *Impact of aircraft NO_x emissions. Part 2: Effects of lowering the flight altitude*. In: *Meteorologische Zeitschrift*, vol. 11, no. 3, pp. 197–205.
Available from: https://doi.org/10.1127/0941-2948/2002/0011-0197
Archived at: https://perma.cc/L2JF-56U3

HARLASS, Theresa, 2024. *Measurement report: In-flight and ground-based measurements of nitrogen oxide emissions from latest-generation jet engines and 100% sustainable aviation*

fuel. In: *Atmospheric Chemistry and Physics*, vol. 24, pp. 11807–11822.
Available from: https://doi.org/10.5194/acp-24-11807-2024
Archived at: https://perma.cc/DFF5-HJME

HERNDON, Scott C., 2004. *NO and NO_2 Emission Ratios Measured from In-Use Commercial Aircraft during Taxi and Takeoff*. In: *Environmental Science and Technology*, vol. 38, no. 22, pp. 6078–6084.
Available from: https://doi.org/10.1021/es049701c (Closed Access)

HERTEL, Ole, 2013. *Utilizing Monitoring Data and Spatial Analysis Tools for Exposure Assessment of Atmospheric Pollutants in Denmark*. In: *Occurrence, Fate and Impact of Atmospheric Pollutants on Environmental and Human Health*, Chap.6, pp. 95–122.
Available from: https://pubs.acs.org/doi/abs/10.1021/bk-2013-1149.ch006 (Closed Access)

HURTECANT, Daan, 2021. *Launch of an Ecolabel for Passenger Aircraft*. Master's Thesis.
Available from: https://www.fzt.haw-hamburg.de/pers/Scholz/arbeiten/TextHurtecant.pdf
Archived at: https://perma.cc/R5A8-MD7T

ICAO, 2014. *Local Air Quality and ICAO Engine Emissions Standards*. Presentation by Dr. Neil Dickson, Environment Branch, ICAO Air Transport Bureau. International Civil Aviation Organization.
Available from: https://www.icao.int/Meetings/EnvironmentalWorkshops/Documents/2014-Kenya/4-1_LAQ-Technology_notes.pdf
Archived at: https://perma.cc/7U86-3PWL

ICAO, 2025. *Committee on Aviation Environmental Protection (CAEP)*
Available from: https://www.icao.int/environmental-protection/pages/caep.aspx
Archived at: https://perma.cc/PT45-P9HU

JARAVEL, Thomas, 2023. *Evaluation of the climate impact of aviation NO_x emissions using a chemistry-climate model*. PhD Thesis.
Available from: https://theses.hal.science/tel-04244436/file/Jaravel.pdf
Archived at: https://perma.cc/A7ZQ-MNSL

KLAPMEYER, Michael E., & MARR, Linsey C., 2012. *CO_2, NO_x, and Particle Emissions from Aircraft and Support Activities at a Regional Airport*. In: *Environmental Science & Technology*, vol. 46, no. 20, pp. 10974–10981.
Available from: https://doi.org/10.1021/es302346x (Closed Access)

KOUDIS, George S., HU, Simon J., MAJUMDAR, Arnab, JONES, Roderic, & STETTLER, Marc E.J., 2017a. *Airport emissions reductions from reduced thrust take-off operations*. In: *Transportation Research Part D: Transport and Environment*, vol. 52, pp. 15–28.
Available from: https://doi.org/10.1016/j.trd.2017.02.004 (Closed Access)

KOUDIS, George S., HU, Simon J., NORTH, Robin J., MAJUMDAR, Arnab, & STETTLER, Marc E.J., 2017b. *The impact of aircraft takeoff thrust setting on NO_x emissions*. In: *Journal of Air Transport Management*, vol. 65, pp. 191–197.
Available from: https://doi.org/10.1016/j.jairtraman.2017.06.009 (Closed Access)

LEE, David S., 2021. *The contribution of global aviation to anthropogenic climate forcing for 2000 to 2018*. In: *Atmospheric Environment*, vol. 244, art. 117834.
Available from: https://doi.org/10.1016/j.atmosenv.2020.117834 (Closed Access)

MATTAUSCH, Pascal, 2024. *Environmental Labels in Aviation – Aircraft Label, Airline Label, Flight Label*. Master's Thesis.
Available from: https://www.fzt.haw-hamburg.de/pers/Scholz/arbeiten/TextMattausch.pdf
Archived at: https://perma.cc/B5UG-TNY4

MAZUR, Marek, 2017. *Experimental study of combustion noise in an aeronautic type combustion chamber – Étude expérimentale du bruit de combustion dans un foyer de type aéronautique*. PhD thesis.
Available from: https://www.researchgate.net/publication/319538089_Experimental_study_of_combustion_noise_in_an_aeronautic_type_combustion_chamber_-_Etude_experimentale_du_bruit_de_combustion_dans_un_foyer_de_type_aeronautique (Closed Access)

MIAKE-LYE, Richard C., & HAUGLUSTAINE, Didier, 2022. *Impacts of Aviation NO_x Emissions on Air Quality, Health, and Climate*. In: ICAO Environmental Report 2022, Chap.3, pp.74–76. International Civil Aviation Organization (ICAO).
Available from: https://www.icao.int/environmental-protection/Documents/EnvironmentalReports/2022/ENVReport2022_Art18.pdf
Archived at: https://perma.cc/A6F6-YUD9

MILLER, Cassandra J., PRASHANTH, Prakash, ALLROGGEN, Florian, GROBLER, Carla, SABNIS, Jayant S., SPETH, RaymondL., & BARRETT, Steven R. H., 2022. *An environmental cost basis for regulating aviation NO_x emissions*. In: *Environmental Research Communications*, vol. 4, no. 5, art. 055002.
Available from: https://iopscience.iop.org/article/10.1088/2515-7620/ac6938
Archived at: https://perma.cc/7SC8-3UYQ

MORAN, John, 2007. *Engine Technology Development to Address Local Air Quality Concerns*. Presented at ICAO Colloquium on Aviation Emissions with Exhibition, 14–16 May 2007, Montréal, Canada. International Civil Aviation Organization (ICAO).
Available from: https://www.icao.int/environmental-protection/documents/env_report_07.pdf
Archived at: https://perma.cc/MSQ5-5MS2

BRINK ,Lukas Frederik Jakob, 2020. *Modeling the Impact of Fuel Composition on Aircraft Engine NOx, CO and Soot Emissions*.
Available from: https://dspace.mit.edu/bitstream/handle/1721.1/129181/1227278199-MIT.pdf?sequence=1&isAllowed=y (Closed Access)

Oxford University Press, 2023. *Aircraft*. In: *Oxford Advanced American Dictionary*.
Available from: https://www.oxfordlearnersdictionaries.com/definition/american_english/aircraft?q=aircraft

PITARI, Giovanni, & MANCINI, Eva, 2002. *Impact of future supersonic aircraft on the distribution of stratospheric tracers: Chemical and dynamical perturbations*. In: *Meteorologische Zeitschrift*, vol. 11, no. 3, pp. 215–223.
Available from: https://doi.org/10.1127/0941-2948/2002/0011-0215
Archived at: https://perma.cc/ZAQ7-6XDN

RIDAO VELASCO, Alejandro, 2020. *Environmental Information for Aviation Passengers*. Bachelor's Thesis.
Available from: https://www.fzt.haw-hamburg.de/pers/Scholz/arbeiten/TextRidaoVelasco.pdf
Archived at: https://perma.cc/H285-Z8SF

SCHAEFER, M., & BARTOSCH, S., 2013. *Overview on fuel flow correlation methods for the calculation of NO_x, CO and HC emissions and their implementation into aircraft performance software*. Report no. IB-325-11-13. DLR Institut für Antriebstechnik.
Available from: https://www.researchgate.net/publication/271210746
Archived at:https://perma.cc/5Y9B-WTJK

SCHUMANN, Ulrich, 1997. *The impact of nitrogen oxides emissions from aircraft upon the atmosphere at flight altitudes—results from the aeronox project*. In: *Atmospheric Environment*, vol. 31, no. 12, pp. 1723–1733.
Available from: https://doi.org/10.1016/S1352-2310(96)00326-3 (Closed Access)

SCHUMANN, Ulrich, 1995. *AERONOX: The Impact of NO_x Emissions from Aircraft Upon the Atmosphere at Flight Altitudes 8–15 km*. Final Report to the Commission of European Communities.
Available from: https://elib.dlr.de/32299/1/at-env-1723-1997.pdf
Archived at: https://perma.cc/QM6L-F2MG

SCHOLZ, Dieter, 2023. *Kondensstreifen*. Memo. Aircraft Design and Systems Group (AERO), HAW Hamburg.
Available from: https://purl.org/aero/M2023-10-20
Archived at: https://perma.cc/2SQN-PXK2

SCHOLZ, Dieter, 2024. *The Aircraft and Alternative Modes of Transport – Environmental Impact: Energy Consumption and Global Warming*
Available from: https://doi.org/10.5281/zenodo.11630497

Archived at: https://perma.cc/S9HZ-GKGT

SCHÜRMANN, Gregor, SCHÄFER, Klaus, JAHN, Carten, HOFFMANN, Herbert, BAUER-FEIND, Martina, FLEUTI, Emanuel, & RAPPENGLÜCK, Bernhard, 2007. *The impact of NO_x, CO and VOC emissions on the air quality of Zurich airport*. In: *Atmospheric Environment*, vol. 41, no. 1, pp. 103–118.
Available from: https://doi.org/10.1016/j.atmosenv.2006.07.030 (Closed Access)

SHIRMOHAMMADI, Farimah, SOWLAT, Mohammad H., HASHEMINASSAB, Sina, SAFFARI, Arian, Ban-WEISS, George, & SIOUTAS, CONSTANTINOS, 2017. *Emission rates of particle number, mass and black carbon by the Los Angeles International Airport (LAX) and its impact on air quality in Los Angeles*. In: *Atmospheric Environment*, vol. 151, pp. 82–93.
Available from: https://doi.org/10.1016/j.atmosenv.2016.12.005 (Closed Access)

STATISTA, 2024. *Marktanteile der Hersteller von Flugzeugtriebwerken weltweit in den Jahren 2015 bis 2022*.
Available from: https://de.statista.com/statistik/daten/studie/270936/umfrage/marktanteile-der-hersteller-von-flugzeugtriebwerken/ (Closed Access)

STETTLER, M.E.J., EASTHAM, S., & BARRETT, S.R.H., 2011. *Air quality and public health impacts of UK airports. Part I: Emissions*. In: *Atmospheric Environment*, vol. 45, no. 31, pp. 5415–5424.
Available from: https://doi.org/10.1016/j.atmosenv.2011.07.012 (Closed Access)

STEVENSON, David S., & DERWENT, Richard G., 2009. *Does the location of aircraft nitrogen oxide emissions affect their climate impact?*. In: *Geophysical Research Letters*, vol. 36, no. 17, 2009GL039422.
Available from: https://doi.org/10.1029/2009GL039422 (Closed Access)

SYNYLO, Kateryna, 2017. *Comparison between modelled and measured NO_x concentrations in aircraft plumes at Athens International Airport*. In: (Details missing).
Available from: http://dx.doi.org/10.1504/IJSA.2017.10011233 (Closed Access)

TECHNICAL SECRETARIAT OF THE TFTEI, 2023. *Reduction of NO_x emissions*. Online resource.
Available from: https://tftei.citepa.org/en/industrial-sources/reduction-of-nox-emissions
Archived at: https://perma.cc/YR7A-HDY5

TEOH, R., SCHUMANN, U., GRYSPEERDT, E., SHAPIRO, M., MOLLOY, J., KOUDIS, G., VOIGT, C., & STETTLER, M. E. J., 2022. *Aviation contrail climate effects in the North*

Atlantic from 2016 to 2021. In: *Atmospheric Chemistry and Physics*, vol. 22, no. 16, pp. 10919–10935.
Available from: https://doi.org/10.5194/acp-22-10919-2022
Archived at: https://perma.cc/LG37-AETE

TSILINGIRIDIS, Georgios, 2008. *Aircraft air pollutant emissions in Greek airports*. Online resource.
Available from: https://journal.gnest.org/sites/default/files/Journal%20Papers/528-534_557_Tsiligiridis_11-4.pdf
Archived at: https://perma.cc/33NX-Q7UA

UNAL, Alper, HU, Yonhtao, CHANG, Michael E., ODMAN, M. Talat, & RUSSELL, Armistead G., 2005. *Airport related emissions and impacts on air quality: Application to the Atlanta International Airport*. In: *Atmospheric Environment*, vol. 39, no. 32, pp. 5787–5798.
Available from: https://doi.org/10.1016/j.atmosenv.2005.05.051 (Closed Access)

VEDANTHAM, Anu, & OPPENHEIMER, Michael, 1998. *Long-term scenarios for aviation: Demand and emissions of CO_2 and NO_x*.
Available from: https://doi.org/10.1016/S0301-4215(98)00021-4 (Closed Access)

WASIUK, D.K., KHAN, M.A.H., SHALLCROSS, D.E., & LOWENBERG, M.H., 2016. *The impact of global aviation NO_x emissions on tropospheric composition changes from 2005 to 2011*. In: *Atmospheric Research*, vol. 178–179, pp. 73–83.
Available from: https://doi.org/10.1016/j.atmosres.2016.03.012 (Closed Access)

WINTHER, Morten, KOUSGAARD, Uffe, ELLERMANN, Thomas, MASSLING, Andreas, NØJGAARD, Jacob Klenø, & KETZEL, Matthias, 2015. *Emissions of NO_x, particle mass and particle numbers from aircraft main engines, APU's and handling equipment at Copenhagen Airport*. In: *Atmospheric Environment*, vol. 100, pp. 218–229.
Available from: https://doi.org/10.1016/j.atmosenv.2014.10.045 (Closed Access)

XU, Hao, FU, Qingyan, YU, Yamei, LIU, Qizhen, PAN, Jun, CHENG, Jinping, WANG, Zhenwu, & LIU, Linqi, 2020. *Quantifying aircraft emissions of Shanghai Pudong International Airport with aircraft ground operational data*. In: *Environmental Pollution*, vol. 261, p. 114115.
Available from: https://doi.org/10.1016/j.envpol.2020.114115 (Closed Access)

YU, J.-L., JIA, Q., GAO, C., & HU, H.-Q., 2021. *Air pollutant emissions from aircraft landing and take-off cycles at Chinese airports*. In: *The Aeronautical Journal*, vol. 125, no. 1285, pp. 578–592.
Available from: https://doi.org/10.1017/aer.2020.126 (Closed Access)

Appendix A
Additional Figures and Observations from Engine Dataset

This appendix presents additional graphical evaluations derived from available engine data. Due to limited data availability for certain engine variants, not all configurations are included. In several cases, the small number of valid data points produced unreliable or unrepresentative results, so they were excluded to maintain the interpretive integrity of this work. Additionally, only plots that were analytically or visually relevant were included. Not every possible variable combination has been evaluated graphically, as exhaustive coverage would exceed the intended scope. However, the full dataset enables readers to conduct alternative analyses, including non-linear or multivariate regressions, if they desire further investigation.

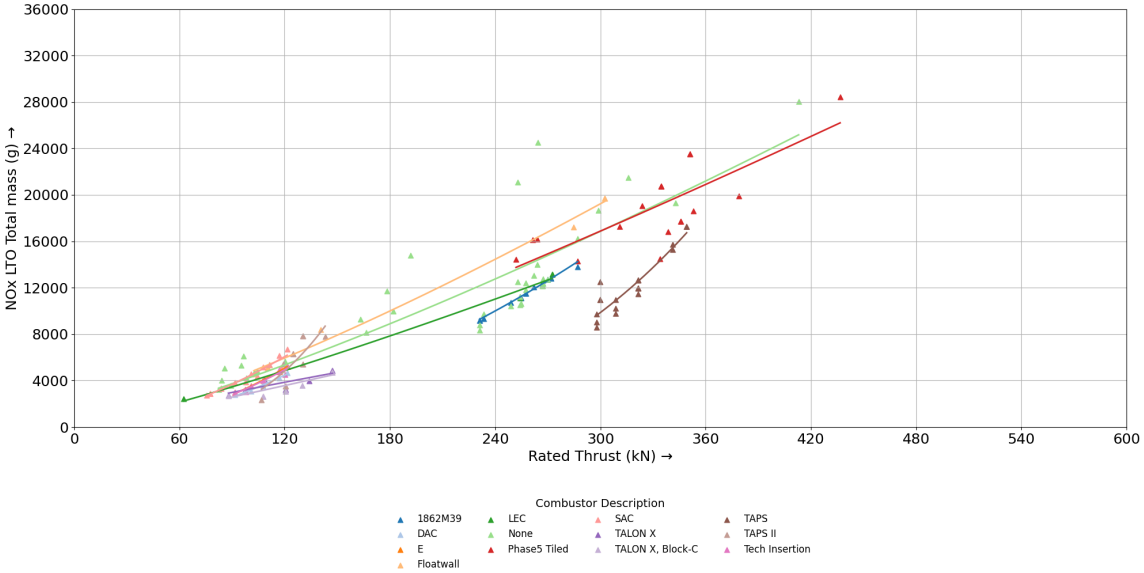

Figure A.1: NO_x LTO total mass (g) as a function of rated thrust (kN) for different combustor configurations. Each color and marker indicates a specific combustor type.

Table A.1: Power-law regression equations for total NO_x mass emissions as a function of take-off thrust T_{TO}

Combustor Type	Equation	R^2	MAPE (%)
1862M39	$NO_{x,LTO} = 0.1944 \cdot T_{TO}^{1.9793}$	0.9843	1.02
DAC	$NO_{x,LTO} = 0.4519 \cdot T_{TO}^{1.9212}$	0.9798	2.69
E	$NO_{x,LTO} = 0.2330 \cdot T_{TO}^{2.0862}$	0.9959	0.92
Floatwall	$NO_{x,LTO} = 12.8783 \cdot T_{TO}^{1.2814}$	0.9937	5.04
LEC	$NO_{x,LTO} = 16.8791 \cdot T_{TO}^{1.1826}$	0.9912	3.83
None	$NO_{x,LTO} = 13.2632 \cdot T_{TO}^{1.2532}$	0.7540	17.57
Phase5 Tiled	$NO_{x,LTO} = 21.1165 \cdot T_{TO}^{1.1718}$	0.6097	10.83
SAC	$NO_{x,LTO} = 1.4929 \cdot T_{TO}^{1.7355}$	0.9360	4.51
TALON X	$NO_{x,LTO} = 52.9920 \cdot T_{TO}^{0.8954}$	0.6201	10.26
TALON X, Block-C	$NO_{x,LTO} = 16.6301 \cdot T_{TO}^{1.1214}$	0.6442	12.46
TAPS	$NO_{x,LTO} = 0.0000 \cdot T_{TO}^{3.4819}$	0.8647	5.80
TAPS II	$NO_{x,LTO} = 0.0005 \cdot T_{TO}^{3.3534}$	0.6023	21.15
Tech Insertion	$NO_{x,LTO} = 0.3321 \cdot T_{TO}^{2.0067}$	0.9331	4.10

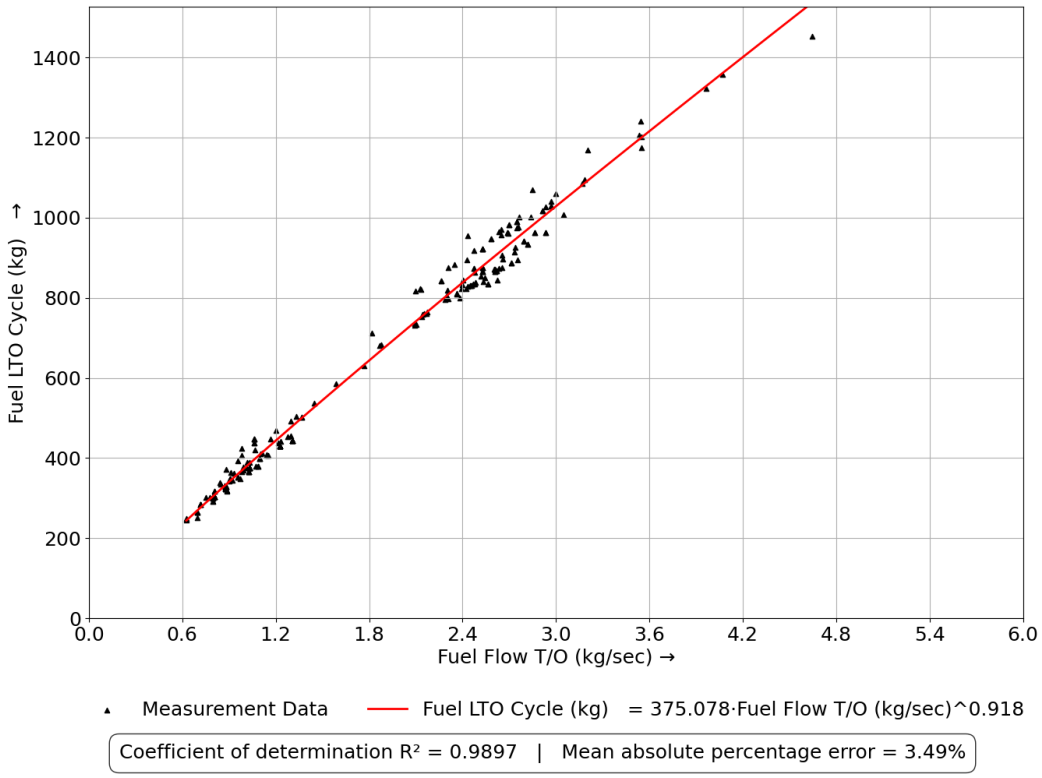

Figure A.2: Fuel mass over the full LTO cycle (kg) as a function of fuel flow rate during the take-off phase for all available engine configurations.

$$m_{f,LTO} = 375.078 \cdot \dot{m}_{f,TO}^{0.918} \tag{A.1}$$

Appendix B
Tools

This project used the AI-based DeepL Write tool by DeepL. It was used to find synonyms and alternative formulations, serving as a means of linguistic support. No text passages or sources were generated autonomously. All information, data and results were independently developed by the authors and are supported by appropriate sources. We take full responsibility for the content of this project paper and confirm that DeepL Write was used strictly for the above purposes.